

**APPLICATION OF PROXIMAL SOIL SENSING FOR ENVIRONMENTAL
CHARACTERIZATION OF AGRICULTURAL LAND**

By

AHMAD SUHAIZI, MAT SU

Department of Bioresource Engineering
Faculty of Agricultural and Environmental Sciences
Macdonald Campus of McGill University
Ste-Anne-De-Bellevue, Montreal, Quebec, Canada

August, 2016

A thesis submitted to McGill University in partial fulfillment of the requirement of the degree
of

Doctor of Philosophy

© Ahmad Suhaizi, Mat Su 2016

*To Siti Amni, Adeeb, and Umar
Who have given me never-ending love and encouragement from the
very beginning*

ABSTRACT

Sustainable high-intensity agriculture involves optimizing yield and profitability without compromising the environment. High chemical inputs have the potential to accelerate soil systems' biological activity and emission of greenhouse gasses (GHG; e.g., CO₂, CH₄, and N₂O) without increasing the yield. Quantifying emissions from agricultural soils is critical to assessing the sustainability of farming practices. Usually, estimates of agriculture-driven GHG emissions are based on a small number of sampling sites. Inherent differences in soil climatic and physical properties and crop management activities can significantly affect an agricultural field's spatial and temporal patterns of GHG emissions. Accordingly, a close knowledge of soil heterogeneity is critical for improving the reliability of GHG emission estimates. In this project, stability estimates of apparent soil electrical conductivity (EC_a) measurements by electromagnetic induction (EMI) and galvanic contact resistance (GCR) instruments were assessed by testing for both temporal and operational effects of a sodden lawn (soil EC_a = 5-15 ms m⁻¹). Operational effects on the instrument included height above ground (0 or 0.10 m), roll angle (0° and ±10°), and pitch angle (0° and ±10°). Among EMI measurements, the perpendicular coplanar (PRP) operating mode of the DUALEM-21S provided the most stable measurements. Changes in height and roll within tolerance had no effect on soil EC_a measurements, but increasing pitch reduced measurement values. From a practical point of view, soil EC_a measurements varied little within the height tolerance of 0.10 m, and roll and pitch tolerance of ±10°. In a second study, a database management methodology was developed to analyze the >30,000 GHG samples. This methodology included a means for data format standardization and flux/emission calculation based on 103 fixed sampling locations across Eastern Canada using a suite of automated MATLAB scripts. Flux estimates were determined using the median slope of temporal change of concentration, thereby filtering outliers arising from erroneous measurements. In a third study, temporal variations in GHG emissions under different soil physical properties and soil organic matter decomposition rates were monitored in three sites with replicated water treatment plots (sprinkler irrigation vs. no irrigation), using a network of wireless sensors that monitored soil matric potential, volumetric water content and soil temperature. Muck soils tended to emit more N₂O under relatively wet and cool conditions, whereas CH₄ fluxes peaked in fully wet soils, while moderate soil moisture levels and warm temperatures promoted CO₂ emissions. Correlations between GHG fluxes and measured soil properties were rather weak, limiting the potential for modeling GHG fluxes and emissions. In a fourth and final study, placement of GHG monitoring

sites was optimized for an agricultural field with variable soil conditions. Nine locations were selected and monitored to detect levels of GHG fluxes and emissions representing the most extreme soil conditions present in the chosen field. Different soil types, as well as soil moisture and temperature dynamics, resulted in different levels of GHG emissions. Due to high soil moisture content caused by a field depression, methane emissions were highest in muck (vs. mineral) soils. Assessment of spatial and temporal variations in soil physical characteristics can clarify GHG emission dynamics, allowing a more accurate quantification of modern farming systems' environmental impact.

RÉSUMÉ

L'agriculture durable peut être définie comme l'optimisation du rendement et la rentabilité sans compromettre l'environnement. Nécessitant des taux élevés de composés chimiques, qui accélèrent l'activité biologique des sols, les pratiques d'agriculture intensive entraînent l'émission de gaz à effet de serre (GES; CO₂, CH₄, et N₂O), sans pour autant obtenir de meilleurs rendements. Quantifier les émissions de GES provenant des sols agricoles devient alors essentiel lors de l'évaluation de la durabilité des pratiques agricoles. N'ayant pas tenu compte de l'hétérogénéité des champs, les estimations d'émissions de gaz du passé ne consistaient qu'en une extrapolation à partir des émissions d'un petit nombre de sites d'échantillonnage. Des différences inhérentes quant aux propriétés physiques et climatiques des sols et des activités de gestion des cultures peuvent affecter significativement la répartition spatiale (à l'horizontale et en profondeur) et temporelle des émissions de GES. Conséquemment, l'amélioration de la fiabilité d'estimation des émissions de GES est étroitement liée à une connaissance approfondie de l'hétérogénéité des sols. En une première étude, la qualité de la cartographie de la conductivité apparente du sol (EC_a), évaluée par induction électromagnétique (IEM) avec des instruments de contact à résistance galvanique (CRG) fut évaluée en examinant les effets temporels et opérationnels d'une pelouse trempée ($EC_a = 5-15 \text{ ms m}^{-1}$). Les effets opérationnels ont inclus la distance au-dessus de la surface (0 ou 0.10 m), et les angles de roulis et de tangage (0° et $\pm 10^\circ$). Parmi les mesures d'EMI, le capteur DUALEM-21S en mode d'opération de conductivité perpendiculaire coplanaire (CPC) a offert les mesures les plus stables. Les variations en hauteur et roulis inférieures à la tolérance évaluée n'affectèrent pas l' EC_a du sol, mais les variations en tangage par rapport à 0° ont réduit l' EC_a . D'un point de vue pratique, les mesures de l' EC_a du sol ont très peu varié à l'intérieur d'une tolérance en hauteur de 0.10 m, et de roulis et tangage de $\pm 10^\circ$. Face à de gros volumes de données (>30,000 échantillons de gaz) provenant de multiples (103 chambres à gaz à 6 sites) et divers (c.-à-d. sol, récolte, irrigation) emplacements dans l'est du Canada, une seconde étude s'adressa à la gestion des bases de données, le format de normalisation, et aux problèmes de calcul des flux et émissions. Pour ce faire, une série de scripts MATLAB furent développés. L'estimation des flux et émissions utilisa les pentes médianes de régressions linéaires, une méthode permettant de filtrer les mesures erronées. Dans une troisième étude, les variations temporelles des émissions de GES sous différentes combinaisons de propriétés physiques et taux de décomposition de sols organiques à trois sites disposant de parcelles irriguées ou non irriguées furent suivies à l'aide de réseaux de capteurs

sans fil pour le potentiel matriciel du sol, l'humidité du sol, et sa température. Les sols de terre noire émettent plus de N_2O lorsque le sol était relativement humide et les conditions climatiques fraîches, tandis que les flux en CH_4 furent plus élevés dans les sols détrempés. Les émissions de CO_2 furent les plus élevées lorsque l'humidité du sol était modérée et les températures chaudes. Les corrélations entre les flux de GES et les propriétés du sol se révélèrent plutôt faibles, limitant le potentiel de modélisation des flux et des émissions de GES. En une dernière étude, l'optimisation du placement des sites de surveillance des émissions de GES fut entreprise pour un champ agricole. Neuf emplacements furent choisis et instrumentés pour détecter différents niveaux différents de flux de GES selon les différents types de sols considérés. La teneur en eau et la température de différents types de sols menèrent à différents niveaux d'émissions de GES. Les émissions en CH_4 étaient particulièrement élevées pour les terres noires (vs sols minéraux) principalement en raison de dépressions dans le champ et de la haute teneur en eau du sol dans ces dépressions. L'évaluation des variations spatiales et temporelles dans les caractéristiques physiques des sols peut aider à mieux comprendre la dynamique des émissions de GES, permettant ainsi de quantifier plus précisément les effets environnementaux des systèmes agricoles modernes.

ACKNOWLEDGEMENTS

I owe my gratitude to all the people who have made this dissertation possible and it is because of them that my graduate experience has been one that I will cherish forever.

Foremost, partial funding for this research was provided by Canada Foundation for Innovation (CFI), Agriculture and Agri-Food Canada (AAFC) – Agricultural Greenhouse Gases Program (AGGP), Ministry of Education of Malaysian (MOEM), and Universiti Putra Malaysia (UPM) is gratefully acknowledged.

I wish to offer my sincerest thanks and deepest gratitude to Prof. Dr. Viacheslav Adamchuk, for having given me the opportunity to work on these projects. His insight value of being a great *shifu* since I began as his student in 2008-2009 as an MS student, and I admire him greatly for his work ethic, problem-solving ability, and knowledge of both academic and daily life. His leadership, scrupulous planning, organizational skills, and drive for perfection were not only the means by which this project was completed, but have also had an invaluable influence on my work ethic and professional career.

I offer my appreciation to the Department Chair of Bioresource Engineering, Prof. Dr. Valérie Orsat, and Director of Graduate Program of Bioresource Engineering, Mrs. Susan Gregus, who continuously provided their support and guidance throughout my Ph.D. program. I'm also grateful to Prof. Dr. Joann Whalen for being on my supervisory committee, Dr. Asim Biswas for being on my dissertation examination committee. I would like to extend my sincere thanks to Prof. Dr. Chandra Madramootoo, Prof. Dr. Joann Whalen, Prof. Dr. Caroline Begg, and Prof. Dr. Vijay Ragavan for being the committee members for my Ph.D. comprehensive examination and who provided suggestions on the preliminary work of this research. Also, I acknowledge active and valuable contributions from the co-authors of the manuscripts of this research; Prof. Dr. Asim Biswas and Dr. Wenjun Ji for their research questions and reviewing my writing for publication. Their input provided me with a wider perspective and understanding this research. Also to Trevor Stanhope, who provides an editorial work in some part of my thesis, and Antoine Poliot, for his help in French translation work.

I also want to extend my thanks to all my colleagues in the McGill Precision Agriculture and Sensor System team with whom I shared many cheerful moments and were a source of support, motivations, and friendship; Dr. Luan Pan, Dr. Nandkishor Dhawale, Hsin-Hui Huang, Yue Su, Frederic Rene-Laforest, Florian Reumont, Francisco Ruiz de la Macorra, Bharath Sudarsan,

Maria Mastorakos, Jasmeen Kaur, and others; at Brace Centre team; Kerri Edward, Angela Grant, Pernilla Talec, Kaitlin Lloyd, Cynthia Crézé, Kenton Ollivierre, Eduardo Ganem Cuenca and others, and to the summer students who participated in the fieldwork.

Thank you to Prof Dr. Ir. Mohd Amin Mohd Soom, Prof. Dr. Ir. Azmi Yahya, and Prof Dr. Aimrun Wayayok, my former project advisors during my work as a research assistant at UPM, who provided opportunity and guidance for my enthusiasm in agricultural research as general.

Sincere gratitude goes to my family members, siblings, and my wife for their great, great, great patience, encouragement, and support. Their unconditional love and support have always been my source of inspiration.

Finally, to The Almighty God to whom I pay my due respects, I offer my obedience and gratefulness for leading me to this blessed path.

TABLE OF CONTENTS

ABSTRACT	III
RÉSUMÉ	V
ACKNOWLEDGEMENTS	VII
TABLE OF CONTENTS	IX
LIST OF TABLES	XIV
LIST OF FIGURES	XVI
FORMAT OF THE THESIS	XIX
CONTRIBUTIONS OF AUTHORS	XXI
NOMENCLATURE	XXIII
CHAPTER 1	1
Introduction	1
1.1 General Introduction.....	1
1.2 Statement of Rationale and Objectives of the Research	2
1.2.1 Statement of Rationale.....	2
1.2.2 Objectives of the Research	3
CHAPTER 2	4
General Review of Literature.....	4
2.1 Proximal Soil Sensing	4
2.1.1 Method of Soil EC _a Measurement and its Uncertainty Issues	4
2.2 GHG Emission Estimation.....	6

2.3 Temporal GHG emission.....	7
Connection Text to Chapter 3	11
CHAPTER 3	12
Temporal and Operational–Induced Apparent Soil Electrical Conductivity Stability .	12
Abstract.....	12
3.1 Introduction	12
3.2 Materials and Methods	14
3.2.1 Instruments	14
3.2.2 Experimental Procedure.....	16
3.2.3 Data analysis.....	17
3.3 Results and Discussions	19
3.3.1 Temporal Test.....	19
3.3.2 Operational Test.....	23
3.4 Conclusion	27
Connection Text to Chapter 4	28
CHAPTER 4	29
Streamlined analysis of agricultural greenhouse gases fluxes and annual emission	29
Abstract.....	29
4.1 Introduction	30
4.2 Materials and Methods	32
4.2.1 Study Site.....	32
4.2.2 Gas Sampling.....	34
4.2.3 Gas Concentration and Threshold Criteria	35

4.2.4 Flux Estimation.....	38
4.2.5 Annual Emission Estimation.....	39
4.3 Results and Discussions	40
4.3.1 Slope and Flux Estimation.....	40
4.3.2 Emission Estimation	43
4.4 Conclusion	52
Connection Text to Chapter 5	53
CHAPTER 5	54
Predicting Changes in Greenhouse Gases Emissions in Muck Soil Using Physical Observations	54
Abstract.....	54
5.1 Introduction	55
5.2 Materials and Methods	56
5.2.1 Site Description	56
5.2.2 Data Collection	57
5.2.3 Data Analysis	59
5.3 Results and Discussion	61
5.4 Conclusion	64
Connection Text to Chapter 6	65
CHAPTER 6	67
Application of Proximal Soil Sensing in Predicting the Spatial and Temporal Agriculture GHG in Eastern Canada	67
Abstract.....	67

6.1 Introduction	68
6.2 Materials and Methods	71
6.2.1 Site Characteristics	71
6.2.2 Field Survey	75
6.2.3 Gas Sampling and Flux Analysis.....	76
6.2.4 Data Analysis	79
6.2.5 Representative monitoring locations (RML) for the GHG fluxes	79
6.3 Results and Discussions	82
6.3.1 Descriptive Statistics	82
6.3.2 Locating the Gas Chambers.....	84
6.3.3 GHG flux and emission	90
6.3.4 N ₂ O–N fluxes and emissions.....	91
6.3.5 CH ₄ –C fluxes and emissions	92
6.3.6 CO ₂ –C fluxes and emissions.....	94
6.3.7 Correlation between on-the-go measurements and soil properties .	94
6.3.8 Identification of the representative chamber location	104
6.4 Conclusions.....	108
CHAPTER 7	109
Summary and General Conclusions.....	109
7.1 Summary.....	109
7.2 General Conclusions	110

CHAPTER 8	111
Contributions To Knowledge And Suggestions for Future Research	111
8.1 Contributions to Knowledge	111
8.2 Suggestions for Further Research.....	112
REFERENCES	113
APPENDICES	123
A. MATLAB programs for data analysis, flux and emission estimation (Chapter 4).....	123

LIST OF TABLES

Table 1: Instrument specifications	15
Table 2: List of recorded measurements	16
Table 3: Experimental timeline	18
Table 4: EC _a [mS/m] measurements for temporal tests.	22
Table 5: Pearson coefficients of correlation between EC _a measurements and measurement conditions.	23
Table 6: EC _a [mS/m] measurements for operational tests.	26
Table 8. Descriptive statistic of nitrous oxide, methane and carbon dioxide emission (g.m ⁻²) for 2012 season.....	46
Table 9. Descriptive statistic of nitrous oxide, methane and carbon dioxide emission (g.m ⁻²) for 2013 season	47
Table 10. Descriptive statistic of nitrous oxide, methane and carbon dioxide emission (g.m ⁻²) for 2014 season.....	48
Table 11: Mean and standard error of the GHG fluxes, and monitored soil physical properties.....	61
Table 12. Wide range of soil series and its characteristic at F26	74
Table 13. Gamma ray specifications	76
Table 14. Descriptive statistics of the 5x5 m data on-the-go measurement; SD, standard deviation; CV, coefficient of variation; N = 4467.	82
Table 15. Descriptive statistic of soil EC _a , gamma ray measurement, and other soil properties measured at all 9 locations.....	84
Table 16. Actual data set at 9 sampling locations.....	85
Table 17. Average of measured properties under organic and mineral soil.	87
Table 18: Pearson correlation of GHG and soil properties (N = 306).....	102
Table 19: Correlation coefficient (r) between the soil EC _a and other soil parameters.	103
Table 20: Correlation coefficient between the Gamma ray and site and soil parameters (N= 56).....	103
Table 21: Correlation coefficient between the soil EC _a and Gamma ray.....	104

LIST OF FIGURES

Figure 1: The overall scope of the study of the relationship between the field heterogeneity and GHG flux or emission.	2
Figure 2: GCR sensor Veris Quad EC 1000 (Veris Technologies, 2014).....	14
Figure 3: EMI sensors: EM-38 and DUALEM-21S, modified from Simpson <i>et al.</i> (2009). ..	15
Figure 4: Experimental setup (24-Oct-2013).	17
Figure 5: Operational tests for EMI instruments.	18
Figure 6: Box-and-whiskers plot of environmental conditions: ambient temperature, soil temperature, air humidity, volumetric soil water content, and the internal temperature of DUALEM-21S instrument during temporal tests.	20
Figure 7: An example of 1-s average EC _a measurement logs obtained on 9-Oct-2013. ..	21
Figure 8: The range (minimum and maximum) of soil EC _a measurements during temporal tests.	21
Figure 9: Examples of relationships between EC _a measurements (15-min sampling) and corresponding records of ambient conditions (dash lines show regressions with 18-Sep-2013 data excluded).....	24
Figure 10: The range (minimum and maximum) of operational tests for each recorded measurement.	25
Figure 11: Study locations located across Ontario to the Eastern Canada	33
Figure 12: Illustration of the median slope concept for flux estimation.....	39
Figure 13: The flux values were calculated from the slope of the model line generated from five gas datasets using MFM models: (a) and (b) are the N ₂ O-N, (c) and (d) are the CH ₄ -C, and (e) and (f) are the CO ₂ -C gases responses under normal and noisy dataset, respectively.	42
Figure 14: Temporal variation of the GHG emission over the growing season on individual chamber IDs.	45
Figure 15: Nitrous oxide emission estimation under different water, crop and soil treatments.....	49
Figure 16: Methane emission estimation for different water and soil treatments.....	50
Figure 17: Carbon dioxide emission estimation for different water and soil treatments....	51
Figure 18. Study locations.....	57

Figure 19: A static non-steady state chamber installed for gas sampling.....	58
Figure 20: Wireless sensor network installed at three different location under different water regime (a) The wireless sensor network (b) Field layout for the sensor arrangement for all three stations.....	60
Figure 21: Wireless sensor network installed at three different decomposition rates of organic soil.....	60
Figure 22: The overall soil moisture and temperature relationships between low, medium and high GHG fluxes measured in 2012 and 2013 from an organic soil (a) N ₂ O-N fluxes, (b) CH ₄ -C fluxes, and (c) CO ₂ -C fluxes. The round black dotes (●) represents the average values of each categories.....	63
Figure 23: Soil series map ranged from organic to mineral soil located at F26 (Soil Canada Survey Map, 1971). The letters is the legend as explained in Table 12.....	74
Figure 24: Precipitation data of 2014 at F26. The respective sampling date was marked as "+"	75
Figure 25: Proximal soil sensing survey (a) DUALEM-21S and (b) Gamma ray spectrometer.....	77
Figure 26: Non-steady state chamber design deployed between soybean crop, covered with aluminum sheet to minimized the effect direct thermal from the sun.	77
Figure 27: Comparison of the R ² between various field measured on-the-go soil physical properties; Elevations vs. (a) total count of the gamma ray and (b) 2013 soil EC _a at PRP 1 m mode; and (c) 2013 soil EC _a at PRP 1 m vs. total count of gamma ray.	85
Figure 28: The 5x 5 m grid of soil physical properties measured using on-the-go system; 2013 soil EC _a measured on different configuration of (a) perpendicular 2 m, (b) perpendicular 1 m, (c) horizontal 2 m, and (d) horizontal 1 m.....	88
Figure 29: The 5x5 m grid of (a) the soybean yield (t/ha) measured using yield monitor on the combine harvester, (b) Total count of gamma ray signal, and (c) Elevation and irrigation line map of F26. The conventional sub-irrigation stretched from east to west of the field mainly at the depression area at sub meter depth, spacing approximately from 6-30 m apart.....	89
Figure 30: Soil moisture variability.....	96
Figure 31: Soil temperature variability.	97
Figure 32: N ₂ O–N fluxes variation	98
Figure 33: CH ₄ –C fluxes variation	99
Figure 34: CO ₂ –C fluxes variation	100

Figure 35: Estimated in-season net GHG emissions under organic and mineral soil..... 101

Figure 36: Ranked mean relative different of the fluxes for (a) N₂O-N, (b) CH₄-C, and (c) CO₂-C. The error bars indicate the standard deviation of the MRD of the fluxes. 105

Figure 37: Spatial variation of the average GHG fluxes (mgm⁻²h⁻¹) spread over location ID and chamber ID (labelled as *Ch ID*) the F26 area of (a) N₂O-N, (b) CH₄-C, and (c) CO₂-C. The circles-colored indicate different of GHG fluxes ranges from individual chamber and locations..... 106

Figure 38: Spatial relationship between the average of the N₂O-N fluxes versus (a) OM (b) soil EC_a, (c) field elevation and (d) total count. CH₄-C, and (c) CO₂-C. The circles-colored indicate different of GHG fluxes ranges from individual chamber and locations..... 107

Figure 39: Spatial relationship between the average of the CH₄-C fluxes versus (a) OM (b) soil EC_a, (c) field elevation and (d) total count..... 107

Figure 40: Spatial relationship between the average of the CO₂-C fluxes versus (a) OM (b) soil EC_a, (c) field elevation and (d) total count..... 108

FORMAT OF THE THESIS

This thesis is submitted in the format of papers suitable for journal publication. This thesis format has been approved by the Faculty of Graduate and Postdoctoral Studies, McGill University, and follows the conditions outlined in the Guidelines Concerning Thesis Preparation, which are as follows:

“As an alternative to the traditional thesis format, the dissertation can consist of a collection of papers of which the student is an author or co-author. These papers must have a cohesive, unitary character making them a report of a single program of research. The structure for the manuscript-based thesis must conform to the following Candidates have the option of including, as part of the thesis, the text of one or more papers submitted, or to be submitted, for publication, or the clearly-duplicated text (not the reprints) of one or more published papers. These texts must conform to the "Guidelines for Thesis Preparation" with respect to font size, line spacing and margin sizes and must be bound together as an integral part of the thesis. (Reprints of published papers can be included in the appendices at the end of the thesis).

The thesis must be more than a collection of manuscripts. All components must be integrated into a cohesive unit with a logical progression from one chapter to the next. In order to ensure that the thesis has continuity, connecting texts that provide logical bridges between the different papers are mandatory.

The thesis must conform to all other requirements of the "Guidelines for Thesis Preparation" in addition to the manuscripts. The thesis must include the following

A table of contents;

An abstract in English and French;

An introduction which clearly states the rationale and objectives of the research;

A comprehensive review of the literature (in addition to that covered in the introduction to each paper);

A final conclusion and summary;

As manuscripts for publication are frequently very concise documents, where appropriate, additional material must be provided (e.g., in appendices) in sufficient detail to allow a clear and precise judgment to be made of the importance and originality of the research reported in the thesis. In general, when co-authored papers are included in a thesis the candidate must have

made a substantial contribution to all papers included in the thesis. In addition, the candidate is required to make an explicit statement in the thesis as to who contributed to such work and to what extent. This statement should appear in a single section entitled "Contributions of Authors" as a preface to the thesis. The supervisor must attest to the accuracy of this statement at the doctoral oral defense. Since the task of the examiners is made more difficult in these cases, it is in the candidate's interest to clearly specify the responsibilities of all the authors of the co-authored papers".

CONTRIBUTIONS OF AUTHORS

List of publications and scientific presentations related to the thesis

A. Thesis chapters submitted for publication in peer-reviewed journals

1. **Ahmad Suhaizi M.S.** and V.I Adamchuk. 2016. Temporal and operation-induced variability of apparent soil electrical conductivity measurements. *Journal of Applied Geophysics* (under review)
2. **Ahmad Suhaizi M.S.** V.I. Adamchuk, C.A. Madramootoo, J.K. Whalen, F.J. Reumont, and H.Hui Huang. Unbiased flux calculation for greenhouse gas emissions estimation. *Canadian Journal of Soil Science* (to be submitted).
3. **Ahmad Suhaizi M. S.** V.I. Adamchuk, J.K. Whalen, C.A. Madramootoo, A. Biswas, F. Reumont, F.R De Le Macorra, and W. Ji. Application of Proximal Soil Sensing in predicting the spatial and temporal agriculture GHG in Eastern Canada. *Agriculture, Ecosystems and Environment* (to be submitted).

B. Non-referred conference proceedings

1. Wenjun Ji, Viacheslav I. Adamchuk, Asim Biswas, **Ahmad S. Mat Su** and Zhou Shi. Simultaneous measurement of multiple soil properties through proximal sensors fusion. In 4th Global Workshop on Proximal Soil Sensing. Zhejiang University, Hangzhou, China, May 12–15, 2015.
2. **Mat Su, A. S.**, V. I. Adamchuk, C. A. Madramootoo, J. K. Whalen, Katina Tam, H.H Huang, and Hicham Beslim. 2014. Predicting changes in Greenhouse Gases Emission in muck soil using physical observations. 2014 ASABE and CSBE/SCGAB Annual International Meeting.
3. K. P. Edwards, C. A. Madramootoo, J. K. Whalen, V. I. Adamchuk, **A.S. Mat Su**, H. Benslim. 2014. Greenhouse gas emission from drip irrigation fields. 2014 ASABE and CSBE/SCGAB Annual International Meeting. Paper Number: 141899456
4. **Mat Su, AS.** V.I Adamchuk. Evaluation of the temporal and operational stability of apparent soil electrical conductivity measurements. July 20-23 2014. 12th ICPA Conference. Sacramento, CA, USA. Link (https://www.ispag.org/proceeding_module/authors/default/details/abstract_id/1465)

C. Published abstracts

1. **Mat Su, A. S.**, V. I. Adamchuk, C. A. Madramootoo, J. K. Whalen, H.H Huang. 2013. Estimating greenhouse gas emissions using experimental data. In: *Scientific Program of CSSS/MSSS/CSAFM Joint Meeting*, Winnipeg, Manitoba, 21-25 July 2013, 70. Winnipeg, Winnipeg, CSSS.
2. Sebastian Belliard, **Ahmad S. Mat Su**, Kerri Edwards, Elaina Hurst, Katina Tam, Hicham Benslim, Joann K. Whalen, Viacheslav I. Adamchuk and Chandra A. Madramootoo. Comparison of nitrous oxide emission factors for Quebec and Ontario

with empirical results from agroecosystems under contrasting water management regimes. CGU-CSSS meeting in Banff, Alberta. May 4–7 2014.

3. Dhawale, N.M., V.I Adamchuk, S.O. Prasher, J.K. Whalen, L. Pan, & **A.S. Mat Su**. 2013. Rapid measurement of nitrate ion activity using a direct soil sensing approach. *In: Poster of Scientific Program of CSSS/MSSS/CSAFM Joint Meeting*, Winnipeg, Manitoba, 21-25 July 2013, 99. Winnipeg, Winnipeg, MB, Canada. Link (<http://home.cc.umanitoba.ca/~tenutam/CSSS/CSSS%20MSSS%20CSAFM%20printed%20program%20FINAL.pdf>)

D. Poster presentation

1. **Ahmad Suhaizi Mat Su**, Viacheslav Adamchuk, , Joann Whalen, Chandra Madramootoo, Asim Biswas, Florian Reumont, Francisco Ruiz De Le Macorra, and Wenjun Ji. 2015. Using proximal soil sensing to optimize the assessment of agricultural greenhouse gas emissions. Poster presentation. In *Soil Interfaces for Sustainable Development Joint Meeting of International Union of Soil Sciences, Canadian Soil Science Society, and Association Québécoise de Spécialistes en Sciences du Sol*. McGill University, Montreal, Canada. 5-10 July 2015.
2. Dhawale, N.M., V.I. Adamchuk, S.O. Prasher, J.K. Whalen, L. Pan and **A.S. Mat Su**. 2013. Rapid measurement of nitrate ion activity using a direct soil sensing approach. *In: Poster of Scientific Program of CSSS/MSSS/CSAFM Joint Meeting*, Winnipeg, Manitoba, 21-25 July 2013, 99. Winnipeg, Winnipeg, CSSS.

E. Awards and recognition

1. Guy Mehuys Memorial Award. 2015. Soil Interfaces for Sustainable Development Conference. Commission 2.5 of the International Union of Soil Science, the Canadian Soil Science Society and the Association quebecois de specualistes en science du sol. July 5-10 2015. Montreal, Canada.
2. Outstanding Graduate Student Award. 2014. International Society of Precision Agriculture. Sacramento, California, USA. July 22nd, 2014. Link: <https://www.ispag.org/awards/>
3. Graduate Travel Awards (GREAT) 2014, Department of Bioresource Engineering. McGill University. May 14th, 2014.
4. Graduate Training & Travel Award, Bioresource Engineering Department, McGill University. 2012.
5. Federal Scholarship Awards: Skim Latihan Akademik IPTA (SLAI). Malaysians Government. 2011-2015.

NOMENCLATURE

^{232}U	Uranium – 232 (measured using gamma-ray spectrometry)
^{238}Th	Thorium – 238 (measured using gamma-ray spectrometry)
^{40}K	Potassium – 40 (measured using gamma-ray spectrometry)
AAFC	Agriculture and Agri–Food Canada
AGGP	Agricultural Greenhouse Gas Program
ANOVA	Analysis of variance
CH_4	Methane
$\text{CH}_4\text{--C}$	Methane – carbon (flux or emission)
C_m	Measured gas concentration (ppm or mg/kg)
CO_2	Carbon dioxide
$\text{CO}_2\text{--C}$	Carbon dioxide – carbon (flux or emission)
C_v	Measured gas concentration (mg/m^3)
$\text{DUALEM}_{\text{HCP-1}}$	Horizontal coplanar at 1 m distance of DUALEM–21S
$\text{DUALEM}_{\text{HCP-2}}$	Horizontal coplanar at 2 m distance of DUALEM–21S
$\text{DUALEM}_{\text{PRP-1.1}}$	Perpendicular coplanar at 1.1 m distance of DUALEM–21S
$\text{DUALEM}_{\text{PRP-2.1}}$	Perpendicular coplanar at 2.1 m distance of DUALEM–21S
EC_a	Apparent soil electrical conductivity (mS/m)
$\text{EM-38}_{\text{HCP-1}}$	Horizontal dipole at 1 m distance of EM–38
$\text{EM-38}_{\text{VCP-1}}$	Vertical dipole at 1 m distance of EM–38
EMI	Electromagnetic inductance
F26	Field ID 26 of MacDonald Campus, McGill University
GCR	Galvanic contact resistivity
GHG	Greenhouse gas
GNSS	Global Navigation Satellite System
GPS	Global Positioning System
H	Height (m)
HCP	Horizontal coplanar
HR	Harrow site
IPCC	Intergovernmental panel on climate change
K	Potassium
L	Length (m)
LE	Leamington site

MFM	Median flux model
MOEM	Ministry of Education of Malaysia
mol	Mole
MRD	Means relative different
mS/m	millisiemens per meter
N	Nitrogen
N ₂ O	Nitrous oxide
N ₂ O–N	Nitrous oxide-nitrogen (flux or emission)
°C	Degree Celsius
P	Phosphorus
PA	Precision Agriculture
PCHIP	Piecewise Cubic Hermite Interpolating Polynomial extrapolation
PRP	Perpendicular coplanar
PSS	Proximal soil sensing
R ²	Coefficient of determination
RML	Representative monitoring locations
RMSE	Root means square error
SDMRD	The standard deviation of mean relative different
SE	Sainte Emmanuel site
SH	Sherrington site
SL	St. Louis de Blandford site
STD	Standard deviation
T	Temperature (°C)
<i>t</i>	Time (h, min or s)
TR	Truro site
t–test	Student's t–test
UPM	Universiti Putra Malaysia
VCP	Vertical coplanar
W	Width (m)
WSN	Wireless sensors network
γ-ray	Gamma ray spectroscopy
Δt	Time interval (h)
Ψ_w	Soils matric potential (kPa)

CHAPTER 1

INTRODUCTION

1.1 General Introduction

As the global population increases, the need for better management of agricultural resources in food production is a priority. Therefore, local and national policies on both environmental sustainability and food security must consider this trend. Despite the constraints of agricultural resources, modern agriculture has made enormous progress in improving yields and in decreasing the time needed for crop growth. An environmental response to modern agricultural activities is tremendously significant in human life. A future with sustainable agriculture requires an integrated approach for technological advances in precision agriculture, i.e. application of proximal soil sensing (PSS). Precision agriculture aims at implementing 4R nutrient stewardship in terms of "application of the right input, at the right time, and in the right amount" (Mikkelsen, 2011). This implementation means not only maximized economical profitability of crop production, but also significant reduction in its negative environmental impact.

Agricultural terrestrial greenhouse gases (GHG) emissions are a major contributor to climate warming. Thus, the assessment and quantification of the magnitude of GHG emissions has become an imperative for predicting climate change. Quantification of GHG emissions from soils in the atmospheric ozone is essential for mitigation measures. In soil, transformations of mineral N via denitrification-reduction events are the main process leading to N₂O emissions from agriculture soils. Exceeding concentrations of N₂O and CH₄ in the atmosphere cause hazards to the stratospheric ozone, especially when considering the reaction products of atmospheric nitrous oxide (N₂O), nitric oxide and nitrogen dioxide. On the other hand, the CH₄ is mainly produced by the reduction process, which digests carbon mainly from organic matter, and the methane gas is the byproduct of the digestion by microbial activities. Different weights of the potential harmful gases were suggested by the IPCC (2006) for N₂O, CH₄, and CO₂ were 298, 25, and 1 respectively. The value of the GHG is normally expressed as a carbon equivalent (e.g. Lal, 2004). While CO₂ is the most abundant gas, with the lowest weight-factor, it exhibits a natural balance in the agricultural land ecosystem. The magnitude of these effects has led to efforts to better quantify fluxes of greenhouse gases and to assess the mitigation potential of agricultural management options, as a guide for policy makers.

The understanding of different effects of water management in terms of irrigation scheduling is important to reducing the GHG emissions. Soil moisture content has a direct effect on the rate of reaction of soil processes which produce GHG. In practice, GHG emission can be affected by application of irrigation water in interaction with co-factors such as soil texture, crop type, and temporal changes in soil physical properties. Due to these complex relationships, the process and accuracy of estimating GHG emissions can be improved by assessing the variation in physical soil properties.

1.2 Statement of Rationale and Objectives of the Research

1.2.1 Statement of Rationale

A sustainable agriculture requires an understanding of spatial and temporal variations within agricultural fields when estimating GHG production. Other than the biological controls of GHG emissions, the variations in soil physical properties are intermediate factors that contribute to different levels of GHG emissions (Figure 1).

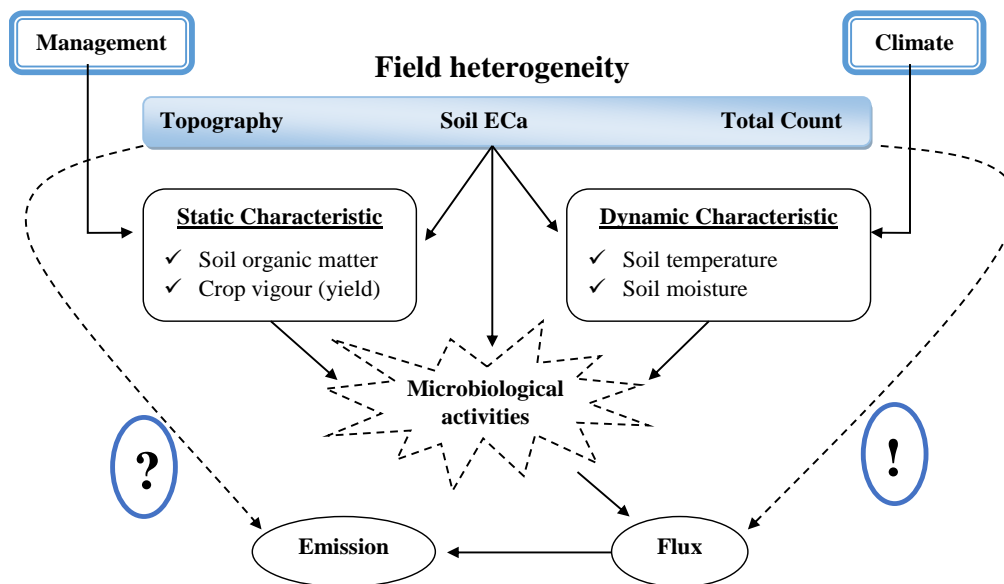


Figure 1: The overall scope of the study of the relationship between the field heterogeneity and GHG flux or emission.

Although measuring apparent soil electrical conductivity (EC_a) is a fast and popular approach to understanding field variability, little attention has been given to quantification methods and data accuracy. Thus, the evaluation of the measurement stability by temporal and operational tests. The measurement of soil EC_a as a co-factor in soil physico-chemical heterogeneity contributes

to the GHG provides fast and reliable measurements and highly dense data. Yet, the study of the relationship between GHG gases and soil EC_a has not yet been established.

Real-time remote monitoring of soil physical properties may enhance the ability to mitigate GHG emissions, specifically with respect to controlling different levels of soil moisture via irrigation schedules and temperature levels due to different water usage. Due to the strong stability of the spatial pattern of the soil physical properties over the growing season, measured using PSS, it provides the details of the agriculture field heterogeneity that could result in varying the soil–gas diffusion production. Soil physical heterogeneity across the agriculture landscape and their associated characteristics provide important prediction parameters for mitigating GHG emissions at the ground level.

1.2.2 Objectives of the Research

The overall goal of this study was to employ PSS technologies to sense soil physical properties, i.e. soil EC_a, γ -ray, soil texture, soil moisture, and soil temperature, for environmental assessment in agricultural land.

The specific objectives of this study are summarized as follows:

- i) To evaluate the temporal and operational stability of soil EC_a using GCR and EMI methods, allowing for decision making of the soil EC_a spatial and temporal stability over time related to the soil properties during the typical mapping exercise (Chapter 3).
- ii) To estimate GHG fluxes using a median flux method of the linear response under different water, soil, and crop management strategies (Chapter 4).
- iii) To monitor GHG emissions spatially under different levels of organic matter decomposition in muck soil under different water management practices (Chapter 5).
- iv) To characterize spatial and temporal variation of GHG emissions in response to field heterogeneity by means of proximally sensed physical soil properties (Chapter 6).

CHAPTER 2

GENERAL REVIEW OF LITERATURE

2.1 Proximal Soil Sensing

Acquisition of the soil properties using PSS in agricultural fields provides an understanding and an evident of temporal and spatial complexity due to soil–plant interaction, or farm management. Characterization of the agricultural field's spatial variability is a fundamental component of a variety of field and landscape–scale concerns including the assessment of the soil quality, solute transport, management–induced changes, and mapping and inventory exercise of soil properties. Therefore, PSS technology has been used in geophysics exploration, and then adapted for agriculture purposes. Of these, the use of wireless sensor network (WSN) to monitor the temporal variability of soil physical properties initiated the assessment of the temporal effects from the different soil–water–plant exchanges during the growing season.

2.1.1 Method of Soil EC_a Measurement and its Uncertainty Issues

Apparent soil electrical conductivity is widely used as the most popular measurement parameter in modern agriculture. The soil EC_a is commonly measured using destructive and non-destructive methods; GCR or EMI, respectively. Both methods involve at least one element causing an electrical current in the soil and at least one element sensing resistance/conductance of the soil media. For GCR, typically a set of rolling discs is used both to transmit and to sense a change in the voltage potential at a fixed distance. The distance between one or more pairs of discs can be configured using Schlumberger, Wenner, Dipole-dipole and other array configurations (Parasnis, 1997; Pan *et al.*, 2014). In contrast, using EMI instruments, alternating current in the transmitter coil generates a primary electromagnetic field causing an eddy current within the soil matrix. The eddy current, in turn, generates a secondary electromagnetic field within the receiving coil. The relationship between currents created from both the primary and the secondary electromagnetic fields allows for the detection of the conducting characteristics of the soil (Allred *et al.*, 2008).

The stability of soil EC_a measurements due to temporal and operational effect was not well reported. In general, soil EC_a measurement provides relatively stable spatial patterns. A few studies compared the different level of uncertainties (Sudduth *et al.*, 2001; Allred *et al.*, 2006; Abdu *et al.*, 2007, Saey *et al.*, 2009; Simpson *et al.*, 2009; Sudduth *et al.*, 2010, and Urdanoz *et al.*, 2012) under different soil EC_a instruments. However, these studies did not focus on the sensitivity of these instruments to temporal and operational noise.

The temporal noise can result from the different degrees of ambient and soil conditions during the mapping exercise (Robinson *et al.*, 2004). On one hand, rapid change of ambient temperature causes heat to build up in the instrument that is directly exposed to sunlight, thus, reducing the soil EC_a measurement (Sudduth *et al.*, 2001, 2010, and Robinson *et al.*, 2004). On the other, cold weather may significantly reduce measured soil EC_a due to a reduction in electrolyte mobility in the soil (Allred *et al.*, 2005). 1 mS/m offset due to the temporal drift on the DUALEM-21S sensor was reported by Taylor and Holladay (2013). Similarly the soil EC_a may impose temporal variations due to an annual change in the top soil layer (Brevik *et al.*, 2004; Farahani *et al.*, 2004).

Operational drift effect resembles the typical soil EC_a mapping exercise. The drift of the soil EC_a measurement could be affected by the internal, thermal drift of the instrument (Allred *et al.*, 2006). In addition, position sensor at certain height above ground (Doolittle *et al.*, 1994; Simpson *et al.*, 2009), distance between the transmitting and receiving coils (Roy 1972; Pan *et al.*, 2014) or as a result of the roll and pitch of the measuring instrument (Adamchuk *et al.*, 2011a). The effect from the crop cover also potentially increases the soil EC_a measurement due to the moisture content in the plant cells (Serrano *et al.*, 2014) or results in a lesser effect from crop residues (Brevik *et al.*, 2003). Variations in different operational factors govern different signal propagation, especially when it differs from the normal position during soil EC_a surveys. Thus, the elusivity of the soil EC_a and the appropriate measurement relationship to other soil properties remains ambiguous.

2.2 GHG Emission Estimation

Two of the most common methods in GHG measurement at the terrestrial level use the closed chamber and the micrometeorological tower. The former method is the main focus of this study. The closed chamber (i.e. non–steady state chamber design) results in a lower foot print, and relatively low cost as compared to the micrometeorological tower. In addition, the chamber method allows for replication of the field treatment, thus, providing higher spatial resolution with repeated treatments (Fowler, 1999).

The flux is normally calculated using the slope or the gradient of the gas concentration over time. The gradient of the GHG flux and emissions can be estimated using linear and non–linear models (Hutchinson and Mosier, 1981). Because the linear response is more versatile, it has become the most popular and commonly used to estimate the flux as well as the emissions in GHG studies. However, less attention has been given to outlier data in flux and emission estimations. Visual individual inspection for each dataset is impractical for large datasets for the purpose of flux calculation. On the other hand, the non–linear model was imposed in the flux calculation mostly due to oscillations in the measurement or downward response of the gas concentration.

Outlier data is the data that behaves abnormally from the rest of the dataset, and does not always represent invalid measurements. The factors contributing to the outlier data may be due to extreme physical air-soil exchanging phenomena events, leakage during gas measurement, sampling error, surface disturbance, and deployment time interval (Venterea *et al.* 2009). Ignoring the appearance of the outlier data during data analysis could result in potential bias especially for the statistical analysis.

2.3 Temporal GHG emission

Sustainable agriculture promotes a good balance between anthropogenic activities and environmental effects, yet optimizes the profits from the crop production for human benefits. Technological advancement helps in increasing food per capita, despite the decline in land to people ratio. This situation strained the agriculture sector's ability to maximize the production per unit of land. Maximizing production and profit may lead to high input usage such as nitrogen based fertilizer, thus, will leading to high greenhouse gas (GHG) emissions.

Agriculture land and ecosystems hold large carbon reserves, thus, the potential for the carbon mitigation and credit (IPCC, 2006). However, the carbon and other gas exchange rate (emit and sink) under specific climate, soil, crop and ecosystems could trigger spatial and temporal variations. Moreover, the mitigation potential was often misestimated when the data was obtained from only a few locations which do not represent field spatial heterogeneity. Introduction of new government incentives and policies for certifying agriculture sustainability and ecosystem services will be crucial if the approach is to meet the demands of improving yields without compromising environmental integrity as well as maintaining public health.

The GHG emission from the agriculture soil is subjected to be mitigated. The main GHG from agriculture soils were nitrous oxide (N_2O), methane (CH_4) and carbon dioxide (CO_2), often reported as CO_2 -equivalent. Significant factors of climate change affiliated with GHG emissions have resulted in local and international efforts in mitigation approaches (Shcherbak *et al.*, 2014; Villarino *et al.*, 2014). Canada is also subject to be caped of the GHG emissions due to about 80 % direct and 20 % indirect GHG sources (United Nations Framework Convention on Climate Change). The trend of the GHG emission from agriculture soil showed exponential increase. Total emissions of 8 % was relatively stable for five years in a row (2005 to 2011) counted for 68 Mt CO_2 -equivalent, however, it is projected to increase with 2 Mt CO_2 -equivalent for 2005-2020 (Environment and Climate Change Canada, 2013). However, despite large seasonal exchanges of CO_2 between the surrounding atmosphere and agriculture lands, the net flux is estimated to be balanced (IPCC 2006).

As it was mentioned, there are two methods in monitoring the GHG from soil, either by destructive (non-steady state chamber (NSS) design or non-destructive eddy covariance method). In this study, NSS method will be focus of the gas sampling technique. Various designs of the NSS used to monitored the GHG fluxes either square, rectangular or cylinder chamber shape, with relatively light weight, and follow the standard design (Livingston *et al.*, 2005;

Pedersen *et al.*, 2010; Rochette, 2011). The NSS method offers simplicity in the treatment design, cost effectiveness, provides low foot print as compared to the eddy covariance, yet high resolution over multi chamber replications. The inference of the overall GHG emissions measured from the small scale area often were made by up-scaling of the GHG measurements over long term scenarios and the large area (Li *et al.*, 2010). Monitoring the GHG emissions at the soil surface is not necessarily a measure of real time net soil GHG production because these GHG transport from source site vary in time and space, in response to the changing soil environment. Different locations for the chamber placement can affect the rate of these processes by influencing soil temperature, soil water content, soil disturbance, barometric pressure fluctuations and root activity. Consequently, changes in soil properties during NSS chamber deployment and measurement may bias flux estimates by altering gas production and transport processes. Therefore, one of the keys to minimizing the effect of soil variation is by considering the soil spatial variation prior the chamber placement. Thus, up-scaling from a small area of interest may underestimate the actual rate GHG responses.

Reported broad spectrum of GHG source from agricultural soils can be divided into several sub sectors such as crop production fields, monoculture (Wagner-Riddler *et al.*, 2007), and perennial crops (Reijnders and Huijbregts, 2008), natural or cultivated forested soils (Sathaye *et al.*, 1995; Smyth *et al.* 2014), pasture for livestock (Rochette *et al.* 2014; McGinn *et al.*, 2014), and organic farming (Wood *et al.*, 2006). In agricultural soil, which is the focus of this study, other than microbial activities, surface soil GHG emissions seems to be co-influenced by soil characteristics related to (i) farm management activities-different types of farms e.g. organic versus conventional agriculture (Rehman, 2014), crop type, fertilization in different forms of N i.e. organic or non-organic (Eichner, 1990; Hénault *et al.*, 1998; Snyder *et al.*, 2009), irrigation effects (Lal, 2004), tillage practices (West and Marland, 2002), and combination of multiple factors e.g. fertilizer, tillage and crop (Kern and Johnson, 1993; Halvorson *et al.*, 2008), (ii) available macronutrient content such as organic matter (OM), nitrogen (N), and carbon (C) cycle (Eswaran *et al.*, 1993; Skinner, *et al.* 2014; Sommer and Bossio, 2014), (iii) environmental conditions such as elevation, weather (precipitation, ambient temperature, humidity, and pressure), hence, leading to volatilization (Weiske *et al.*, 2006) and leaching (Nikièma *et al.*, 2012), and (iv) soil physical properties such as soil moisture and temperature (Peterjohn *et al.*, 1994; Mukherjee and Zimmerman, 2014), and water table (Buchanan and Triantafilis, 2009; Berglund and Berglund, 2011).

The costs of conventional agriculture soil-gas monitoring, however, are substantial and the reliability of the results are often limited and questionable. For instance, soil-gas monitoring activity conducted via a network of the sampling points such as grid or transect sampling (Ishizuka *et al.*, 2005 and Allaire *et al.*, 2012), where inferences of spatial distribution were made. This method does not enable a reliable estimation at the field scale. Thus, alternatively PSS technologies was used as a quantitative method to infer spatial patterns across spatial and temporal variability. Such PSS measurements were apparent soil electrical conductivity, and gamma ray spectroscopy. The efficacy using PSS in relation to the GHG emissions lies in understanding spatial and temporal soil property variations. Because there is a limitation of the sensors related to the spatial soil biological activities, the measurement or estimation of soil physical properties can be done via PSS technologies. Other than biological activities, the variation of soil physical properties changed the formation of soil aggregates, pore spaces, and water content, consequently, altering the rate of soil gas diffusion. Alternatively, understanding the soil mineralogy using gamma-ray methods may help in predicting GHG rates.

The use of PSS technology as a method of GHG mitigation from agriculture land is a relatively new approach. Soil EC_a measurements at different times may be used to predict different levels of GHG fluxes; however, local and detail interpretations are imperative. For instance, Allaire *et al.* (2012) used a multi depth soil EC_a profile investigation to co-relate with the CO₂, and found a negative correlation between CO₂ and soil EC_a. To date, there is no comprehensive study on the application of γ -ray spectra in actual GHG production. The closest was the measurement of available soil carbon through a predictive approach. In an early study by Macias and Barker (1978), they attempted to predict bulk available oxygen and nitrogen gas in a coal sample using a gamma ray spectrometer. Along with other interesting properties, the study indicated good correlation ($r > 0.95$). In contrast, recent findings on nitrogen gas by Chapyzhnikov *et al.* (2005) found no significant correlation with nitrogen gas. However, both studies achieved a good correlation of gamma ray spectra of the carbon content. This may lead to better prediction of the CH₄ or CO₂ emissions. The spatial variability of the soil carbon across the field can be predicted using Cesium (¹³⁷Cs) in the soil (Johnston *et al.*, 2004; Dierke and Werban, 2013). These data suggest that measurements of ¹³⁷Cs in soils can be useful for understanding carbon distribution patterns in surface soil. A few studies reported good correlation between γ -ray with texture clay content. Rodrigues *et al.* (2015) performed a combination of soil EC_a and gamma ray measurements in CEC and clay content. In addition, soil chemical properties also resulted in a very significant relationship, for instance, strong correlation with potassium (K) (Piikki *et al.*, 2013).

Bulk density and soil water content also was predicted using γ -ray measurements (Gurr, 1964). Good prediction with potassium (K) content and soil texture in the soil (Wong and Harper, 1999, Wong *et al*, 2010), however, may not hold in all areas due to landscape heterogeneity other than soil forming factors.

Connection Text to Chapter 3

Following the literature review the role of soil EC_a measurements in agricultural soil is to monitor the spatial and temporal heterogeneity that might affect environmental responses (i.e. GHG production). This was done by using PSS technology, specifically CGR and EMI techniques. Although soil EC_a measurements were well established and had become the most popular method in providing field heterogeneity information, different levels of uncertainties caused by different instrument's measurements were not fully reported. In conjunction with spatial and temporal responses, the relationship to other soil properties were discussed in the previous chapters.

This chapter is awaiting to be published as a journal paper. Chapter 3 is related to the first objective of this study as listed in Chapter 1 section 1.2.2. Chapter 3 discusses the principle of soil EC_a measurements using the GCR and EMI methods, and its sensitivity and uncertainties related to the environment and operation factors associated with measurement stability. Prior to illustrating the prospect of using proximally-sensed soil properties in relation to the temporal GHG variation, the quality of the soil EC_a measurement was evaluated in terms of temporal and operation–induced modalities.

The findings provide particularly vital information with respect to the mapping exercise as well as post processing of data. This includes the minimization of measurement temporal drift as well as preventing undesirable "noise" due to inconstant sensor operation.. Different parts of this study were presented at a conference and a manuscript has been submitted to the Journal of Applied Geophysics. The following citations are available at this time:

Ahmad Suhaizi M.S. and V.I Adamchuk. 2016. Temporal and operation-induced variability of apparent soil electrical conductivity measurements. Journal of Applied Geophysics. (In review).

Ahmad Suhaizi M.S. and V.I Adamchuk. 2014. Evaluation of the temporal and operational stability of apparent soil electrical conductivity measurements. In: proceedings of 12th International Conference on Precision Agriculture, July 20-23, 2014, Sacramento, California, USA. Available online at <https://www.ispag.org/presentation/3/1465/>

CHAPTER 3

TEMPORAL AND OPERATIONAL–INDUCED APPARENT SOIL ELECTRICAL CONDUCTIVITY STABILITY

Ahmad Suhaizi M.S. and V.I. Adamchuk

Abstract

Measuring apparent soil electrical conductivity (EC_a), using galvanic contact resistivity (GCR) and electromagnetic induction (EMI) techniques, is frequently conducted to reveal spatial soil heterogeneity. Various studies have demonstrated the possibilities for significant changes in the measured quantities over time with relatively stable spatial structure representations. The objective of this study was to quantify the effects of temporal drift and operational noise for three popular EC_a mapping instruments. The sensors were placed in stationary positions approximately 8 m apart in an area with relatively low EC_a . Temporal drift was assessed using a series of 4.5-h data logs recorded under different weather conditions (from extremely hot to near freezing temperatures). The two EMI instruments were also used to quantify the effect of minor changes in the height, pitch and roll of the sensor with respect to the ground. These operational noise tests were replicated over several days. GCR measurements of EC_a , along with perpendicular coplanar EMI measurements, have shown relatively strong stability over time. Temporal effects introduced measurement uncertainties due to the changes in temperature and soil water content.

Keywords: apparent soil electrical conductivity; electromagnetic inductance; galvanic contact resistivity; temporal; operational; proximal soil sensing

3.1 Introduction

Site-specific crop management has been implemented to increase profitability and reduce the negative environmental impact of modern farming. The application of proximal soil sensing facilitates the understanding of spatial variability of crop growing conditions. Thus, maps of soil EC_a reveal soil heterogeneity related to various physical characteristics affecting the ability of the soil profile to conduct an electrical charge. Soil EC_a has been related to salinity (De Jong *et al.*, 1979; Williams and Hoey, 1987; Lesch *et al.*, 1995; Amidu and Dunbar, 2008), texture (Slavich *et al.*, 1993; Corwin *et al.*, 2003; Tetegan *et al.*, 2012), soil water content (Kachanoski *et al.*, 1988;

Sheets and Hendricks, 1995; Michot *et al.*, 2003; Corwin and Lesch, 2005; Brevik *et al.*, 2006; Brillante *et al.*, 2014) and cation exchange capacity (Paillet *et al.*, 2010).

The most popular methods for measuring soil EC_a on-the-go are based on GCR and EMI techniques. Both involve at least one element causing an electrical current in soil and at least one element sensing resistance/conductance of soil media. For GCR, a set of contact electrodes (typically rolling discs) is used to both introduce the electrical current and to sense a change in the potential at a fixed distance. These electrodes have been configured using Schlumberger, Wenner, Dipole-dipole, and other array configurations (Parasnis 1997; Pan *et al.*, 2014). Alternatively, EMI offers a non-invasive method. An alternating current in the transmitter coil generates a primary electromagnetic field causing an eddy current within the soil matrix. The eddy current, in turn, generates a secondary electromagnetic field within the receiving coil. The relationship between currents created from both the primary and the secondary electromagnetic fields allows for the detection of the conducting characteristics of the soil.

Previous studies have reported on different levels of soil EC_a observed using the same instrumentation (Sudduth *et al.*, 2001; Allred *et al.*, 2006; Abdu *et al.*, 2007; Saey *et al.*, 2009;; Simpson *et al.*, 2009; Sudduth *et al.*, 2010; Urdanoz and Aragüés 2012). Although a few studies reported relatively stable spatial patterns, these research activities did not focus on the sensitivity of these instruments to temporal and operational noise. Differences in ambient and soil conditions (Robinson *et al.*, 2004) may cause the signal to change over time (drift). For example, heat builds up in an instrument that is directly exposed to sunlight and this reduces the measured soil EC_a (Sudduth *et al.*, 2001; Robinson *et al.*, 2004; Sudduth *et al.*, 2010). In contrast, cold weather may significantly reduce measured soil EC_a due to a reduction in electrolyte mobility in the soil (Allred *et al.*, 2005). Taylor and Holladay (2013) found 1 mS/m offset due to the temporal drift on the DUALEM-21S sensor. Likewise, soil EC_a may vary annually due to the temporal dynamics of the top soil layer (Brevik *et al.*, 2004; Farahani *et al.*, 2004). Thus, the elusivity of the soil EC_a relationship to other soil properties remains ambiguous.

Operational drift marks the effect of the typical soil EC_a mapping exercise. The drift of soil EC_a measurements could be affected by the internal, thermal drift of the instrument (Allred *et al.*, 2006). In addition, EC_a measurements were shown to be altered due to small changes in instrument height above the ground (Simpson *et al.*, 2009; Doolittle *et al.*, 1994), distance between the transmitting and receiving coils (Roy 1972; Pan *et al.*, 2014), or as a result of the roll and pitch of the measuring instrument (Adamchuk *et al.*, 2011a). The vegetative cover on the

ground could potentially increase the soil EC_a due to the moisture content in the plant cells (Serrano *et al.*, 2014), and minor effects from annual crop residues (Brevik *et al.*, 2003). In general, different operational factors govern the signal propagation and when it differs from the normal position during soil EC_a surveys, EC_a measurements will vary.

Since service providers have to consider a combination of factors causing temporal and operational noise when mapping agricultural fields, the objective of this study was to quantify the deviation of stationary EC_a measurements produced using different instruments over time (both, short-term and long-term), and due to different operational uncertainties (height, roll and pitch)..

3.2 Materials and Methods

3.2.1 Instruments

Three different instruments were used to simultaneously measure soil EC_a [mS/m] within the same area. These included a GCR sensor Veris Quad EC 1000 (Veris Technologies, Inc., Salina, Kansas, USA) shown in Figure 2 and two EMI instruments: DUALEM-21S (Dualem, Inc., Milton, Ontario, Canada) and EM-38 (Geonics Limited, Mississauga, Ontario, Canada) shown in Figure 3. Table 1 summarizes the main parameters of these instruments.

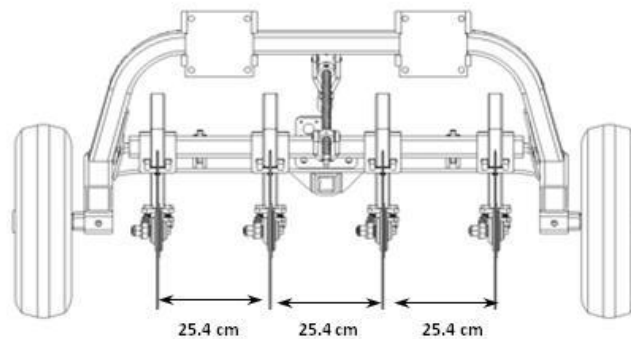


Figure 2: GCR sensor Veris Quad EC 1000 (Veris Technologies, 2014).

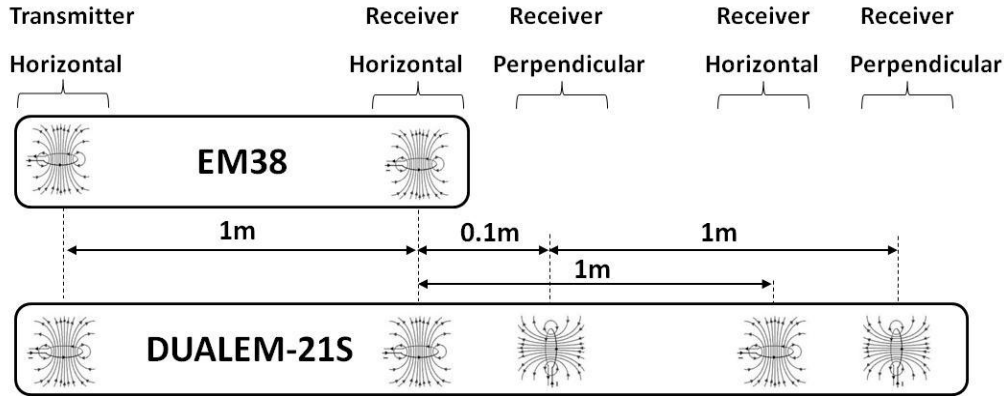


Figure 3: EMI sensors: EM-38 and DUALEM-21S, modified from Simpson *et al.* (2009).

Table 1: Instrument specifications

Specification	Veris Quad EC 1000	EM-38	DUALEM-21S
Method	GCR	EMI	EMI
Dimensions, m	1.43 x 1.50 x 0.69	1.06 x 0.15 x 0.13	2.41 x 0.09 x 0.09
Mass, kg	136	3	5
Power supply	12 V DC external	9 V DC internal	12 V DC external
Number of depths	1	2	4
Operating frequency	20 Hz	14.6 kHz	9 kHz
Data output rate	1 Hz	14 Hz	5 Hz
Year of manufacture	2012	2004	2012

The Veris EC used in this study consisted of four rolling coulters and provided output related to shallow (0-30 cm) soil EC_a (Veris Technologies, 2014). The DUALEM-21S consisted of a 2.41 m long tube and had one transmitter coil and four receiving coils. Two of these four coils form a horizontal coplanar (HCP) array at 1 m ($DUALEM_{HCP-1}$) and 2 m ($DUALEM_{HCP-2}$) distances whereas the other two form a perpendicular coplanar (PRP) array at 1.1 m ($DUALEM_{PRP-1.1}$) and 2.1 m ($DUALEM_{PRP-2.1}$) distances. The effective sensing depths for all configurations can be found in Table 2. Finally, the EM-38 had only one pair of coplanar coils 1 m apart. The unit can be positioned in a horizontal dipole or a vertical dipole mode producing EC_a measurements related to 0.75 and 1.55 m deep soil profiles, respectively. This unit was calibrated before each use according to the manufacturer's recommendations. Since the vertical dipole is the same as HCP, $EM-38_{HCP-1}$ and $DUALEM_{HCP-1}$ measurements are comparable (Saey *et al.*, 2009), the EM-38 instrument was tested only in the vertical dipole configuration. All instruments went through the warming up period for about 5 minutes before each test event.

Table 2: List of recorded measurements

Recorded measurement	Instrument	Array configuration	Distance, m	Effective sensing depth (75% response), m
Veris EC	Veris Quad EC 1000	Wenner	0.254	0.30
EM-38 _{HCP-1}	EM-38	Vertical dipole	1	1.55
DUALEM _{HCP-1}	DUALEM-21S	Horizontal coplanar	1	1.55
DUALEM _{PRP-1.1}	DUALEM-21S	Perpendicular coplanar	1.1	0.54
DUALEM _{HCP-2}	DUALEM-21S	Horizontal coplanar	2	3.18
DUALEM _{PRP-2.1}	DUALEM-21S	Perpendicular coplanar	2.1	1.03

A LabView (National Instruments, Cor., Austin, Texas, USA) application has been developed to automatically log data from the three sensors at individual data rates. A Watch Dog 2700 weather station (Spectrum Technologies, Inc., Aurora, Illinois, USA) was used to record ambient conditions that might affect instrument performances. Monitored parameters were logged with a 5-min interval and included: air temperature and humidity, wind speed and direction, and rainfall. The same station was used to monitor soil temperature and water content 30 cm below the surface using an installed SMEC 300 (Spectrum Technologies, Inc., Aurora, Illinois, USA) stationary probe.

3.2.2 Experimental Procedure

The instruments were placed in stationary positions approximately 8 m apart and about 6 m from the data logging station, as shown in Figure 4. The test area at Macdonald Farm of McGill University, Quebec, Canada, was a regularly cut lawn approximately 2 m from the edge of a corn field. The soil type at the test location was identified as Chicot series, sandy loam with moderate water holding capacity, and moderate to poor drainage (Paul 1960) and had generally low EC_a.

A series of five 4.5-h data recordings were conducted from August to October 2013. Each time, the instruments were placed in the same marked locations. The GCR coulter disks were pushed down gently (about 5 – 10 cm deep) to ensure good contact with the soil. At the same time, the EMI instruments were placed on the flat ground with the roll and pitch of the instruments as close to 0° (normal position) as possible. Another set of 5-min data recordings was conducted over several days from September to November with artificially introduced operational noise. Evaluated factors included: a) 10 cm height above the ground simulating an inconsistent distance between the instrument and soil surface, b) +10° and -10° pitch simulating potential raising of one

end of the instrument, and c) $+10^\circ$ and -10° roll simulating deviation of the instrument from its vertical orientation (Figure 5). Table 3 summarizes all data acquisition events that allowed five replicates of temporal and three replicates of operational tests for every instrument.

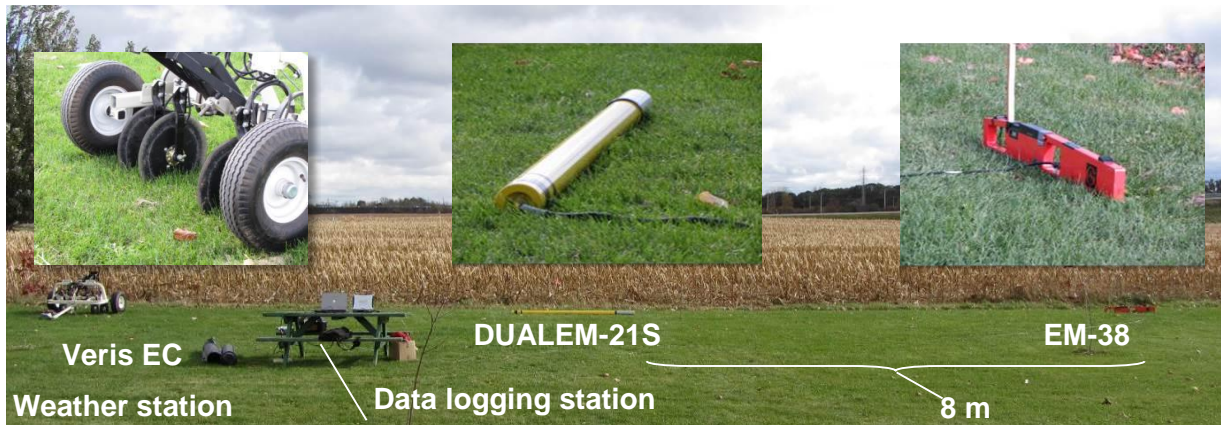


Figure 4: Experimental setup (24-Oct-2013).

3.2.3 Data analysis

Data analysis was based on a comparison of 1-s average data obtained at the highest possible rate without any filtering. While the temporal tests quantify the potential data drift from the beginning to the end of a single mapping exercise, the operational tests reveal the influence of typical uncertainties of the position of the instrument with respect to the ground. In addition, the test replicates show the influence of ambient conditions along with the possible uncertainties of sensor repositioning and other feasible inconsistencies between test replicates.

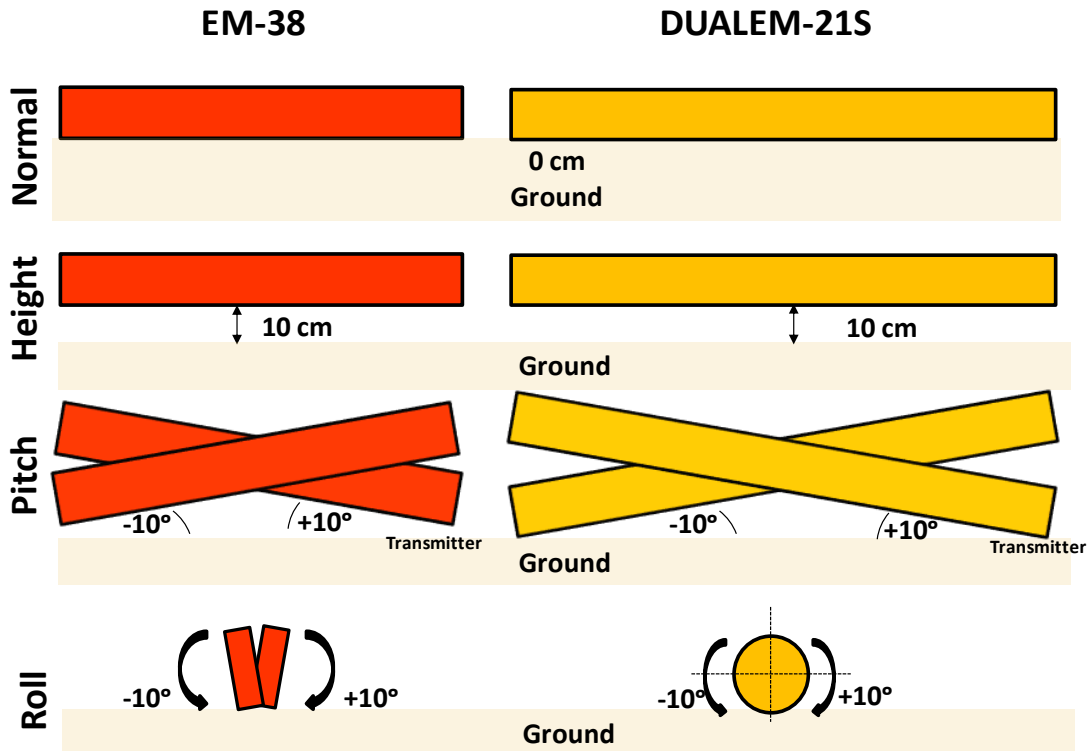


Figure 5: Operational tests for EMI instruments.

Table 3: Experimental timeline

Instrument and operation	Replicates				
	1	2	3	4	5
Temporal test (normal operation)					
Veris EC	12-Aug-2013	13-Aug-2013	18-Sep-2013	09-Oct-2013	24-Oct-2013
EM-38	13-Aug-2013	18-Sep-2013	09-Oct-2013	24-Oct-2013	29-Oct-2013
DUALEM-21S	13-Aug-2013	18-Sep-2013	09-Oct-2013	24-Oct-2013	29-Oct-2013
Operational test					
EM-38	Normal	16-Sep-2013	17-Sep-2013	23-Oct-2013	
	10 cm height	16-Sep-2013	17-Sep-2013	23-Oct-2013	
	+ 10° roll	16-Sep-2013	17-Sep-2013	23-Oct-2013	
	Normal	16-Sep-2013	10-Oct-2013	23-Oct-2013	
	- 10° roll	16-Sep-2013	17-Sep-2013	23-Oct-2013	
	+ 10° pitch	16-Sep-2013	10-Oct-2013	23-Oct-2013	
DUALEM-21S	Normal	10-Oct-2013	23-Oct-2013	23-Oct-2013	
	- 10° pitch	16-Sep-2013	17-Sep-2013	23-Oct-2013	
	Normal	17-Sep-2013	22-Oct-2013	23-Oct-2013	
	10 cm height	17-Sep-2013	10-Oct-2013	23-Oct-2013	
	+ 10° roll	17-Sep-2013	22-Oct-2013	10-Oct-2013	
	Normal	17-Sep-2013	22-Oct-2013	23-Oct-2013	
	- 10° roll	17-Sep-2013	22-Oct-2013	10-Oct-2013	
	+ 10° pitch	17-Sep-2013	10-Oct-2013	23-Oct-2013	
	Normal	23-Oct-2013	23-Oct-2013	23-Oct-2013	
	- 10° pitch	17-Sep-2013	10-Oct-2013	23-Oct-2013	

For both temporal and operational tests, descriptive statistics, such as mean and standard deviation (STD) of each test replicate, were calculated using Microsoft Excel. Root mean square errors (RMSE) for the temporal tests were estimated using the following equation:

$$RMSE = \sqrt{\frac{1}{m(n-1)} \sum_{i=1}^m \sum_{j=1}^n (\overline{EC_{ai}} - EC_{aij})^2} \quad (1)$$

where n is the number of 1-s measurement averages within any specific data log; m is the number of different logging events.

The Levene's test of equal variances was conducted to compare mean square error (MSE) values corresponding to different instruments. However, due to a very large number of data records, high degrees of freedom made relatively similar variance estimates significantly different from each other. Therefore, a subjective grouping of similar RSME estimates was performed to facilitate the discussion. A simple linear regression was applied to the relationships between EC_a measurements and ambient conditions, including soil and air temperature, soil water content, air humidity, and internal temperature of the DUALEM-21S instrument. In terms of the operational test, a t-test was used to compare the means of three operational test replicates to the mean of nine replicates representing normal operation of the instrument (i.e., zero height, roll and pitch).

3.3 Results and Discussions

3.3.1 Temporal Test

Figure 6 demonstrates the range of air and soil temperatures, relative humidity, soil water content, and recorded internal instrument temperature of DUALEM-21S during each 4.5-h temporal test. These tests generally cover all reasonable operational conditions when soil EC_a data are normally collected. The weather data captured from the weather station showed ambient and soil temperatures varying from 23.3 °C to nearly freezing (– 0.1 °C) and 29.5 to 7.6 °C, respectively. The latter measurements slightly vary within the same measurement date; however, they change greatly from one test event to another. The internal temperature of the DUALEM-21S ranged from 40 to 6 °C across the test dates. The increase in soil moisture on 9-Oct-2013 was due to rainfall events during the two days prior to the test event (6 mm of total precipitation).

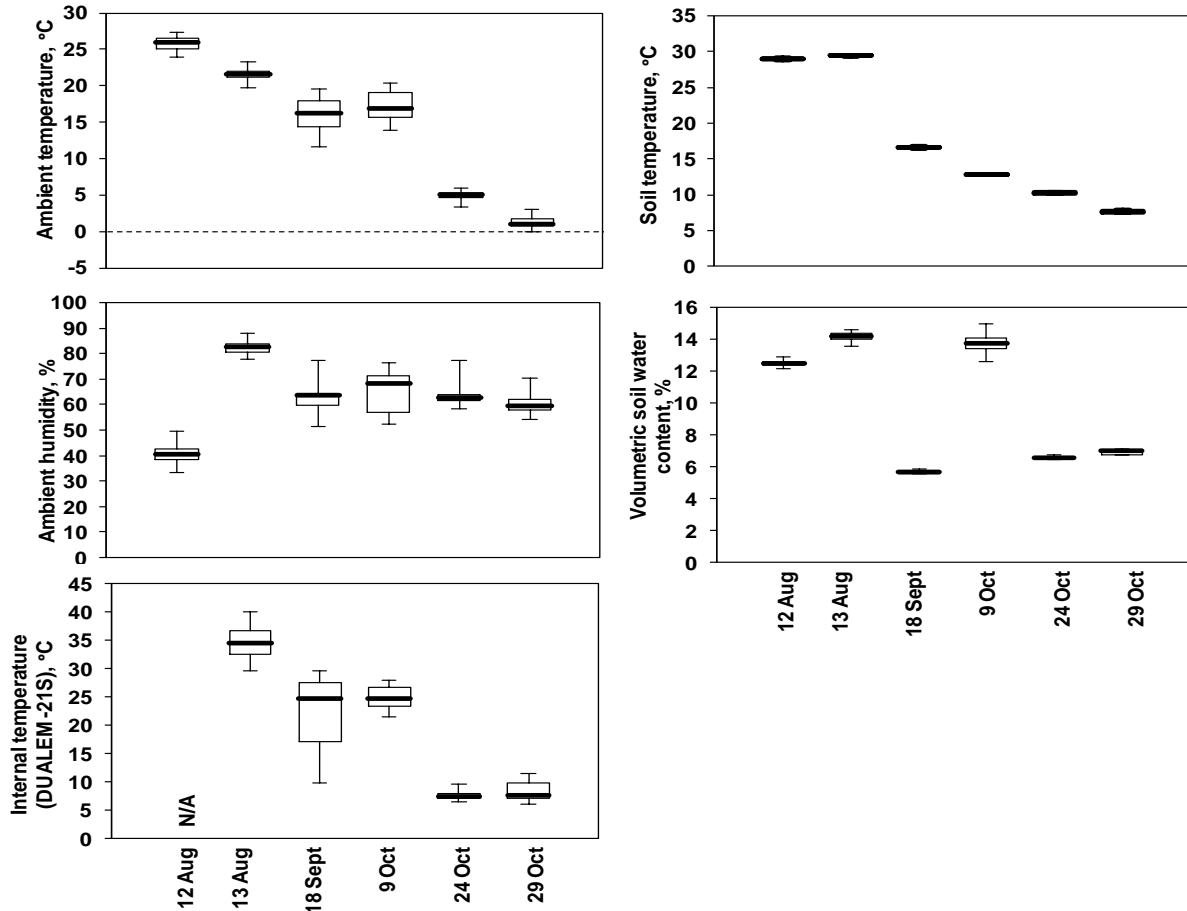


Figure 6: Box-and-whiskers plot of environmental conditions: ambient temperature, soil temperature, air humidity, volumetric soil water content, and the internal temperature of DUALEM-21S instrument during temporal tests.

Figure 7 illustrates data logs for four different measurements obtained during the 9-Oct-2013 test. The ranges (minimum and maximum) for unprocessed soil EC_a measurements for the entire temporal test are presented in Figure 8. Table 4 summarizes the average, STD, and RMSE (Equation 1) values. The most stable soil EC_a measurements were from the GCR instrument. Earlier, Serrano *et al.* (2014) observed a similar level of consistency of CGR measurements. Both DUALEM PRP measurements produced RMSE values 5-10 times smaller than those from EM-38 or DUALEM HCP measurements. In addition to the 4.5-h drift of EC_a measurements, there were noticeable changes from day to day. For an unknown reason, the most apparent reduction in EC_a measurements was noted on 18-Sep-2013 for both DUALEM HCP measurements, but not for PRP. That day, the initial internal and ambient temperatures were similar (10.4 and 11.6 °C), but a steady increase of the ambient temperature with relatively low wind speed (around 2 km/h)

may have resulted in rapid solar warming of the instrument. This typically reduces soil EC_a measurements. However, the certain reason for this sensor behaviour is unknown.

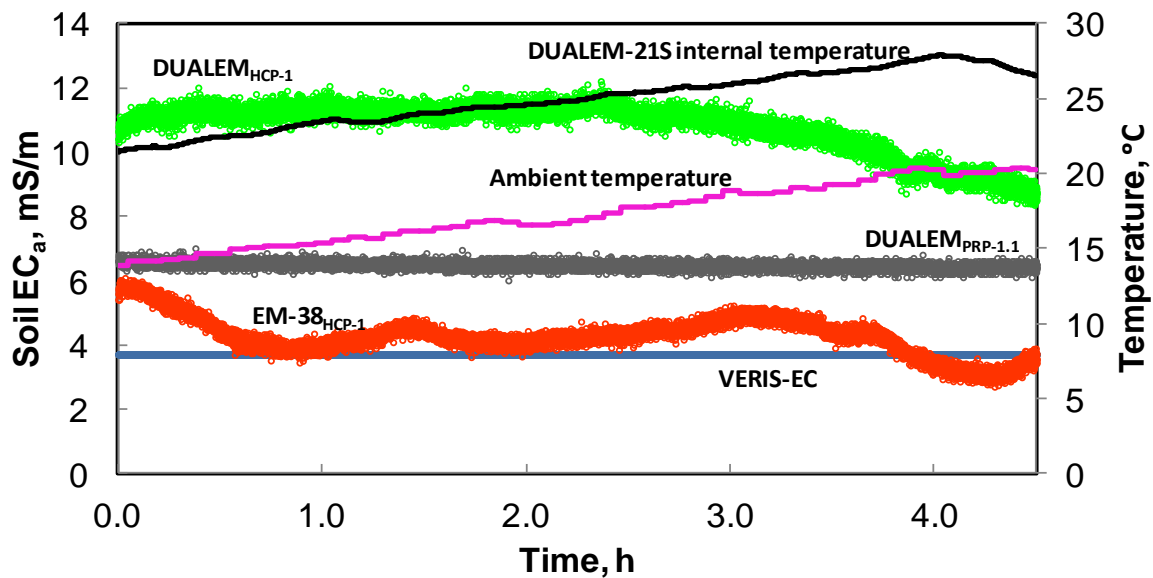


Figure 7: An example of 1-s average EC_a measurement logs obtained on 9-Oct-2013.

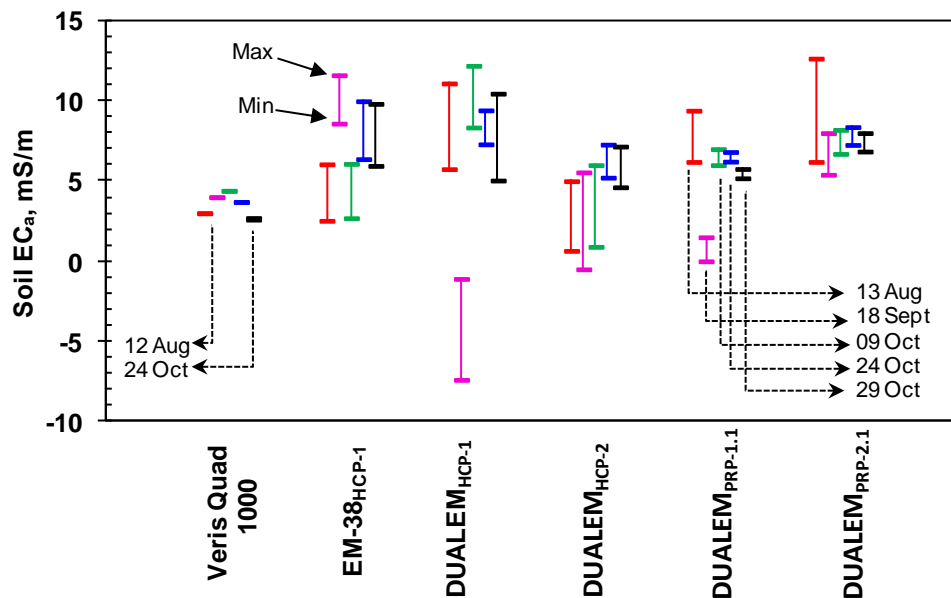


Figure 8: The range (minimum and maximum) of soil EC_a measurements during temporal tests.

Table 5 summarizes the correlation coefficients for a linear regression between ambient conditions and recorded measurements. Figure 9 demonstrates the relationships between air, soil and internal DUALEM instrument temperatures with several EC_a measurements. It is obvious that an anomaly, such as the 18-Sep-2013 drop in DUALEM HCP measurements, affected the

observed relationships. This anomaly cannot be explained by ambient conditions and may be affiliated with a number of unaccounted for factors, such as instrument positioning and conditions of surrounding vegetation. When disregarded, it appears that the EM-38 measurements are negatively correlated with ambient and internal temperatures. According to Allred *et al.* (2006), low soil water content and high temperature normally reduces soil EC_a. Sudduth *et al.* (2001) reported that the drift over 10 % of EC_a observed during field mapping using the EM-38 might be due to the change of internal temperature rather than ambient temperature variation. Corwin and Lesch (2005) recommend converting EC_a measurements at a specific temperature to measurements at a reference temperature (e.g., 25°C). Naturally, this would mean that temperature-compensated Veris EC and DUALEM-21S measurements would not be affected by ambient conditions to the extent of non-compensated EM-38 measurements. However, the presented data have not revealed temperature-induced changes in EM-38 measurements greater than other effects, such as instrument repositioning. The effects of soil temperature and water content are less quantifiable since they did not change significantly during individual tests.

Table 4: EC_a [mS/m] measurements for temporal tests.

Measurement	Replicate					Average EC _a (STD) between replicates, mS/m	RMSE, mS/m
	1	2	3	4	5		
Veris EC	3.00 (0.01)*	4.00 (<0.01)	4.00 (<0.01)	3.70 (<0.01)	2.70 (<0.01)	3.56 (0.70)	< 0.01a
EM-38HCP-1	4.28 (0.58)	9.12 (1.79)	4.28 (0.58)	8.64 (0.89)	8.53 (0.88)	6.97 (2.46)	1.08c
DUALEMHCP-1	8.34 (1.01)	-2.98 (1.60)	10.79 (0.78)	8.64 (0.27)	8.79 (0.83)	6.72 (5.51)	1.03c
DUALEMHCP-2	2.79 (0.74)	1.50 (1.57)	2.95 (0.87)	6.41 (0.38)	5.96 (0.41)	3.92 (2.15)	0.99c
DUALEMPRP- 1.1	7.49 (0.11)	0.68 (0.10)	6.48 (0.09)	6.56 (0.07)	5.47 (0.07)	5.34 (2.70)	0.10b
DUALEMPRP- 2.1	8.51 (0.22)	6.78 (0.17)	7.43 (0.15)	7.81 (0.13)	7.40 (0.13)	7.59 (0.64)	0.17b

* = Average and standard deviation (in parenthesis) of replicated tests. a = Temporarily most stable measurements. b = Temporarily relatively stable measurements. c = Temporarily relatively unstable measurements

Table 5: Pearson coefficients of correlation between EC_a measurements and measurement conditions.

Measurement	Temperature, °C			Air humidity, %	Soil water content, %
	Ambient	Soil	Internal DUALEM		
Veris EC	0.369	0.145	0.867*	0.064	0.029
EM-38 _{HCP-1}	- 0.663	- 0.525	- 0.724*	- 0.449	- 0.896*
DUALEM _{HCP-1}	- 0.173	- 0.132	- 0.052	0.102	0.552
DUALEM _{HCP-2}	- 0.823*	- 0.555	- 0.816*	- 0.152	- 0.309
DUALEM _{PRP-1.1}	- 0.009	0.157	0.082	0.368	0.638
DUALEM _{PRP-2.1}	0.527	0.561	0.332	0.616	0.588

* = Significant relationship ($\alpha = 0.05$)

3.3.2 Operational Test

Figure 10 provides the results of the operational tests for both EMI sensors. Each 5-min data log represented a particular test configuration that was repeated on three different occasions during at least two different days in random order. Since normal operation (zero height, pitch and roll) was part of each operational test, this configuration has been replicated nine times. Table 6 shows the individual soil EC_a test average, STD and t-test *p*-values. In this case, the average of three operational test replicate means were compared with the mean of nine normal operation means.

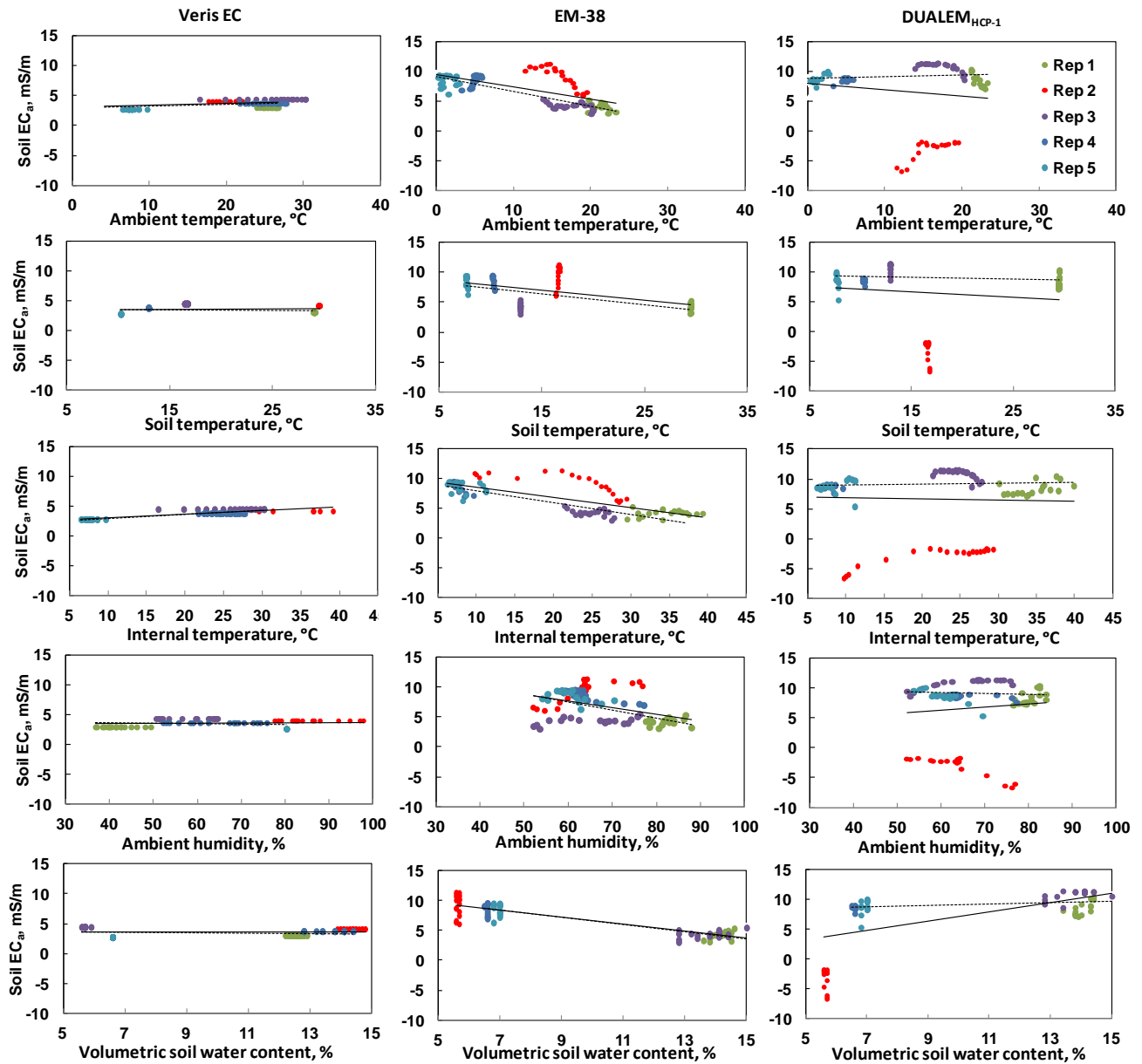


Figure 9: Examples of relationships between EC_a measurements (15-min sampling) and corresponding records of ambient conditions (dash lines show regressions with 18-Sep-2013 data excluded).

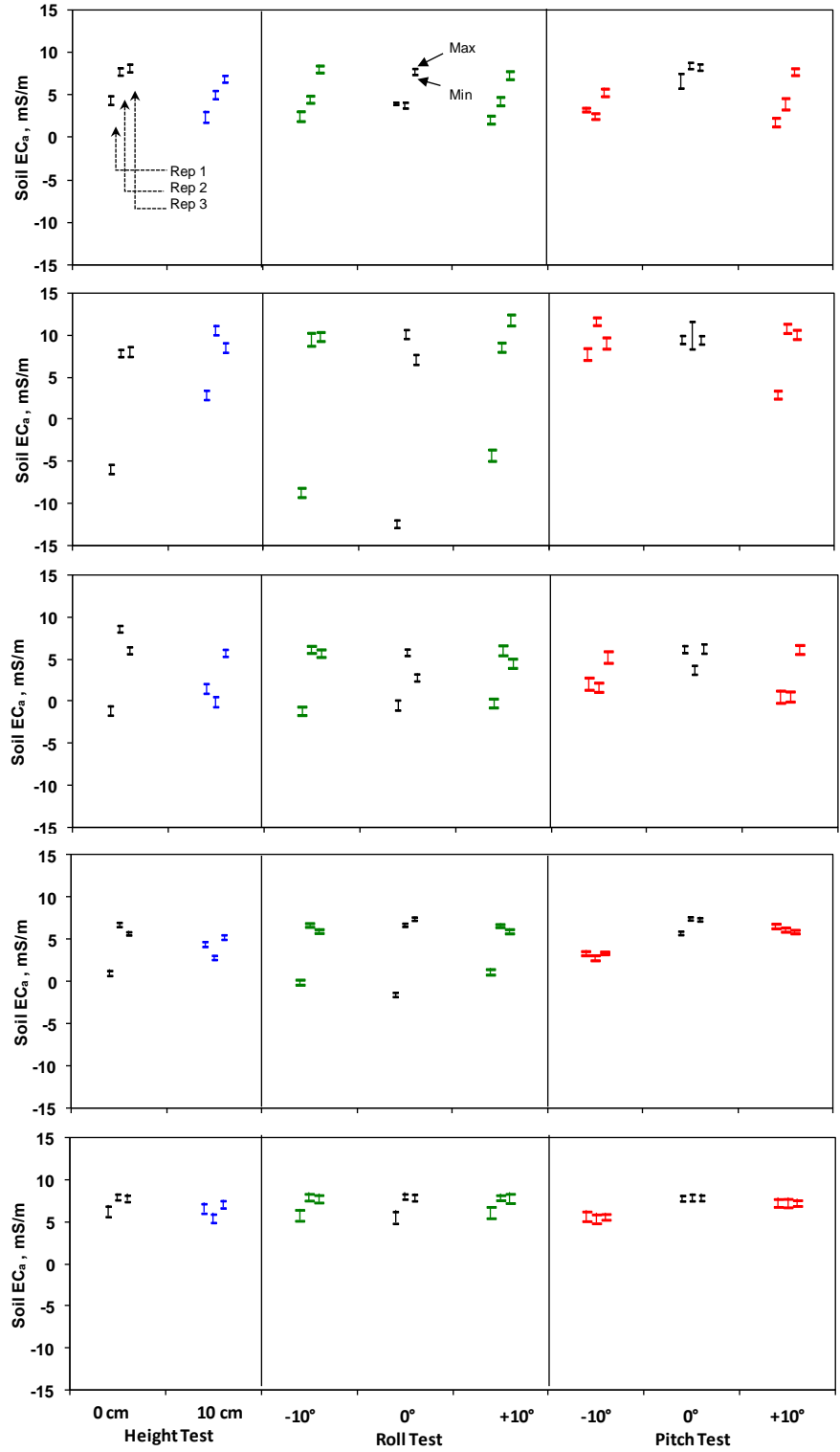


Figure 10: The range (minimum and maximum) of operational tests for each recorded measurement.

Table 6: EC_a (mS/m) measurements for operational tests.

Measurement	Height effect test				
	0 cm	10 cm	<i>p</i> -value		
EM-38 _{HCP-1}	6.59 (1.93)	4.67 (2.31)	0.13		
DUALEM _{HCP-1}	4.81 (8.2)	7.28 (4.02)	0.26		
DUALEM _{HCP-2}	4.16 (3.26)	2.36 (2.96)	0.21		
DUALEM _{PRP-1.1}	5.19 (3.25)	4.16 (1.24)	0.24		
DUALEM _{PRP-2.1}	7.51 (0.92)	6.40 (0.84)	0.06		
Roll effect test					
	0°	-10°	<i>p</i> -value	+10°	<i>p</i> -value
EM-38 _{HCP-1}	6.59 (1.93)	4.55 (2.63)	0.14	4.95 (2.8)	0.20
DUALEM _{HCP-1}	4.81 (8.2)	5.33 (8.51)	0.47	3.50 (10.64)	0.43
DUALEM _{HCP-2}	4.16 (3.26)	3.40 (3.27)	0.37	3.51 (4.11)	0.41
DUALEM _{PRP-1.1}	5.19 (3.25)	4.56 (3.03)	0.39	4.22 (3.68)	0.35
DUALEM _{PRP-2.1}	7.51 (0.92)	7.35 (0.92)	0.40	7.25 (1.1)	0.36
Pitch effect test					
	0°	-10°	<i>p</i> -value	+10°	<i>p</i> -value
EM-38 _{HCP-1}	6.59 (1.93)	4.51 (3.01)	0.16	3.52 (1.5)	0.02**
DUALEM _{HCP-1}	4.81 (8.2)	7.87 (4.39)	0.23	9.49 (2)	0.10
DUALEM _{HCP-2}	4.16 (3.26)	2.33 (3.24)	0.22	2.9 (1.99)	0.23
DUALEM _{PRP-1.1}	5.19 (3.25)	6.24 (0.37)	0.20	3.19 (0.32)	0.07
DUALEM _{PRP-2.1}	7.51 (0.92)	7.32 (0.02)	0.28	5.61 (0.15)	< 0.01**

* Average and standard deviation (in parenthesis) of replicated tests

** Significantly different at $\alpha = 0.05$

It appears that raising the instrument did not contribute to greater EC_a measurement change than the differences between replicates. In most cases, HCP measurements decrease when the instrument is raised in the air, but this may not be the case if high EC_a soil overlays less conductive subsoil for some sensor configurations. A marginal significance of the drop in average EC_a caused by the raised instrument was found for DUALEM_{PRP-2.1} was due to the relatively low EC_a difference between replicates rather than the magnitude of this change. In terms of the pitch and roll tests, it appears that the 10° deviations from the normal operation also did not have a significant effect on the measurements recorded. The exceptions were EM-38_{HCP-1} and DUALEM_{PRP-2.1} when the end of the instrument containing the transmitting coil was raised above ground.

From a practical standpoint, the results of this study indicate that GCR sensing of EC_a may be less sensitive to temporal effects than EMI measurements and may have an appeal in many

environments. However, the non-contact nature of EMI measurements provides versatility with respect to the measurement environment and, when designing the deployment platform (e.g., sled), these instruments should stay close to the ground with zero pitch and roll. It was determined to be very important to keep the transmitting coil close to the ground. Minor deviations from these conditions do not affect measurements to a greater degree than replications.

3.4 Conclusion

A set of stationary tests of one GCR and two EMI instruments revealed the degree of temporal and operation-induced variations on observed measurements of EC_a . While the GCR instrument was relatively immune to long-term data drifts, repositioning the EMI instruments on the soil surface at different times of the year (different soil conditions and ambient temperatures) provided more noticeable differences. Furthermore, EMI measurements were less stable during 4.5-h log periods than the CGR instrument. Also it was noted that the PRP configuration was more stable over time than the HCP operation. The same applies to the operational tests. The effects of the instrument height, roll and pitch were smaller than the differences from test event to test event, which could be attributed to a number of uncontrolled factors, including exact position of the instrument and different environmental parameters. However, practitioners should avoid, or minimize, raising the transmitting coil end of the instrument due to the reported sensitivity of EC_a measurements to this experimental treatment.

Connection Text to Chapter 4

Chapter 4 is a manuscript awaiting publication in 2016. The manuscript was authored by several researchers responsible for different parts of data collection and processing. All literature cited in this chapter is listed in the reference section.

Agricultural greenhouse gas is complex, dynamic, and governed by differing diffusion characteristics of soil–gas. Many factors contribute to this variation such as soil type, availability of water in the soil, and the crop itself. Despite GHG naturally varying across the agricultural field, the best estimation of GHG fluxes monitored using the non–steady state chamber design were one of the challenges that needed to be addressed. The approach of streamlining a large quantity of data is crucial to avoiding calculation errors. The MATLAB scripts developed in this work have been applied to several studies in flux and emission estimation.

This manuscript addresses the second objective as listed in Chapter 1, which deals with GHG flux and emission estimation by taking into account the spatial and temporal effect of in–season GHG production. This study is intended to aid the prediction GHG (3rd objective) using physical soil properties. However, GHG fluxes using the non–steady state chamber design may produce large variations in gas responses and lead to outliers in the dataset. Thus, the optimization method in flux calculation was established using the median flux value to estimate the GHG flux in agricultural fields. In depth interpretation of the results between respected treatments in each experimental site has been done by other collaborating researchers, and, therefore, has not been addressed in this thesis. Different parts of this study were presented at a series of conferences and a manuscript has been finalized to be submitted to the Canadian Soil Science Journal.

The following citations are available at this time:

Ahmad Suhaizi M.S. V.I. Adamchuk, C.A. Madramootoo, J.K. Whalen, F.J. Reumont, and H.Hui Huang. 2016. Unbiased flux calculation for greenhouse gas emissions estimation. Canadian Journal of Soil Science (to be submitted).

Mat Su, A. S., V. I. Adamchuk, C. A. Madramootoo, J. K. Whalen, H.H Huang. 2013. Estimating greenhouse gas emissions using experimental data. In: Scientific Program of CSSS/MSSS/CSAFM Joint Meeting, Winnipeg, Manitoba, 21-25 July 2013, 70. Winnipeg, Winnipeg, CSSS.

CHAPTER 4

STREAMLINED ANALYSIS OF AGRICULTURAL GREENHOUSE GASES FLUXES AND ANNUAL EMISSION

Ahmad Suhaizi Mat Su, Viacheslav I. Adamchuk, Chandra A. Madramootoo,
Joann K. Whalen, Florian J. Reumont, and Hsin-Hui Huang

Abstract

The objective of this work was to develop a robust and rapid method for calculating greenhouse gas (GHG) fluxes and annual emissions with consideration of the outlier dataset removal approach. The dataset contained the nitrous oxide (N_2O), methane (CH_4) and carbon dioxide (CO_2) concentrations for more than 30,000 headspace gas samples collected during 2012, 2013 and 2014 from 103 stationary non-steady state chambers, located at six agricultural sites across Eastern Canada. These sites were under different agricultural practices, (i.e., soil type, cropping system, and water management). MATLAB scripts were developed to: i) automatically filter data records based on threshold concentrations of N_2O , CH_4 and CO_2 , ii) estimate GHG fluxes from each chamber on each sampling date, and iii) estimate the annual emissions of GHG from each chamber during the growing season. The GHG fluxes were determined from the median slopes of gas concentrations measured at five sampling points (0, 15, 30, 45 and 60 min) during chamber deployment. Generally, CO_2 concentration increased, whereas CH_4 and N_2O concentrations were variable during the chamber deployment period. Streamlined approach resulted relatively fast data processing handling with about 10,000 data per year (total of >30,000 dataset) with maximum of 3 min of the processing time for all six sites per season using operating system of Window 7, 64-bit processor. The model proposed shows the lowest RMSE as compared to the standard average regression model. The results from this finding could be used as benchmark values for the Tier II of the IPCC database.

Key words: greenhouse gas, non-steady-state chamber, emission, bias data, uncertainty

4.1 Introduction

Mitigation of greenhouse gases (GHG) - particularly nitrous oxide (N_2O), methane (CH_4) and carbon dioxide (CO_2) - from agricultural soils is important in reducing the impacts of climate change (IPCC, 2006). Agricultural practices affect the spatial and temporal fluxes of these GHG, as well as the annual emissions of N_2O , CH_4 and CO_2 . Variations in gas production from soils can be evaluated with chamber and micrometeorological techniques, the chamber method being better suited to assess punctual, small-scale gas fluxes with a lower footprint than the micrometeorological approach. Typically, static non-steady-state chambers are selected to measure fluxes from 0.1-10 m^2 , which provides greater accuracy and higher spatial resolution with repeated treatments (Fowler 1999). Replicated chamber allow for investigations on soil-air gas exchanges in experimental field plots with various agricultural practices (i.e., irrigation, crop type and soil properties) or along pre-defined biogeochemical gradients.

In practice, the quantification of GHG fluxes is affected by temporal variability in the headspace gas concentrations of chambers, which can be described using linear and non-linear regressions. The potential flux of trace gases is often calculated by the slope (or gradient) technique, and was adapted for stationary chambers on soil by Hutchinson and Mosier (1981) and Hutchinson and Livingston (1993). In their approach, the gas concentrations (y-axis) in three consecutive headspace gas samples were plotted against time (x-axis) with linear regression to estimate gas flux from the chamber headspace. Although this simplified technique is straightforward, it lacks robustness because it fails to consider the uncertainty arising from outliers and small sample sizes. Moreover, sporadic flux readings are expected because gases can be produced (net source) and consumed (net sink) simultaneously from chambers due to biological processes (Chapuis-Lardy *et al.*, 2007). In such a case, the method of Hutchinson and Mosier (1981) is inaccurate.

The most common method of calculating fluxes was via a simple linear regression model wherein the gradient was calculated based on the average slope value (Venterea, 2010). A minimum number of samples per total duration of measurement had a small effect on the variation, thus often the approach in flux calculation is simply by taking an average. If the outlier data was ignored, the flux could deviate significantly from the flux estimate and lead to overestimation. This can be resulted from the direct linear regression equations that have to consider a line that fit all the points as to minimize the errors (e.g. John, 1995). The outlier data

may have resulted from accidental measurement errors or site-specific soil-gas exchange. High variation in the dataset could potentially lead to high discrepancies in flux estimates.

The median flux model (MFM) technique was used to discard outliers and the corresponding bias in flux estimation. The MFM technique provides several advantages: (i) calculated flux and estimated emission are not affected by extreme high or low variations from the set of measurements, (ii) the original data set, holding valuable information, is maintained (iii) it is independent of equal time intervals, sequence or sampling durations, (iv) concentration corrections such as in Hutchinson and Mosier (1981) are not required, and (v) unlimited number of sample observation, but with a minimum of three, as shown by Pedersen *et al.* (2010) and Parkin *et al.* (2012). However, neither of these studies considered outlier datasets. The outlier data can be analyzed using the median values, as example, explained by Blessing (1997), which will give a robust and resistance of the averaging weight of the slope for the flux calculation.

Discrete gas measurements may be a part of outlier data. In this case visual inspections would be required for quality control of both linear and non-linear regression flux estimation techniques. Such a qualitative examination of outlier data is impractical for large datasets. Standard approach to remove the outlier dataset is by analysing each individual data set for its standard deviation and mean values or using the quartile methods. However, these methods are not valid since the flux dataset is from temporal dataset and in the time series data format. While the outlier data may represent valid measurements, e.g. reflecting extreme physical air-soil exchange events, considering outliers in data analysis could result in a potential bias during statistical analysis (i.e., a distorted mean and variance). There are different potential mechanisms that could also impose bias, such as deployment time interval, surface disturbance during measurement, chamber design, and gas sampling procedures (Venterea *et al.* 2009). The method presented in this study have been through the standard procedure for the gas sampling and analysis in systematic manner, that suitable for the automatic and standardized flux calculation. Thus a model, or procedure, that performs effective, robust, efficient and unbiased flux estimations is necessary. Moreover, the study also anticipated only one value of the GHG emission i.e. annual carbon equivalent GHG for each individual site.

The objective of this study was to develop an automated MATLAB-based data processing method for N₂O, CH₄ and CO₂ concentrations in headspace gases of stationary chambers to: i) remove the bias imposed by outlier data, ii) calculate fluxes of GHG, and iii) estimate seasonal GHG emissions under various agriculture practices.

4.2 Materials and Methods

4.2.1 Study Site

Study sites were located in across Eastern Canada: Harrow (HR), Leamington (LE), St. Emmanuel (SE), Sherrington (SH), St. Louis de Blandford (SL), and Truro (TR), as shown in Figure 11. Each site represented a unique combination of agricultural practices (water management, soil types, and cropping systems), as summarized in Table 7. Water treatments included conventional drainage, subsurface irrigation, surface irrigation, sprinkler irrigation, and non-irrigated fields. Soil types consisted of muck (pure organic to mineralized organic soil), sandy, highly fine loamy sand and loamy clay soils. Cropping systems included grain crops, vegetables, cranberries and pasture. During the study period (2012, 2013 and 2014 growing seasons), a total of 103 static non-steady-state chambers were installed and geo-referenced using Garmin eTrex Legend handheld Global Positioning System (GPS) receiver (Garmin International, Inc., Olathe, KS, USA).

Each site received at least one water treatment repeated in the three year study, either under similar or different crop rotations with different soil texture (Table 7). However, no gas sampling was conducted in 2014 for the LE or SL sites. HR received 4 replicates of irrigation and 2 replicates of fertilizer treatment (CD_i and CD_m) which were either organic (solid manure) or inorganic and gas sampling involved 6 chambers per replicated water treatment (for a total of 24 chambers). At the LE site five chambers were deployed per water treatment of SSd at 15 cm depth. The SH site was treated with sprinkler irrigation or no irrigation (3 x replicates each) and four gas chambers were installed at each water treatment locations. The SH site was considered unique as it was under a muck soil with various decomposition levels as compared to the typical mineral agriculture soil at the other study sites. The water table for the subsurface irrigation site at the SE was maintained at about 1 m below ground surface. Without water or fertilization treatment, the naturally grown cranberry in the surrounding bog area (organic) acted as a control plot, which occurs only at SL site. Five chambers were replicated for each treatment for a total of 15 chambers. Four gas chambers were deployed for each of the water treatments and two for the control site at the TR site.

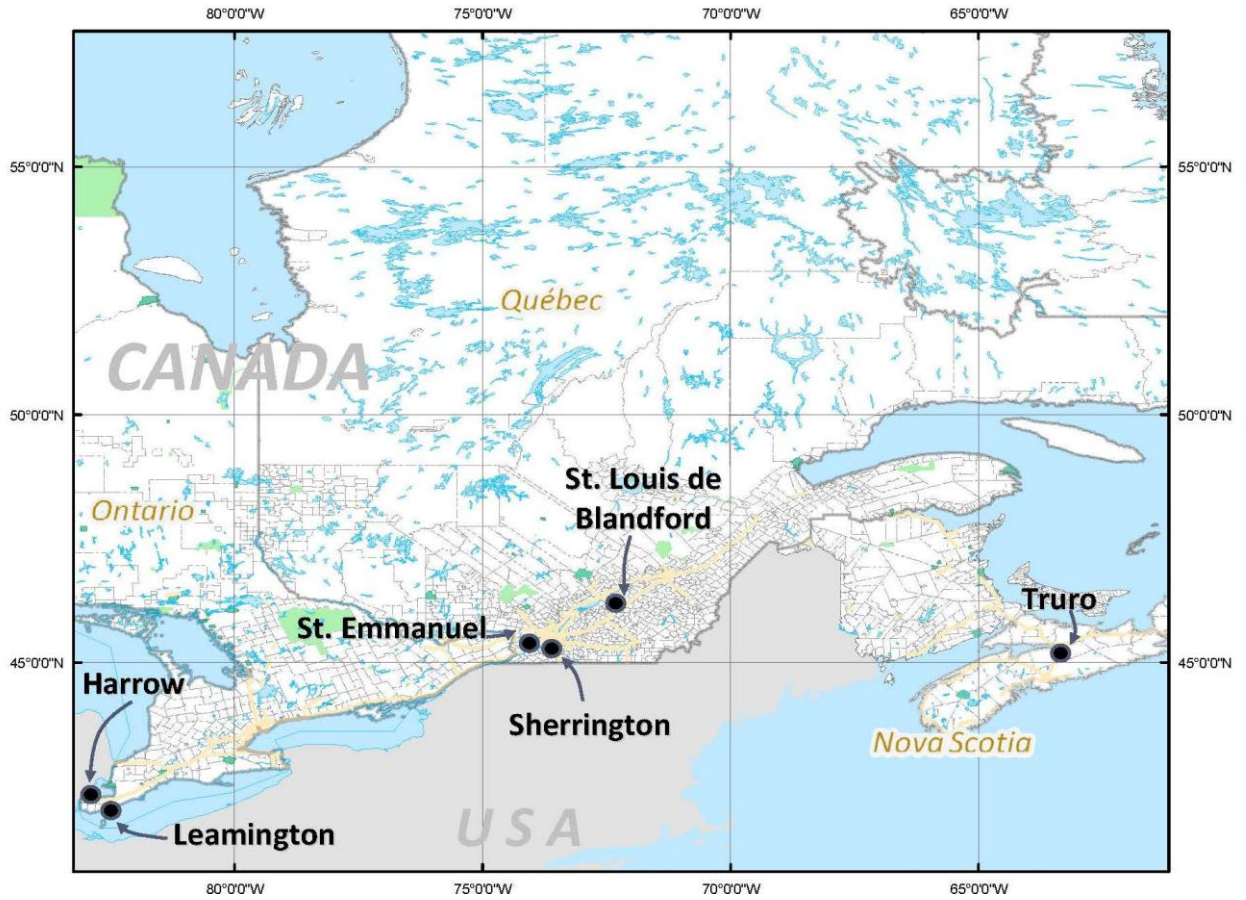


Figure 11: Study locations located across Ontario to the Eastern Canada

Table 7. Details of the sampling activities under different agriculture practices

Site	Start of Sampling	End of Sampling	Sampled Days	Treatment		
				Water	Soil	Crop
HR	7-June-2012	22-Oct-2012	20	2 x CD _i 2 x CD _m	Clay loam	Corn
	18-June-2013	1-Oct-2013	16			Soybean
	11-July-2014	14-Nov-2014	19			Corn
LE	10-May-2012	15-Oct-2012	20	1x SS _d 1 x S _d	Sandy loam	Tomato
	15-May-2013	20-Sep-2013	17			
SH	24-May-2012	29-Aug-2012	11	3 x SP 3 x NI	Muck (Organic)	Onion
	29-Apr-2013	17-Oct-2013	16			
	20-May-2014	3-Nov-2014	16			
SE	18-May-2012	7-Sep-2012	9	3 x CD 3 x SS	Fine loam	Yellow bean
	26-Apr-2013	7-Nov-2013	14			Corn
	15-May-2014	4-Nov-2014	21			Corn
SL	30-May-12	4-Nov-12	20	2 x SP 1 x B	Loamy sand, organic	Cranberry
	22-Apr-2013	24-Oct-2013	22			
TR	3-May-2012	7-Nov-2012	20	1 x NI, 2 x CD 2 x SS	Sandy loam, loamy sand	Pasture,
	8-May-2013	24-Oct-2013	11			bluegrass or mixed with red clover
	7-May-2014	1-Oct-2014	9			

HR = Harrow; LE = Leamington; SE = St. Emmanuel; SH = Sherrington; SL = St. Louis De Blandford; TR = Truro; CD_i = Conventional drain-inorganic fertilizer; CD_m = subsurface drain-manure fertilizer; SS_d = Subsurface drip; S_d = Surface drip; CD = Conventional drain; SS = Subsurface irrigation or control drainage; SP = Sprinkler; B = Bog area; NI = No irrigation

4.2.2 Gas Sampling

The gas chamber used in this study consisted of a chamber cover and base which was left installed and undisturbed in the soil throughout the sampling and growing period. The base was made of a flexi-glass frame with dimensions: 0.556 x 0.556 x 0.140 m, (W x L x H) and vented to avoid pressure perturbations. The chamber cover size was 0.564 x 0.564 x 0.130 m. The chamber base was installed at the beginning of the summer, and gently pushed down until about 4 cm remained above the soil surface. The effective height of the chamber base from the soil surface was frequently measured, adjusted at desired height (if needed) and manually noted to ensure a consistent height prior to starting the gas sampling procedure. All chamber bases were installed prior to, or a few days after, crop seeding to avoid interference of gas measurement from the top soil profile either due to the crops soil movement or root system. In some cases, the bases were removed and reinstalled at the same location due to farming activity (e.g. fertilizer or pesticide application). The chamber cover was protected with an aluminum cover to reflect heat and minimize the temperature effect during gas measurements (Rochette and Eriksen-Hamel,

2008). A soft cushion tape was placed on the contact surface of each chamber cover to seal the chamber system and eliminate gas leakage.

Gas samples were collected at least once per week throughout the growing season. At each sampling event, five gas samples (20 ml each) were taken with a syringe at 15 minute intervals (labeled t_0 , t_{15} , t_{30} , t_{45} , and t_{60}) over a total of one hour. These five gas concentrations allowed the flux to be calculated via simple linear regression. All samples were then injected into a 12 ml vacuumed exetainer (Labco, Wycombe, UK) fitted with an extra 60 ml (equal to 1/16th of an inch or 0.0625 in) of Teflon-silicon septa (National Scientific, Rockwood, TN, USA). All samples were brought immediately to the Soil Ecology Research Laboratory of Macdonald Campus, McGill University, where they were stored in a temperature controlled location. All samples were analyzed for the three main trace GHG gases: N_2O , CH_4 and CO_2 using a customized Bruker-Varian 450 gas chromatograph (Bruker, Bremen, Germany). All sites followed the same gas sampling procedure, except for the Truro site during the 2012 and 2014 seasons when only 3 gas samples were collected at 15 minute-intervals over a total of 30 min using round PVC chambers (0.25 m in height and 0.203 m in outer-diameter). The gas was sampled for approximately 100 days each year. In-season day time gas samples were collected from the soil surface from the time of planting to harvesting, i.e. from mid-May to mid-November.

4.2.3 Gas Concentration and Threshold Criteria

In order to facilitate the flux calculations, the gas concentrations from the lab analysis were first converted from a volumetric to a mass basis (ppm to $mg \cdot m^{-3}$) using the following equation (Holland *et al.* 1999):

$$C_v = (C_m \cdot M \cdot P) / R \cdot T \quad (2)$$

where C_v denotes the gas concentration in $mg \cdot m^{-3}$ of a particular trace gas species, C_m denotes the gas concentration in ppm (or $mg \cdot kg^{-1}$), M denotes the molecular weight of a particular trace gas species (i.e., N_2O : $\mu g \text{ N } \mu mol^{-1} N_2O^{-1} = 28.0134 \text{ g mol}^{-1}$; CH_4 : $\mu g \text{ C } \mu mol^{-1} CH_4^{-1} = 12.0107 \text{ g mol}^{-1}$, and CO_2 : $\mu g \text{ C } \mu mol^{-1} CO_2^{-1} = 12.0107 \text{ g mol}^{-1}$), P denotes the atmospheric pressure at 1 atm, R denotes the universal gas constant, $0.0821 \text{ L atm K}^{-1} \text{ mol}^{-1}$, and T denotes the room temperature (293K).

By replacing the parameters with the given values for each trace gas, Equation 2 can be simplified as:

$$C_{v(N_2O-N)} = 1.1660 \cdot C_{m(N_2O)} \quad (3)$$

$$C_{v(CH_4-C)} = 0.4999 \cdot C_{m(CH_4)} \quad (4)$$

$$C_{v(CO_2-C)} = 0.4999 \cdot C_{m(CO_2)} \quad (5)$$

where $C_{v(X)}$ is the volumetric concentration of gas element X in $\text{mg}\cdot\text{m}^{-3}$, and $C_{m(\text{gas})}$ is the measured gas concentration from the lab analysis in ppm or $\text{mg}\cdot\text{kg}^{-1}$. The conversion factors per ppm unit for each trace gases were $1.1660 \text{ mg}\cdot\text{m}^{-3}\cdot\text{ppm}^{-1}$ for N_2O-N , and $0.4999 \text{ mg}\cdot\text{m}^{-3}\cdot\text{ppm}^{-1}$ for both CH_4-C and CO_2-C calculated using Equation 2 above.

Two different threshold values (lower and upper) were predefined prior to the flux analysis. The data was filtered using the imposed lower threshold for all three gases, and the upper threshold for two of the three gasses, N_2O and CO_2 . While the lower threshold was fixed for each gas, the upper threshold was a dynamic threshold dependent on the previous ($i-1$) and subsequent samples ($i+1$):

$$C_{m(N_2O)_i} = \begin{cases} N/A & \text{for } (C_{m(N_2O)})_i \leq 0.15 \text{ ppm} \vee \dots \\ & ((C_{m(N_2O)})_i \geq 2.5 \times (C_{m(N_2O)})_{i-1} \wedge (C_{m(N_2O)})_i \geq (C_{m(N_2O)})_{i+1}) \\ (C_{m(N_2O)})_i & \text{Otherwise} \end{cases} \quad (6)$$

$$C_{m(CH_4)_i} = \begin{cases} N/A & \text{for } (C_{m(CH_4)})_i \leq 1.7 \text{ ppm} \\ (C_{m(CH_4)})_i & \text{Otherwise} \end{cases} \quad (7)$$

$$C_{m(CO_2)_i} = \begin{cases} N/A & \text{for } (C_{m(CO_2)})_i \leq 300 \text{ ppm} \vee \dots \\ & ((C_{m(CO_2)})_i \geq 2.5 \times (C_{m(CO_2)})_{i-1} \wedge (C_{m(CO_2)})_i \geq (C_{m(CO_2)})_{i+1}) \\ (C_{m(CO_2)})_i & \text{Otherwise} \end{cases} \quad (8)$$

Where i denotes the sample number.

The minimum value for which different gases were fixed at the lower threshold was chosen upon the minimum spectral detection limit of gas chromatography. In Equation 6, the minimum for N_2O was 0.15 ppm. Equation 6 holds when the upper threshold, constituting of measured N_2O , is equal to or greater than 2.5 times than the previous gas, AND (\wedge) is equal to or greater than the subsequent gas sample. If the conditions hold (e.g., true for lower OR (\vee) upper thresholds), the equation's output is "not a number" (N/A). The same rules and equation were applied to the CO_2 gas (Equation 8), but using a different lower threshold, specifically a detection limit of 300 ppm. Conversely, if one of the upper OR lower threshold conditions does not hold, then the

condition returns the true measured value. Due to the possibility that CH₄ sourced from pockets exploding (i.e., air bubbles, creating spikes in the data set) filtration for CH₄ (Equation 7), was evaluated using only a fixed lower threshold value of 1.7 ppm. The outliers (spikes), mainly from CH₄ gas, were the result of a natural phenomenon, and should therefore not be removed. Furthermore, no high pass filter nor maximum detection limits were set in the filtration process due to the uncertain response of the maximum of possible concentration of trace gases to local variation.

The dynamic upper threshold used for N₂O and CO₂ was implemented to condition the data pattern by removing outlier samples regardless of the range of the data set. A dynamic threshold can be applied on data sets with small variances as well as those with large variances assuming they both show linear responses. Equation 6-8 were created during data processing via MATLAB scripts to facilitate an automatic filtering process for abnormally low or high values. The post-processing procedure, including visual and manual checks, was implemented only when the data was extremely sporadic. This procedure included using the ambient gas result from each sampling event as a benchmark for minimum threshold values, since ambient gas samples were the natural gas concentration that occurred in the air prior the sampling.

After applying the low and high pass filter, the flux was calculated using the concentration gradients of the GHG of interest over the total measured duration. The most common method of calculating fluxes was via a simple linear regression model wherein the gradient was calculated based on the average slope value (Venterea, 2010). A minimum number of samples per total duration of measurement had a small effect on the variation, thus often the approach in flux calculation is simply by taking an average. If the outlier data was ignored, the dataset source could have deviated significantly from the flux estimate and could have led to overestimation. The outlier data may have resulted from accidental measurement errors or site-specific soil-gas exchange. High variation in the dataset could potentially lead to high discrepancies in flux estimates.

The median flux model (MFM) technique was used in this study to discard outliers and the corresponding bias in flux estimation. The MFM technique provides several advantages: (i) calculated flux and estimated emission are not affected by extreme high or low variations from the set of measurements, (ii) the original data set, holding valuable information, is maintained (iii) it is independent from equal time intervals, sequence or sampling durations, (vi) concentration corrections such as in Hutchinson and Mosier (1981) are not required, and (v) unlimited number

of sample observation, but with a minimum of three, as similarly shown in Pedersen *et al.* (2010) and (Parkin *et al.* 2012). However, neither of these studies consider outlier datasets.

4.2.4 Flux Estimation

Five gas samples were collected simultaneously in 15 min intervals totalling one hour of sampling time. While Hutchinson and Mosier (1981)'s study fitted a linear regression to three measured gas concentrations, this study applied a simple linear relationship to every two gas measurements. As shown in the following equation, a slope or gradient was calculated by dividing the difference of two gas concentrations by the difference in sampling time:

$$Slope = \frac{\Delta C_v}{\Delta t} = \frac{C_j - C_i}{t_j - t_i} \text{ with } i = 0 \text{ to } 3 \text{ and } j = i \text{ to } 4 \quad (9)$$

where *Slope* denotes the slope or gradient value in $\text{mg}\cdot\text{m}^{-3}\cdot\text{h}^{-1}$, ΔC_v denotes the difference in gas concentrations in $\text{mg}\cdot\text{m}^3$ (e.g., $C_1 - C_0$, $C_2 - C_1$, $C_3 - C_2$, $C_4 - C_3 \dots$) and Δt denotes the difference between two measurements (e.g. $t_1 - t_0$, $t_2 - t_1$, $t_3 - t_2$, $t_4 - t_3 \dots$ although not necessarily subsequent).

Only the median value of the ten slopes was used to calculate the flux. The use of the median value reduced the effect of bias data from erroneous measurements (i.e., outliers). After the median value of the slopes was identified, the flux of each chamber was calculated via:

$$Flux = \frac{\Delta C_v}{\Delta t} \cdot \frac{V}{A} = H \cdot \frac{C_{v,j} - C_{v,i}}{t_j - t_i} = H \cdot Slope_{median} \quad (10)$$

where *Flux* denotes the hourly flux in $\text{mg}\cdot\text{m}^{-2}\cdot\text{h}^{-1}$, *V* denotes the volume of the chamber in m^3 with $V = \text{height } (H) \times \text{length } (L) \times \text{width } (W)$, *A* denotes the total soil surface area covered by the chamber in m^2 , *H* denotes the sum of the active height of the chamber measured from the inner dimensions of the chamber cover and the chamber base in m, and $Slope_{median}$ denotes the median value of the ten calculated slopes in $\text{mg}\cdot\text{m}^{-3}\cdot\text{h}^{-1}$.

In estimating the flux at ideal conditions, if all the ten slopes of the trace gas species measured in term of concentration versus time have equal slopes, then the flux can be estimated from the single value of the same gradient (Figure 12).

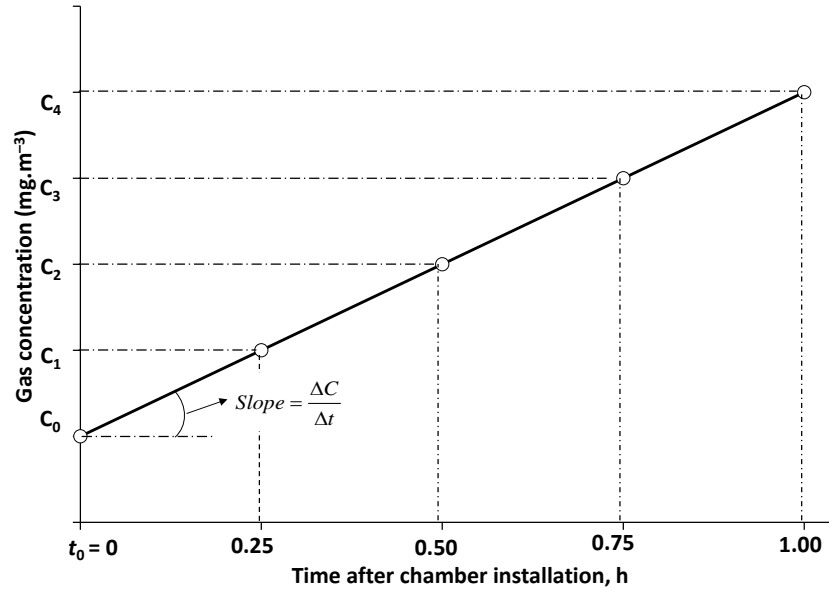


Figure 12: Illustration of the median slope concept for flux estimation.

4.2.5 Annual Emission Estimation

Over the long term, the response of the flux or emission during the growing season is rarely monotonic in practice and tends to fluctuate. Thus, to understand the temporal variability trend in a localized environment for in-season gas emissions, the emission value was estimated using the Piecewise Cubic Hermite Interpolating Polynomial (PCHIP) extrapolation technique (MATLAB). Detailed equations are mentioned in Fritsch and Carlson (1980). The PCHIP interpolation technique was employed to predict the fluxes at any given date between the sampling dates, and functioned even when the sampling dates did not have equal intervals. This method produced a smooth curve at each defined point for each flux despite for unequal distance (i.e., days) of the gas sampling date. This eliminates overestimation and less oscillation in the case of highly fluctuated and/or sporadic flux data source. The total cumulative emissions were calculated for each chamber using Equation 11. The total cumulative emissions were calculated for each chamber using the following equation:

$$Emission = \frac{24}{1000} \cdot \sum_{i=1}^n Flux_i \quad (11)$$

where *Emission* denotes the total cumulative emission of trace gases over the growing season in g·m⁻², *Flux* denotes the hourly flux at a chamber for a given date in mg·m⁻²·h⁻¹ calculated via Equation 10, and *n* and *i* respectively denote the first date and last date of sampling.

The total estimated emissions for a particular chamber location were the accumulation of daily fluxes for the period of the growing season. After the flux and emission calculation procedures were completed for all sites, the data variation was presented through descriptive statistics of the estimated emissions result for each chamber and the corresponding site. A plot of side-by-side comparison of the GHG emission for all three years study was also presented. These steps were conducted in Microsoft Excel.

4.3 Results and Discussions

4.3.1 Slope and Flux Estimation

The variations in the gas concentrations demonstrate the challenge of calculating flux when using the non-steady state chamber technique. Some of the gas concentrations were also scattered and difficult to distinguish for direct linear relationships over the measurement period. A few factors that contributed to inaccurate predictions were identified. Low soil-gas diffusivity, especially with methane gas, varied within and between gas data sets at very low concentrations. At $t = 0$ h, methane tended to have a higher concentration at the subsequent sampling times. Furthermore, a gas leakage from the chamber may have promoted a non-linear response, especially when the soil surface was uneven, the soil was highly porous (e.g., low moisture content in organic and high clay soil texture) or when the soil expanded or contracted throughout the summer. A large variation in gas concentrations was observed as well as fluxes from one chamber to another. This is consistent with the conclusions from Fowler (1999). As similarly being reported by Venterea (2010), the total height (H) of the chambers is the most critical parameter in the flux calculation, regardless of the chamber design. A slight variation in the height changes the total chamber volume, significantly affecting flux estimation. Thus, measuring the H variation of the chambers over the growing season must be validated prior to the flux calculation.

For the data analysis in the flux calculation and emission estimation, we frequently used Excel functions using a standard regression line model (e.g., LINEST function). However, this method tends to overestimate the initial gas concentration ($t=0$) and overall (average slope) flux values and cannot distinguish outliers from large datasets (Venterea, 2010). The MFM method allows discrimination of data originating from erroneous measurements, thus, removing biased data automatically. We employed this method for our estimation of the flux using the slope over the measurement period, as previously shown in Equation 6.

Figure 13 shows an illustration of response patterns from the individual gas concentration model calculated using Equations 1 through 5. In addition, the RMSE also was calculated where the values labelled as $RMSE_{Actual}$ is the RMSE measured from the standard average linear regression, and $RMSE_{Model}$ is the RMSE calculated from the MFM linear model. Most of the model plotted using the MFM methods resulted lower RMSE relative to the standard average linear regression. The consideration in flux calculation for non-linear regression will provide greater systematic error as reported by Kroon *et al.* (2008). The model provided better flux estimation with the minimum gas sample of three uniform slopes over the measured time. Figure 13 (a), (c) and (e) show how the model eliminates outlier data in the gas measurement, thus, avoiding flux overestimation. The model eliminated the noisy dataset (Figure 13 (b), (d) and (f)). A very low flux, which almost showed a plateau response (zero flux) may have also occurred during flux analysis. The MFM model may not line up exactly on the top of each actual measured data point, since the MFM model only considers the gradient of the response, and not the intercept.

In general, the CH_4 and N_2O gas concentrations show the most sporadic variations throughout the sampling period, whereas CO_2 shows the most stable linear response trend. The CO_2 and N_2O gases were generally positively emitted, and CH_4 was mostly consumed (sink) by agricultural soils. The flux estimation for trace gases was calculated using the median slope technique in MFM. MFM provides an alternative to the method offered by Hutchinson and Mosier (1981), with the advantages of reducing bias from small numbers of gas samples and eliminating outliers from datasets. This simple linear relationship procedure also offers unlimited discrete measurements of replication observation, independent time interval, while maintaining the similar trend of the measured trace gas.

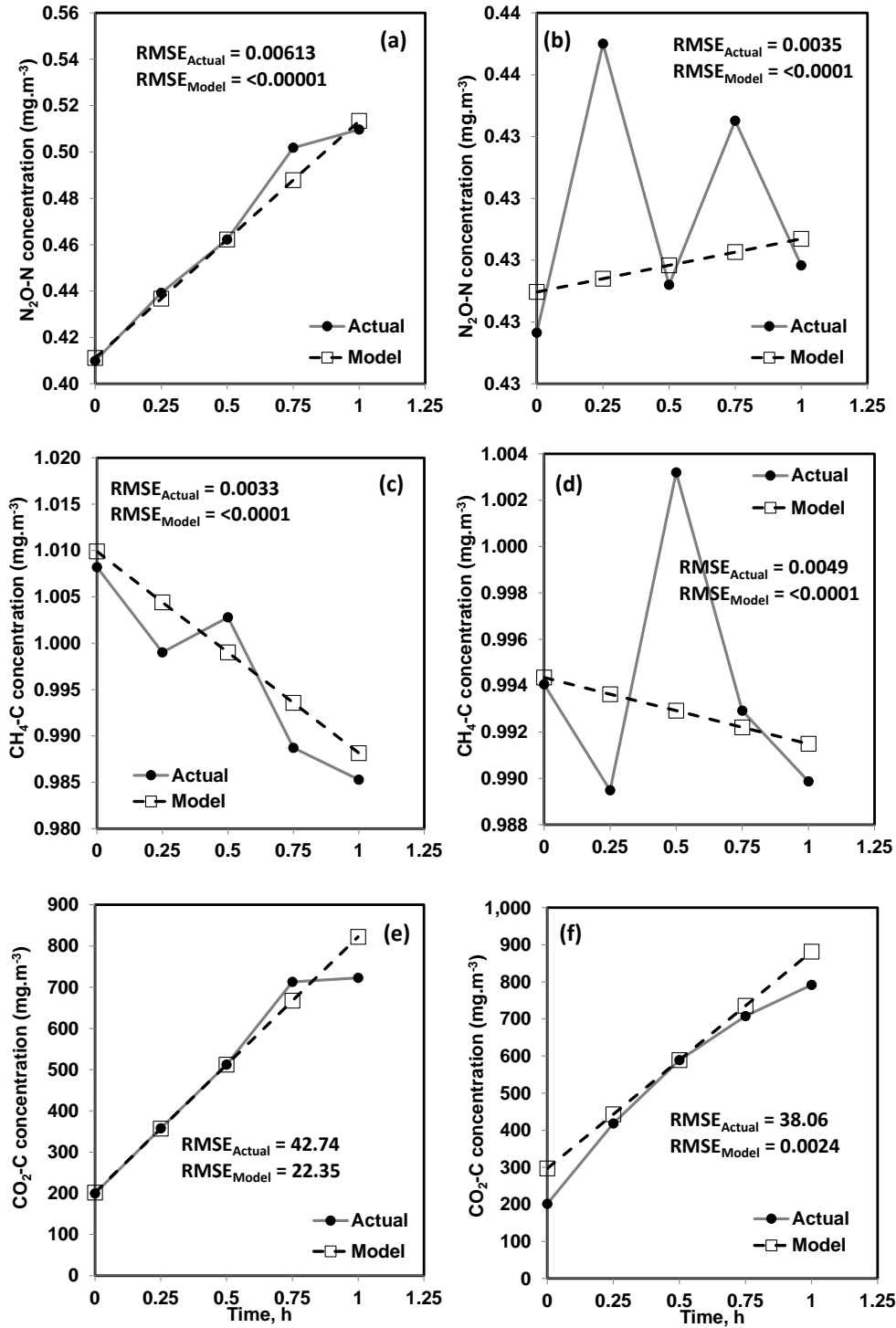


Figure 13: The flux values were calculated from the slope of the model line generated from five gas datasets using MFM models: (a) and (b) are the N₂O-N, (c) and (d) are the CH₄-C, and (e) and (f) are the CO₂-C gases responses under normal and noisy dataset, respectively.

4.3.2 Emission Estimation

Using Equation 11, the cumulative daily (diurnal) GHG emission per chamber based on different treatments over the growing season was estimated as shown in Figure 14. It illustrates high fluctuations of the trace gases emissions of the trace gases throughout the season and the variation between chambers. The emissions were estimated using the PCHIP one-dimensional data array interpolation. However, the results were underestimations. The data was interpolated from the first until the last day of sampling on a per chamber basis. PCHIP was the most appropriate method of interpolation since it did not result in an overshoot curve from the point data of the emissions estimation and produced a smooth curve over the oscillating fluxes for the measured period. The inconsistent gap between sampling days was also taken into account. This method performed better than a normal polynomial line, which tends to overestimate the total emissions.

A simple descriptive statistic for the minimum, medium, maximum, mean and standard deviation of estimated total diurnal emission of main three gases is presented in Tables 8, 9 and 10 for seasons in 2012, 2013 and 2014, respectively. Unfortunately, in 2014 there were no studies conducted at the LE and SL sites. These estimated emissions data were calculated on a per chamber basis using a 1-D array data interpolation via the PCHIP method as previously discussed.

At the LE site in 2012 and 2013, based on the mean value, the source of, $\text{N}_2\text{O-N}$ emissions had a mean of about 0.253 g.m^{-2} (2012) and 0.262 g.m^{-2} (2013). Additionally, in 2013, the SE and the SH sites also fell within the same range of emissions (0.267 and 0.262 g.m^{-2} respectively). In 2014, the SE site produced the highest $\text{N}_2\text{O-N}$ emissions, with a mean of 0.394 g.m^{-2} . In both years 2012 and 2013, the SL site was shown to be the main $\text{N}_2\text{O-N}$ sink, with a mean of $<0.001 \text{ g.m}^{-2}$, and -0.001 g.m^{-2} .

$\text{CH}_4\text{-C}$ emissions were highest at the SL site and released 6.107 g.m^{-2} and 0.990 g.m^{-2} in the first two consecutive years of 2012 and 2013. This was a result of emissions from the bog area. In 2012, $\text{CH}_4\text{-C}$ was mostly consumed by the soil at the LE and TR sites, and in 2013 the TR, LE and SH sites showed a similar pattern ($< 0 \text{ g.m}^{-2}$ based on average value). Interestingly, the TR site in 2012 and 2013, but not 2014, also indicated absorption of $\text{CH}_4\text{-C}$ under a free pasture field. This may have been a result of the relatively wet season in 2014 at the TR site.

For all seasons, the $\text{CO}_2\text{-C}$ emissions were mostly emitted from the TR site at about 1424 g.m^{-2} , 368 g.m^{-2} and 105 g.m^{-2} . However, potentially due to chamber leakage and sampling error,

the latter results indicate high variation. In contrast, the lowest CO₂-C emissions were observed at SH in 2012 and HR in both 2013 and 2014.

Figure 15, 16 and 17 illustrates the side-by-side comparison of annual GHG emissions from different sites based on varying irrigation treatments, soil texture and crop species. N₂O-N emissions were observed in all sites, except for the few data points that show N₂O-N consumption at the TR site. The TR site was quite consistent over the study period. The LE site produced the highest N₂O-N emissions relative to the other sites. In the 2012 study, the HR site indicated that different sources of fertilization clearly resulted in differences in N₂O-N emissions regardless of different types of irrigation, settled between 0.03 to 0.26 g.m⁻². However, in 2013, there was no obvious indication of the irrigation treatment difference since no fertilization was applied to the soybean crop. The results from the LE site in 2012 showed differences between subsurface and surface irrigation. There was a large variation in N₂O-N emissions within each individual treatment and a disparity in 2013. There was almost no difference in emissions under the different treatment of water and varying soil organic decomposition rate (observed at the SH site populated within 0 to 0.07 g.m⁻² in 2012) but higher variation of emissions observed within 0.01 to 0.9 g.m⁻² in 2013. At the SE site, conventional drainage showed no difference with subsurface in N₂O-N emissions in 2012, but there was a large disparity in 2013. There were also almost no differences detected at the SL and TR sites. In 2013, the data at the TR site showed the potentially significant effect of water management on the same type of pasture area.

Methane emissions had the most sporadic response and no differences were observed between different water treatments, fertilizers and soils at every site in all years 2012 through 2014. (Figure 15). The most populated CH₄-C emission level settled between -0.10 to 0.10 g/m² of average emissions for both years 2012 and 2013. For 2014, most of the CH₄-C emission levels were fluctuated and higher than measured in previous two years. At the SL and TR sites, where most of the CH₄-C, ranging from 0.02 to 0.35 g/m² (2012) and 0.01 to -0.10 g/m² (2013), was emitted and consumed respectively. The SL site claimed the largest CH₄-C emissions during two consecutive years 2012 and 2013. High methane emissions may have occurred at the SL site.

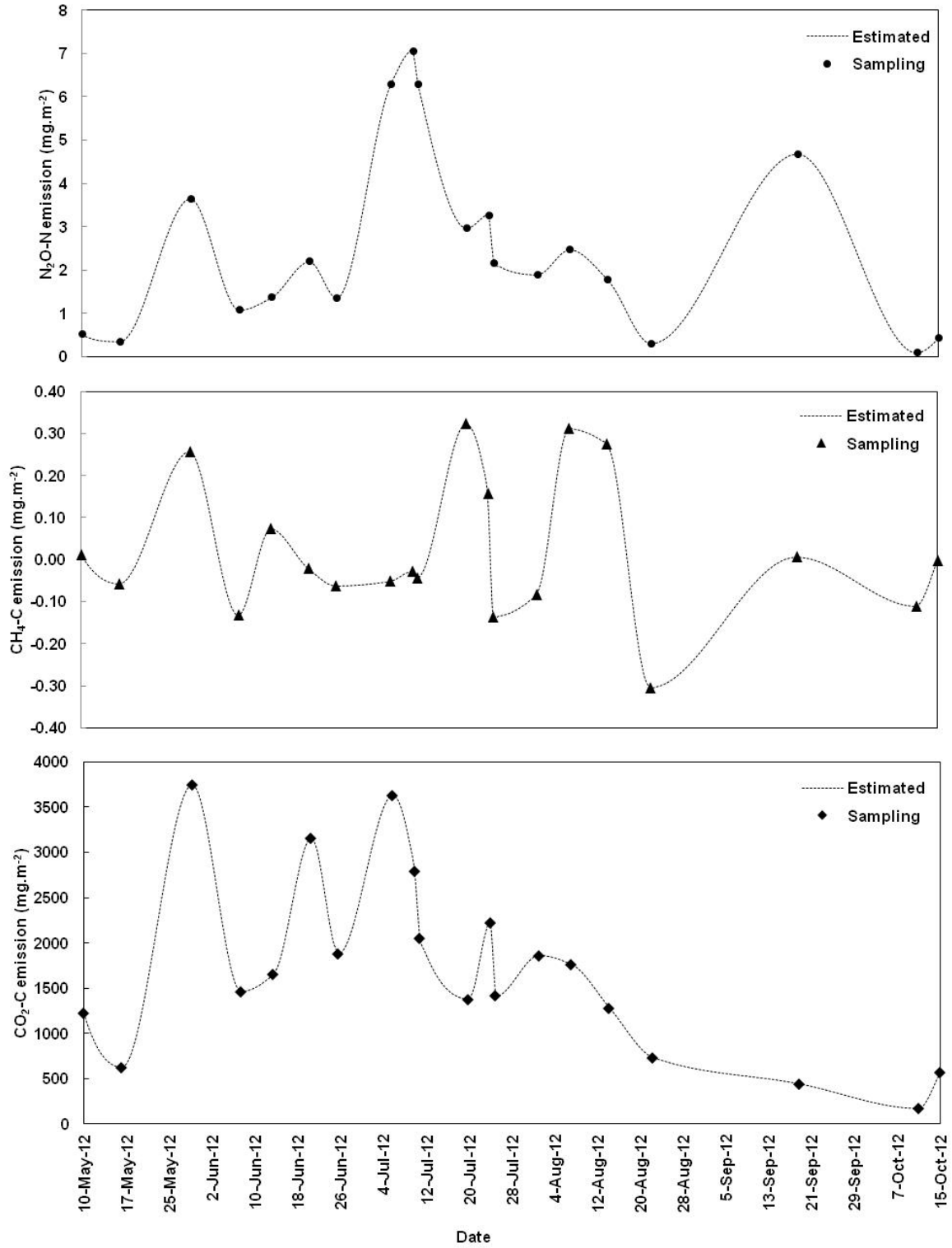


Figure 14: Temporal variation of the GHG emission over the growing season on individual chamber IDs.

Table 8. Descriptive statistic of nitrous oxide, methane and carbon dioxide emission ($\text{g}\cdot\text{m}^{-2}$) for 2012 season

Year	Emission (g/m^2)	Site	N	Minimum	Median	Maximum	Mean	Std. Deviation
Season 2012	$\text{N}_2\text{O-N}$	HR	24	0.029	0.054	0.259	0.075	0.055
		LE	10	0.094	0.203	0.612	0.253	0.161
		SH	24	0.002	0.014	0.066	0.017	0.012
		SE	12	0.012	0.040	0.086	0.036	0.020
		SL	15	-0.003	<0.001	0.003	<0.001	0.002
		TR	18	-0.169	0.046	0.284	0.067	0.105
	$\text{CH}_4\text{-C}$	HR	24	-0.097	-0.016	0.344	0.009	0.105
		LE	10	-0.280	-0.019	0.000	-0.066	0.103
		SH	24	-0.175	-0.004	0.062	-0.011	0.040
		SE	12	-0.141	-0.006	0.014	-0.017	0.041
		SL	15	-0.106	0.024	42.748	6.107	12.591
		TR	18	-0.359	-0.039	0.032	-0.063	0.088
	$\text{CO}_2\text{-C}$	HR	24	108	150	207	157	29
		LE	10	102	169	242	168	49
		SH	24	55	155	254	149	49
		SE	12	26	177	401	207	110
		SL	15	35	137	354	164	94
		TR	18	576	1432	2294	1424	375

HR = Harrow; LE = Leamington; SE = St. Emmanuel; SH = Sherrington; SL = St. Louis De Blandford; TR = Truro; N = Number of chamber

Table 9. Descriptive statistic of nitrous oxide, methane and carbon dioxide emission (g.m-2) for 2013 season

Year	Emission (g/m ²)	Site	N	Minimum	Median	Maximum	Mean	Std. Deviation
Season 2013	N ₂ O-N	HR	24	-0.001	0.027	0.093	0.036	0.026
		LE	10	0.049	0.187	0.716	0.262	0.228
		SH	24	0.011	0.064	0.865	0.210	0.277
		SE	12	0.095	0.235	0.490	0.267	0.134
		SL	15	-0.006	<0.001	0.007	-0.001	0.004
		TR	18	-0.348	0.034	0.183	0.013	0.105
	CH ₄ -C	HR	24	-0.009	-0.003	0.044	0.000	0.012
		LE	10	-0.016	-0.006	0.001	-0.006	0.005
		SH	24	-0.015	-0.005	0.003	-0.005	0.005
		SE	12	-0.020	-0.002	0.003	-0.004	0.006
		SL	15	0.004	0.059	7.794	0.990	2.439
		TR	18	-0.024	-0.011	-0.002	-0.012	0.007
	CO ₂ -C	HR	24	56	120	163	120	23
		LE	10	135	200	245	195	39
		SH	24	163	315	528	310	96
		SE	12	124	241	398	252	90
		SL	15	31	138	234	126	62
		TR	18	36	389	603	368	178

HR = Harrow; LE = Leamington; SE = St. Emmanuel; SH = Sherrington; SL = St. Louis De Blandford; TR = Truro; N = Number of chamber

Table 10. Descriptive statistic of nitrous oxide, methane and carbon dioxide emission (g.m⁻²) for 2014 season

Year	Emission (g/m ²)	Site	N	Minimum	Median	Maximum	Mean	Std. Deviation
Season 2014	N ₂ O-N	HR	24	0.037	0.194	0.891	0.249	0.195
		LE	10	-	-	-	-	-
		SH	24	0.036	0.088	0.640	0.143	0.158
		SE	12	0.109	0.409	0.923	0.394	0.222
		SL	15	-	-	-	-	-
		TR	18	-0.613	0.002	0.198	-0.024	0.169
	CH ₄ -C	HR	24	-0.012	-0.004	0.001	-0.004	0.003
		LE	10	-	-	-	-	-
		SH	24	-0.019	-0.005	0.007	-0.005	0.005
		SE	12	-0.023	-0.006	0.002	-0.008	0.008
		SL	15	-	-	-	-	-
		TR	18	-1006.071	-14.700	765.527	-99.661	548.520
	CO ₂ -C	HR	24	86	150	262	161	53
		LE	10	-	-	-	-	-
		SH	24	152	292	528	304	81
		SE	12	91	349	513	325	121
		SL	15	-	-	-	-	-
		TR	18	-1611	219	1312	105	860

HR = Harrow; LE = Leamington; SE = St. Emmanuel; SH = Sherrington; SL = St. Louis De Blandford; TR = Truro; N = Number of chamber

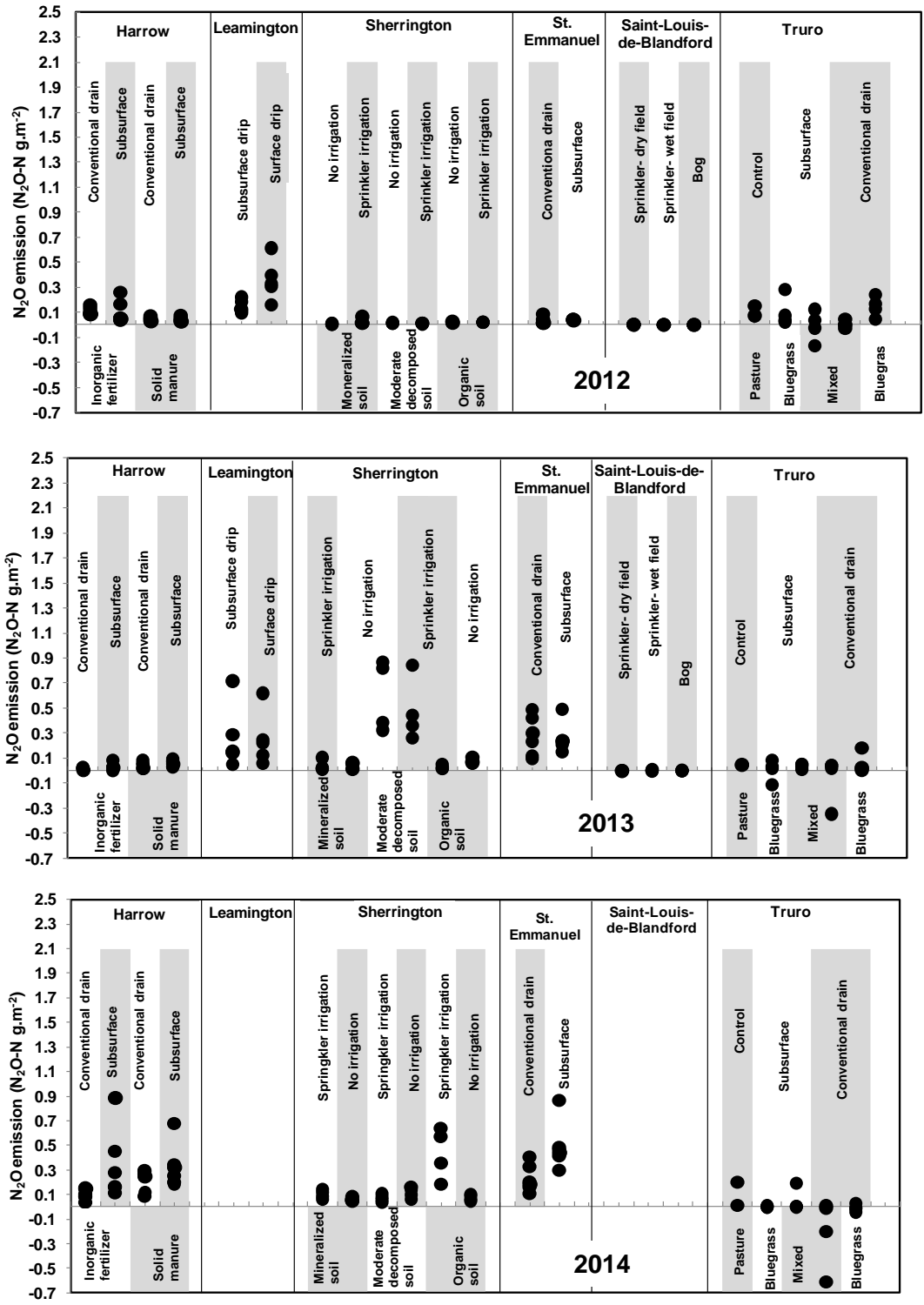


Figure 15: Nitrous oxide emission estimation under different water, crop and soil treatments.

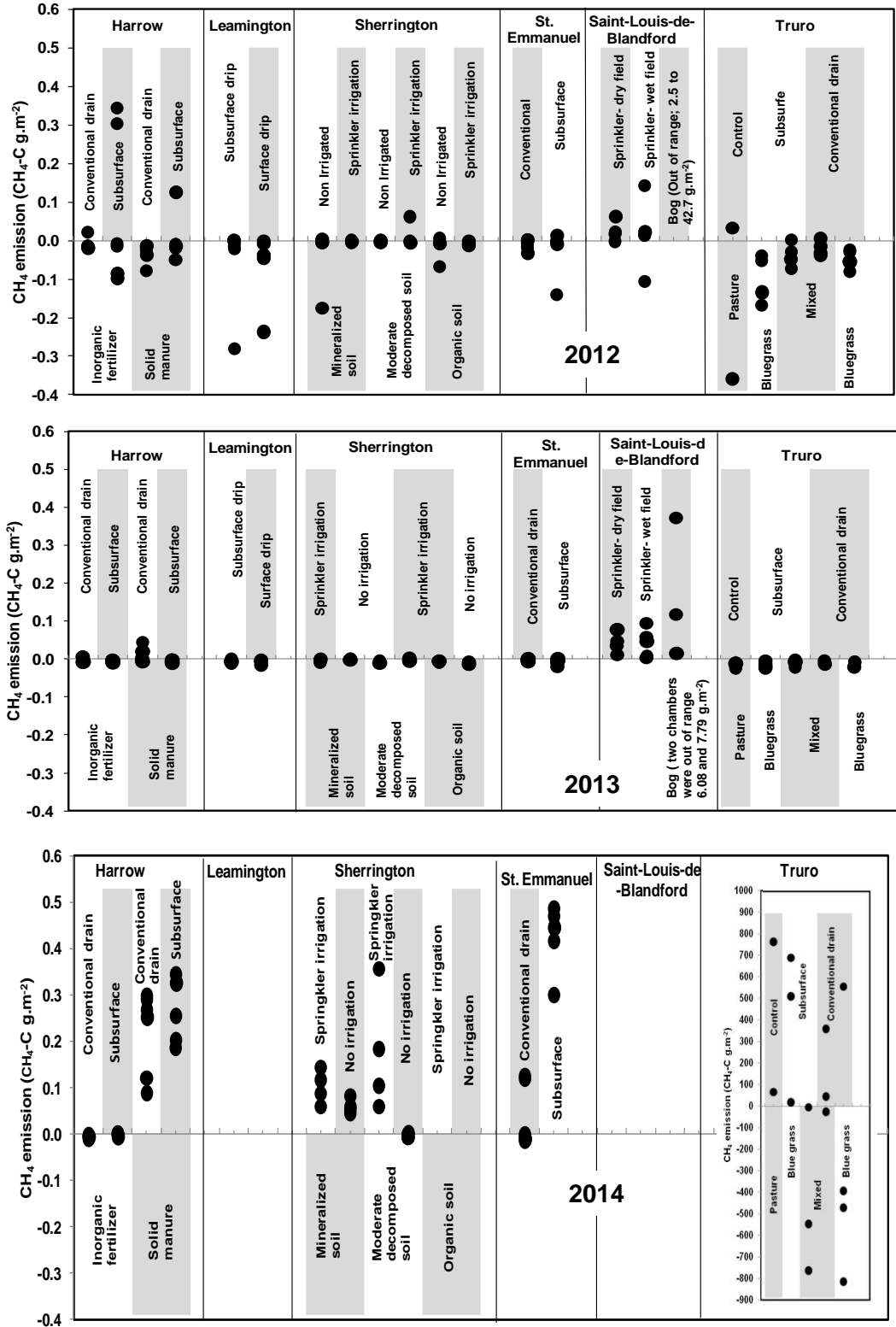


Figure 16: Methane emission estimation for different water and soil treatments.

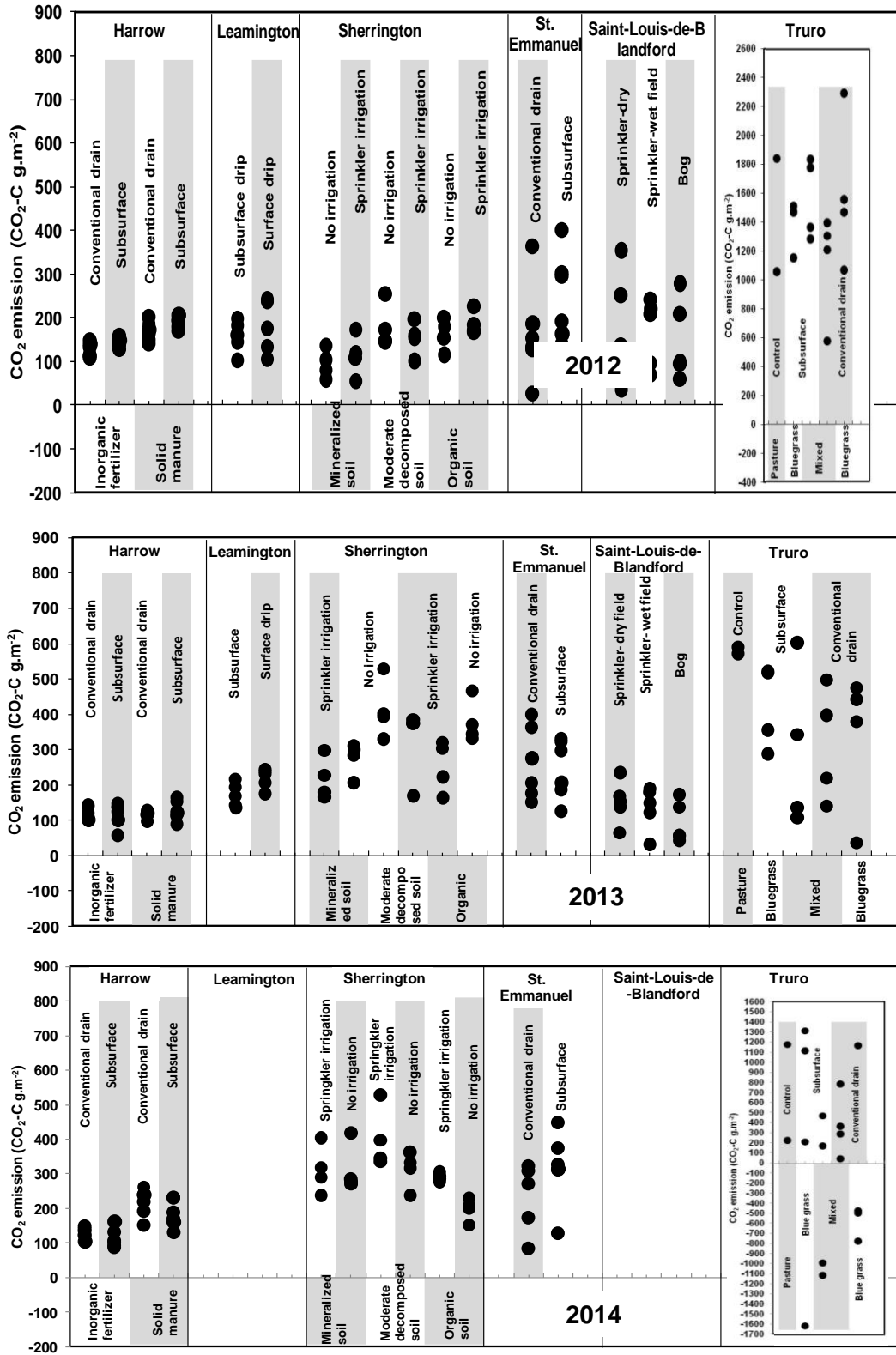


Figure 17: Carbon dioxide emission estimation for different water and soil treatments.

4.4 Conclusion

The method, proposed in this paper to disregard outliers and to calculate the flux, is the use of the MFM which is offered as one solution for handling large datasets especially when the measurements also contain noisy data. Thus, this procedure establishes a standard automatic data processing for this study whose purpose is estimating emissions across sites and treatments. In addition, this procedure also offers unlimited discrete measurements of replication observations, with no concentration correction required, while maintaining the original pattern and the magnitude of the measured trace gas. The total height of the chamber deployed during the gas sampling is the most critical parameter to be considered in overall flux and emission estimation. Based on the total estimated emission, the SL site under sprinkler irrigation with cranberry, emitted the largest amount of CH₄-C, and was the main source of N₂O-N sink especially at the beginning of the growing season. On the other hand, the TR site, under a wide range of irrigation practices and pasture production, became the main source of CH₄-C sink in both consecutive years. Overall, GHG emissions for all six sites across Eastern Canada were observed using MFM under water, soil and crop treatment for the 2012, 2013 and 2014 data collections.

Connection Text to Chapter 5

Chapter 5 relates to the third objective listed in Chapter 1. As discussed in Chapter 3, physical soil properties (i.e. soil moisture, soil temperature and EC_a) were the most important factors to monitor in term of estimating levels of GHG in agricultural soil. However, the spatial variability of GHG emissions measured with the chamber-method for multiple combinations of treatments (water, crop and soil) is not well documented for Eastern Canada. This relationship is particularly important since most vegetables are grown in muck soil (organic) which have spatially variable GHG emissions when compared to other soils. Intensive farming practices during both wet and dry seasons increase decomposition in muck soil. Hence, the ability of the soil to emit, or sink, temporally is a subject of interest for monitoring temporal GHG and real time physical soil properties.

Thus, Chapter 5 is focused on the temporal relationship between GHG fluxes and local physical soil properties using data collected by a wireless sensor network (WSN). The WSN monitoring system was deployed to collect in-situ soil properties and variations in crop water status. Different parts of this study have been presented at an ASABE conference.

The following citations are available at this time:

Mat Su, A. S., V. I. Adamchuk, C. A. Madramootoo, J. K. Whalen, K. Tam, H.H. Huang, and H. Beslim. Predicting changes in greenhouse gases emissions in muck soil using physical observations. 2014. 2014 ASABE and CSBE/SCGAB Annual International Meeting

CHAPTER 5

PREDICTING CHANGES IN GREENHOUSE GASES EMISSIONS IN MUCK SOIL USING PHYSICAL OBSERVATIONS

Ahmad Suhaizi Mat Su, Viacheslav I. Adamchuk, Joann K. Whalen, Chandra A. Madramootoo, Hsin-Hui Huang, Katina Tam, and Hicham Benslim

Abstract

Estimating greenhouse gas (GHG) emissions in the field is improved when ancillary soil measurements, like soil moisture, soil water content and soil temperature, are collected. Hand-held probes provide point measurements in the field, but wireless sensor networks (WSN) are more useful for describing the dynamics of soil properties via in-situ probes and can provide insight on the temporal variations in GHG fluxes. WSN probes enable continuous measurements to be gathered from the field easily and at a relatively low cost. This is particularly important in soils that exhibit high temporal variability in GHG fluxes, such as organic (muck) soils. The objective of this study was to relate continuous soil water content and soil temperature measurements with the emissions of nitrous oxide (N_2O), methane (CH_4) and carbon dioxide (CO_2) throughout the growing season of irrigated onion production on muck soils. The GHG fluxes were calculated from regular sampling of static, non-steady state chambers and gas chromatography measurements. Soil water content and soil temperatures were measured using portable sensors in addition to a stationary WSN. Relatively cool and wet soil conditions resulted in greater N_2O fluxes whereas relatively dry and warm soil conditions were associated with more CO_2 release. With respect to sensor technologies, soil matrix potential sensors were better at predicting high GHG fluxes compared to capacitance moisture sensors. The method used in this research is appropriate to quantify GHG emissions from crops produced in muck soils using real-time measurements of soil moisture and temperature conditions. This information also could be used as a benchmark Tier II level under IPCC database platform.

Keywords. wireless sensor network, emissions, organic, carbon dioxide, methane, nitrous oxide.

5.1 Introduction

Agricultural-induced GHG emissions accounted for 9.6 % of the total 2013 GHG in Canada (Environment and Climate Change Canada). Agriculture may be both a source and a sink for GHG, such as N₂O and CH₄, both of which are predominantly due to anthropogenic activities. Agricultural production of fruits and vegetables contributed, on average, \$1476 million CAD in sales in Canada from 2009 to 2011 (Statistics Canada, 2012). Vegetables sales contributed about 53 % of Canadian sales (\$780 million CAD) from the same period. Provincially, Quebec was the second largest vegetable producer, accounting for about \$276 million CAD in sales, second to Ontario, which had \$362 million CAD in sales from 2009 to 2011. Vegetable cultivation occurs primarily on fertile, organic-rich soils. However, GHG emissions caused by vegetable production in Eastern Canada, especially on organic soils, are poorly documented.

The GHG emission from intensively farmed organic soils merits attention because these soils were originally wetlands that were drained for agricultural use. The draining process exposes the organic soil layer to oxygen and the physical disturbance of cultivation further enhances decomposition, leading to CO₂ emissions. Kasimir-Klemedtsson *et al.* (1997) reported that cultivation under organic-rich soil may lead to high N₂O and low CH₄ emissions. As well, N₂O fluxes are enhanced by the N fertilizer inputs and irrigation common in organic soils that are used for vegetable crop production (Rochette *et al.*, 2010).

The dynamics of soil moisture and temperature should explain some of the variability in the biological processes of decomposition, denitrification and methanogenesis that are responsible for the production of CO₂, N₂O and CH₄ gases. For instance, Wiant *et al.* (1967) observed that the rate of CO₂ production increased linearly with a rise in temperature between 20 to 40 °C and Leirós *et al.* (1999) predicted greater GHG emissions as climatic temperature reduced the soil organic matter content. On the other hand, Howard and Howard (1993) found a non-linear relationship between soil moisture and CO₂ flux production on a wide range of agricultural soil types, including peat soil. Linn and Doran (1984) observed that N₂O fluxes increased from 70 to 90% water-filled pore space, as the lack of oxygen created redox conditions that favored denitrification. There must be underlying relationships between soil temperature, soil moisture and GHG emissions, and investigation of these relationships could explain why GHG fluxes vary spatially and temporarily throughout the growing season in organic soils.

Proximal soil sensing is a powerful tool to monitor soil temperature and moisture conditions. Widely used in irrigation management (example from Pan *et al.*, 2013), WSNs provide valuable

real-time information that could be related to agricultural GHG fluxes. Deployment of various proximal sensors to track the dynamic changes in soil temperature and moisture could provide insight into the pattern of GHG emissions in organic soils at a much lower cost than repeated in-field GHG sampling or monitoring of GHG fluxes with microclimatology towers; as far as we know, this has not been tested before. The purpose of this paper was (1) to determine the relationship between soil temperature, soil moisture and GHG fluxes from organic soils under onion production.

5.2 Materials and Methods

5.2.1 Site Description

A wireless sensor network was deployed at a farm in Sherrington, Quebec. This farm is one of the largest vegetable producers in Eastern Canada with approximately 30 hectares cultivated for onion and other vegetables on organic soils. The soil type was classified as muck soil (organic soil), which contains more than 30% organic matter, and has a minimum depth of 40 cm (Canada Soil Survey Committee, Subcommittee on Soil Classification, 1978). The muck soil (classified as the "O" layer) contains mainly litters, fibers, and mosses built up originally from swampy forest saturated with water for prolonged periods. Three locations were selected based on their different decomposition levels, namely: Station 1, 2 and 3 (Figure 18). Each station represents different soil layer classifications – mineralized organic soil (Station 2), moderately mineralized organic soil (Station 1), and organic soil (Station 3) - based on the soil layer structure, bulk density, and organic matter content. At the 0 - 40 cm soil depth, Station 2 was a mineralized organic soils (highly decomposed) mixed with clay soil due to plowing activities. The underlying 40 - 120 cm depth at Station 2 had a clay and hard pan layer blended with marine clay subsoil. Station 1 was a moderately mineralized soil with intermediate decomposition, while Station 3 was newly cultivated land with fresh, organic-rich soil. A deep organic soil layer in the 0 - 120 cm depth was present at Stations 1 and 3. All fields were cultivated for onions (*Allium cepa* L.). With respect to irrigation treatments, all stations were treated with either sprinkler irrigation or no irrigation. Four gas chambers were used for each of the 2 water treatments at each station, which resulted in the deployment of 24 chambers in total.

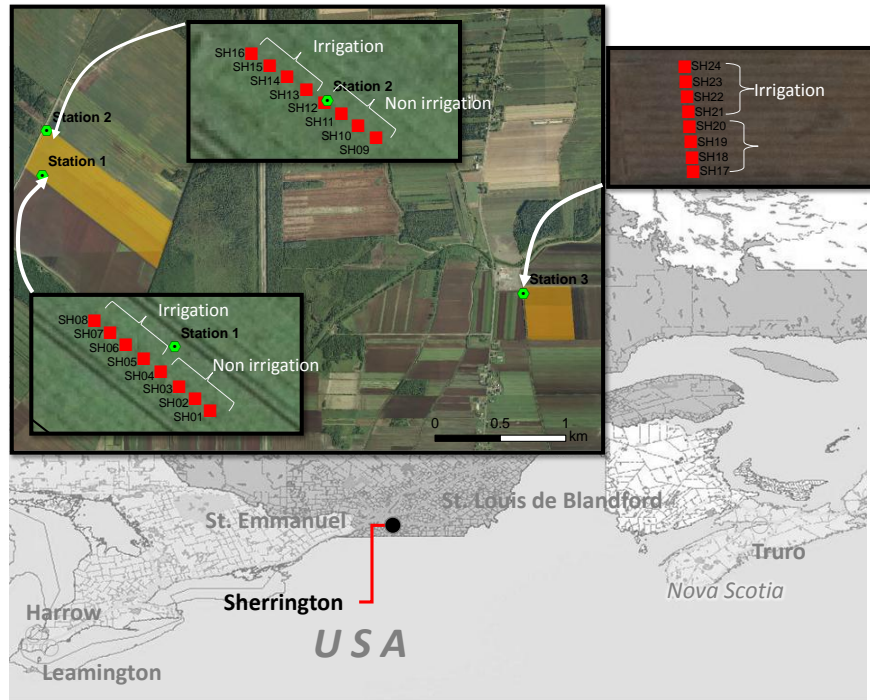


Figure 18. Study locations.

5.2.2 Data Collection

The GHG data was captured using a non-steady state chamber (NSS) design (Figure 19) deployed at each of the 24 locations during the 2012 and 2013 growing seasons. The gas chamber consisted of a chamber cover and base. The base was installed prior to the season and was left in-situ permanently throughout the sampling and growing period to mitigate any effects of disturbance of the soil or root system may have on GHG emissions. Additionally, this setup minimized the leakage of the gas due to the soil surface disturbance during the repeated measurements over the growing season. The base of the chamber was made of a flexi-glass frame with dimensions (W x L x H): 0.556 x 0.556 x 0.140 m, and the chambers were vented to avoid pressure perturbations with a cover of 0.564 x 0.564 x 0.130 m. The chamber base was installed at the beginning of the season and gently hammered into the top soil until 5 cm remained above the soil surface which provided a support for the chamber cover. The chamber cover was protected with an aluminium sheet to reflect heat, thus, minimizing the temperature effect during gas measurements. To prevent gas leaks, a soft cushion tape was placed on the contact surface of the chamber cover to seal the entire chamber system.



Figure 19: A static non-steady state chamber installed for gas sampling

The gas samples were collected at least once a week daily between (7am - 7pm) throughout the growing season. A total of 195 and 135 gas datasets along with other soil physical properties and climate conditions were logged via the WSN for 2012 and 2013, respectively (Figure 20). Geographic locations of the chambers were logged using a Garmin eTrex Legend handheld GPS (Garmin International, Inc., Olathe, KS, USA). The data collection in 2012 started in May and continued until the end of August with a total of 11 sampling dates, and in 2013, sampling was conducted from late April until mid-October, with 16 sampling dates. On each sampled date, five gas samples were taken simultaneously at 15 minute intervals for a total of one hour. Climatic parameters, such as rainfall (mm), ambient relative humidity (%), and temperature ($^{\circ}\text{C}$), wind speed and direction were captured using the wireless sensor network via a weather station (WatchDog 2900ET, Spectrum Technologies, Inc., Aurora, IL, USA). The soil physical properties, such as soil matrix potential (kPa), electrical conductivity (mS/m), temperature ($^{\circ}\text{C}$), and soil moisture (%) were logged at the same 15 minute intervals. All of these datasets were entered into the logger and sent to the host controller via the wireless modem. This data was transmitted over the internet and the data could be viewed and downloaded using software provided by the manufacturer as shown in Figure 21. Although the active telemetry sends wireless data at a 15 min frequency, only data corresponding to the GHG sampling events were considered in this paper.

5.2.3 Data Analysis

All gas samples were extracted using a 20 ml gas exetainer from the headspace using air-tight syringes. All samples were then injected into pre-evacuated or vacuum exetainers of 12 ml (Labco, Wycombe, UK) fitted with an extra 60 mil (1/16 in) Teflon-silicon septa (National Scientific, Rockwood, TN, USA) and stored in cool conditions. All samples were brought immediately to the lab and analyzed for the three main trace GHG gas concentrations (N_2O , CH_4 and CO_2) using a custom Bruker-Varian 450 gas chromatograph (Bruker, Bremen, Germany). The flux of each GHG was calculated based on the change in gas concentration over time. In this method, five concentrations were used to calculate a flux using simple linear regression with a median flux model (MFM) processed via MATLAB scripts. The flux was estimated based on a median slope value of ten slope estimates. The flux of the GHG was classified in three ranges: low (quartile 25 %), medium (quartile 50 %) and high (quartile 75 % or 25 %) over measured soil physical properties.

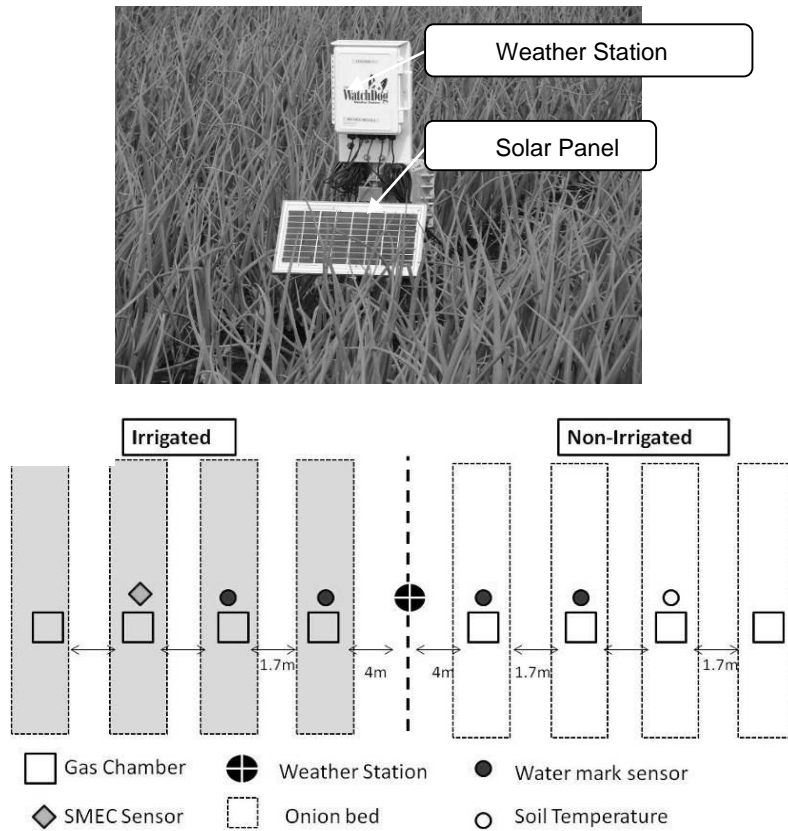


Figure 20: Wireless sensor network installed at three different location under different water regime (a) The wireless sensor network (b) Field layout for the sensor arrangement for all three stations.

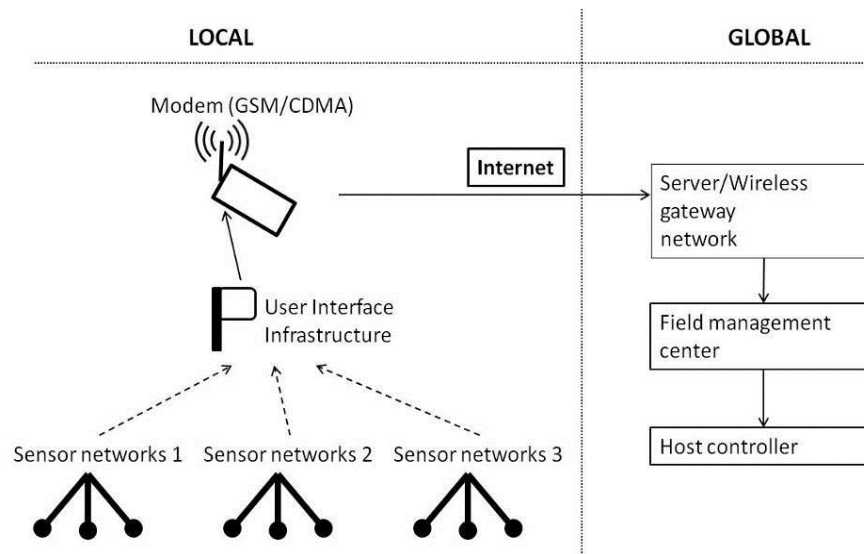


Figure 21: Wireless sensor network installed at three different decomposition rates of organic soil

5.3 Results and Discussion

Considerable variation in GHG fluxes was observed between sampling dates, between field locations, due to the irrigation treatment and even between chambers with the same irrigation schedule at one field station. The CH₄-C and N₂O-N fluxes fluctuated more than the CO₂-C flux during the 2012 and 2013 growing seasons. Table 11 summarizes the mean GHG fluxes measured in the two growing seasons along with soil temperature and moisture. During the two years study, organic soils were a source of N₂O-N and CO₂-C, but a sink for CH₄-C, based on the negative flux values. The N₂O-N flux was $0.0096 \pm 0.0013 \text{ mg.m}^{-2}.\text{h}^{-1}$ in 2012, and was about 9 % greater, on average, in 2013. The CO₂-C flux was $72.14 \pm 5.68 \text{ mg.m}^{-2}.\text{h}^{-1}$ in 2012 with a 25 % increment in 2013. The measured soil temperature was consistent during the study period, with a mean of about 22 °C for both years. Table 12 shows the Pearson correlation between the GHG fluxes and other measured soil parameters i.e. soil moisture, soil temperature and soil matrix potential. In general N₂O-N may provide significant correlation between all measured parameters, however on different magnitude. For instance, N₂O-N fluxes has positive correlation between soil moisture and soil EC, but negative correlation between soil temperature and soil matric potential. CH₄-C fluxes mostly has poor correlation with soil moisture and soil EC (positive correlation) and no significant to other parameters. CO₂-C fluxes have relatively strong positive correlation with soil temperature and soil matric potential, but negative correlation with soil moisture content.

Table 11: Mean and standard error of the GHG fluxes, and monitored soil physical properties.

Year	2012 & 2013
Measurement	Mean \pm Std Error (N = 513)
N ₂ O-N Flux (mg.m ⁻² h ⁻¹)	0.0555 ± 0.0077
CH ₄ -C Flux (mg.m ⁻² h ⁻¹)	-0.0026 ± 0.0019
CO ₂ -C Flux (mg.m ⁻² h ⁻¹)	60.95 ± 3.11
Soil temperature (°C)	21.98 ± 0.13
Soil moisture (VWC %)	20.38 ± 0.15

The structure of the GHG flux data based on the low, medium and high quartiles, in relation to soil moisture and soil temperature conditions, is presented in Figures 22 a-c. The N₂O-N fluxes were more dependent on soil moisture than soil temperature. High N₂O-N fluxes can be clearly seen in Figure 5 (a), with relatively high in soil moisture ranging from about 10 to 80 % of VWC and warm of soil temperature ranged from 5 to 27 °C. Soil moisture is more dominant factor in resulting in higher CH₄-C fluxes compared to soil temperature (Figure 22 (b)). High soil moisture

tends to emit more methane. From the separate analysis (not shown), the 2013 season was a wet season; thus, the CH₄-C fluxes were scattered and not clearly shown on the soil moisture-temperature relationship, but better depicted in low soil matrix potential of less than 30 kPa. Figure 22 (c) shows that CO₂-C was also sporadic across a wide range of soil moisture conditions for both years, but it was governed mainly by hot and warm soil. Both the soil temperature and soil matrix potential failed to establish a strong relationship for high emissions of this gas. However, soil temperature of 20 - 25 °C clearly indicated the majority of the high CO₂-C fluxes production. This suggests that warm temperature initiates more biological activity under relatively wet soil, thus, promoting higher respiration and CO₂-C fluxes.

Table 12: Pearson correlation between the GHG fluxes and measured soil physical properties. ns = not significant; * = significant at 95 % of CI; ** = significant at 99 % of CI

	N ₂ O-N Flux (mg.m ⁻² .h ⁻¹)	CH ₄ -C Flux (mg.m ⁻² .h ⁻¹)	CO ₂ -C Flux (mg.m ⁻² .h ⁻¹)	Soil temperature, °C (manual)	Soil temperature (SMEC sensor), °C	Soil moisture, % (manual)	Soil moisture, % (SMEC sensor)	Soil matrix potential, kPa	Soil EC, mS/cm (SMEC sensor)
N ₂ O-N Flux (mg.m ⁻² .h ⁻¹)	1								
CH ₄ -C Flux (mg.m ⁻² .h ⁻¹)	ns	1							
CO ₂ -C Flux (mg.m ⁻² .h ⁻¹)	0.213**	ns	1						
Soil temperature, °C (manual)	-0.166**	ns	0.324**	1					
Soil temperature (SMEC sensor), °C	-0.179**	ns	ns	0.521**	1				
Soil moisture, % (manual)	0.224**	ns	-0.254**	-0.288**	-0.599**	1			
Soil moisture, % (SMEC sensor)	0.257**	0.116*	ns	-0.356**	-0.314**	0.416**	1		
Soil matrix potential, kPa	-0.215**	ns	0.204**	0.234**	0.415**	-0.391**	-0.375**	1	
Soil EC, mS/cm (SMEC sensor)	0.269**	0.122*	ns	-0.286**	-0.269**	0.421**	0.942**	-0.361**	1

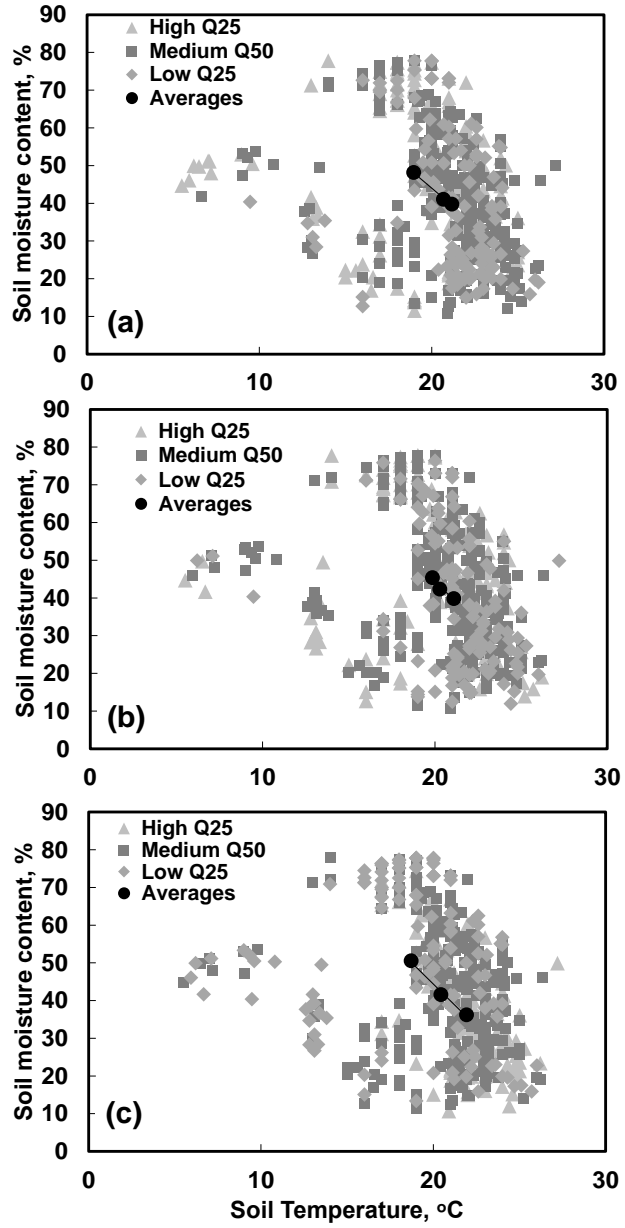


Figure 22: The overall soil moisture and temperature relationships between low, medium and high GHG fluxes measured in 2012 and 2013 from an organic soil (a) N₂O-N fluxes, (b) CH₄-C fluxes, and (c) CO₂-C fluxes. The round black dots (●) represents the average values of each categories.

5.4 Conclusion

Wireless sensor networks along with secondary portable sensors are essential tool for measuring the real-time soil physical conditions. Such systems provide insight into the underlying soil conditions affecting GHG fluxes, both spatially and temporally across the field. The soil matrix potential measurement was the best predictor of GHG-water relationships, mainly affecting for $\text{N}_2\text{O-N}$ and $\text{CH}_4\text{-C}$ fluxes. Higher $\text{N}_2\text{O-N}$ fluxes were associated with higher soil water content (40-70 % of VWC) in the crop root zone at relatively low soil temperatures ($<20^\circ\text{C}$) in organic soil. On the other hand, $\text{CH}_4\text{-C}$ fluxes were sporadic during the growing season as organic soils were generally a sink for $\text{CH}_4\text{-C}$ in the 2012 and 2013 seasons. The $\text{CO}_2\text{-C}$ fluxes were greater in soils having between 40-70 % of VWC at warmer soil temperatures ($24\text{-}25^\circ\text{C}$). The application of a wireless sensor network, along with other secondary datasets, has potential to indirectly estimate the in-season GHG fluxes in an organic soil. This method may provide a cost effective estimate of GHG emissions from agricultural fields during the growing season, while providing valuable information on soil conditions that can improve irrigation scheduling and fertilizer management. The information of the GHG in muck soil will contributed to the IPCC factors as listed under the IPCC (2006) unique for temperate regions.

Connection Text to Chapter 6

Chapter 6 is a manuscript awaiting publication in 2016. The manuscript has been co-authored by several collaborating researchers. All literature cited in this chapter is listed in the reference section.

Since the direct monitoring of temporal and spatial microbial activities related to GHG is limited, it is evident that one approach to estimation GHG emissions is to determine the relationship between GHG production and physical soil properties. The measurements were spatial and temporally varied through space and time. Chapter 3 demonstrated the assessment for ensuring high quality soil EC_a data and understanding the factors in its variation. Subsequently, there is a need to estimate GHG fluxes from agricultural soil under the effect of different water, crop and soil types, and to develop a method for minimizing outliers due to the soil-gas diffusion effect (Chapter 4). Subsequently, Chapter 5 describes the relationship between GHG and the temporal variability in which the fluxes and emissions of the monitored GHG were estimated using the method explained in Chapter 4.

Chapter 6 is related to the fourth objective listed in Chapter 1. In this chapter, the data layer of soil EC_a along with soil mineralogy measurements of on-the-go gamma ray spectroscopy were used to reveal the heterogeneity of the experimental site. Conventional GHG monitoring using NSS gas chambers was either based on systematically or randomly positioning the chambers on agriculture land. However, this approach is not effective for large scale operations and emission estimations based on samples from a subsection of a larger field can be misleading. Thus, PSS technology offers the field heterogeneity information needed to effectively position the NSS chambers. Chapter 6 mainly discusses the predictive approach of GHG using physical soil properties measured using proximal soil sensing technology.

The following citations are available at this time:

Ahmad Suhaizi M. S. V.I. Adamchuk, J.K. Whalen, C.A. Madramootoo, A. Biswas, F. Reumont, F.R De Le Macorra, and W. Ji. 2016. Application of Proximal Soil Sensing in predicting the spatial and temporal agriculture GHG in Eastern Canada. Agriculture, Ecosystems and Environment (to be submitted)

Ahmad Suhaizi Mat Su, Viacheslav Adamchuk, , Joann Whalen, Chandra Madramootoo, Asim Biswas, Florian Reumont, Francisco Ruiz De Le Macorra, and Wenjun Ji. 2015. Using proximal soil sensing to optimize the assessment of agricultural greenhouse gas emissions. Poster presentation. In Soil Interfaces for Sustainable Development Joint Meeting of International

Union of Soil Sciences, Canadian Soil Science Society, and Association Québécoise de Spécialistes en Sciences du Sol. McGill University, Montreal, Canada. 5-10 July 2015.

CHAPTER 6

APPLICATION OF PROXIMAL SOIL SENSING IN PREDICTING THE SPATIAL AND TEMPORAL AGRICULTURE GHG IN EASTERN CANADA

Ahmad Suhaizi Mat Su, Viacheslav Adamchuk, , Joann Whalen, Chandra Madramootoo, Asim Biswas, Florian Reumont, Francisco Ruiz De Le Macorra, and Wenjun Ji

Abstract

Stationary gas chambers are commonly used to monitor greenhouse gas (GHG) fluxes from agricultural fields. Their relatively low cost compared to other methods, such as eddy covariance towers, and their low foot print allow for replicating experiments. However, soil spatial heterogeneity poses a challenge for identifying the right location to set up these chambers. The objective of this study was to identify representative locations in monitoring GHG fluxes based on the spatial and temporal variation of soil properties measured using proximal soil sensing (PSS) technologies. Spatial variation of apparent soil electrical conductivity (EC_a) measured using DUALEM-21S, electromagnetic inductance instrument, radiometric characteristics determined using a gamma ray spectrometer, and elevation were used to delineate the field into representative areas. Nitrous oxide (N_2O), methane (CH_4) and carbon dioxide (CO_2) gas fluxes were monitored at 9 locations with two replicated chambers at each location. The gas sampling was performed 17 times at 2-week intervals through the entire 2014 growing season in a soybean field. A total of 1531 gas samples were collected and analyzed in the laboratory using gas chromatography. Fluxes were estimated using the median slope of the linear time response model. In general, organic soil exhibited greater levels of N_2O and CO_2 emissions as compared to mineral soils. However, no significant correlation was found between N_2O -N fluxes and soil moisture. The estimated CH_4 fluxes were negligible. Substantial differences in the GHG flux estimates between the two chambers at any given location was the main concern limiting the ability to develop high-quality spatial models predicting distributions of GHG across the landscape. However, it was noted that extreme soil environments recognized by the sensors correspond to extreme observations of GHG rates of emission. The most representative chamber location to represent the field GHG fluxes and emission values can be evaluated by using the means relative different (MRD).

Keywords: precision agriculture; proximal soil sensing; soil EC_a; gamma-ray spectroscopy; greenhouse gases; nitrous oxide; methane; carbon dioxide

6.1 Introduction

Sustainable agriculture promotes a balance between anthropogenic activities and environmental effects, yet optimizes profit from crop production for human benefits. Technological advancement helps to increase food per capita, despite the fact that the land to people ratio is declining. This situation strained the agriculture sector to maximize the production per unit land. Maximizing production and profits may lead to high input usage such as inorganic base fertilizers, thus, resulting in high greenhouse gas (GHG) emissions.

Agricultural land holds large carbon reserves, thus the potential for carbon mitigation and credit (IPCC, 2006). However, carbon under specific climate, soil, crop and ecosystems could trigger spatial and temporal variations. Moreover, the mitigation was often over estimated, especially when the data were estimated from only a few sites at similar locations which did not represent field spatial heterogeneity. Introduction of new government incentives and policies for certifying agricultural sustainability and ecosystem services will be crucial.

The main GHG related to agricultural soil were nitrous oxide (N₂O), methane (CH₄) and carbon dioxide (CO₂) and often reported as CO₂-equivalent. Significant factors of climate change affiliated with GHG emissions have resulted in local and international efforts in mitigation approaches (Shcherbak *et al.*, 2014; Villarino *et al.*, 2014). The trend of GHG emissions from agricultural soils showed an exponential increase. In Canada, GHG emission from agricultural soil produced about 80% direct and 20% indirect sources (United Nations Framework Convention on Climate Change). Total emissions of 8% were relatively stable for five years in a row (2005 to 2011) and counted for 68 Mt CO₂-equivalent; however, it is projected to increase by 2 Mt CO₂-equivalent for 2005-2020 (Environment and Climate Change Canada). However, despite large seasonal exchanges of CO₂ between the surrounding atmosphere and agricultural lands, the net flux is estimated to be balanced (IPCC 2007).

GHG sources from agricultural soil are often monitored using a closed chamber i.e. non steady state (NSS) chamber design, or micrometeorology using the eddy covariance method. In this paper, the NSS method is the subject of interest. Various designs of the NSS were used to monitor the GHG fluxes, including square, rectangular or cylinder shapes, relatively light weight, and following a standard design (Livingston *et al.*, 2005; Pedersen *et al.*, 2010; Rochette, 2011). The

NSS method offers simplicity in the treatment design, cost effectiveness, provides a low foot print as compared to the eddy covariance, yet offers high resolution over multi chamber replications. The inference of the overall GHG emissions measured from the small scale area often were made by up-scaling of the GHG measurements over a long term scenario and for a large area (Li *et al.*, 2010). Monitoring the GHG emission at the soil surface is not necessarily a measure of real time net soil GHG production, because GHG transport from their source site vary in time and space in response to changing soil environments. Different locations for the chamber placement can affect the rate of these processes by influencing soil temperature, soil water content, soil disturbance, barometric pressure fluctuations and root activity. Consequently, changes in soil properties during the NSS chamber deployment and measurement may bias flux estimates by altering gas production and transport processes. Therefore, one of the key ways to minimize the effect of soil variation is by considering soil spatial variation prior to chamber placement. Thus, the up-scaling method from a small area of interest may underestimate with respect to the actual rate of GHG responses.

Reported broad spectrum of GHG sources from agricultural soil can be divided into several sub sectors such as crop production fields, monoculture (Wagner-Riddler *et al.*, 2007), and perennial crops (Reijnders and Huijbregts, 2008), natural or cultivated forested soils (Sathaye *et al.*, 1995; Smyth *et al.* 2014), pasture for livestock (Rochette *et al.* 2014; McGinn *et al.*, 2014), and organic farming (Wood *et al.*, 2006). In agricultural soil, which is the focus of this study, other than microbial activities, surface soil GHG emissions seem to be co-influenced by soil characteristics related to (i) farm management activities-different types of farms e.g. organic versus conventional agriculture (Rehman, 2014), crop type, fertilization by different forms of N i.e. organic or non-organic (Eichner, 1990; Hénault *et al.*, 1998; Snyder *et al.*, 2009), irrigation effects (Lal, 2004), tillage practices (West and Marland, 2002), and a combination of all factors e.g. fertilizer, tillage and crop (Kern and Johnson, 1993; Halvorson *et al.*, 2008), (ii) available macronutrient content, such as organic matter (OM), N, and carbon (C) cycle (Eswaran *et al.*, 1993; Skinner, *et al.* 2014; Sommer and Bossio, 2014), (iii) environmental conditions, such as elevation, weather (precipitation, climate temperature and humidity), ambient pressure leads to volatilization (Weiske *et al.*, 2006) and leaching (Nikièma *et al.*, 2012), (iv) soil physical properties, such as soil moisture and temperature (Peterjohn *et al.*, 1994; Mukherjee and Zimmerman, 2014), as well as the level of water table (Berglund and Berglund, 2011).

The costs of conventional agricultural soil-gas monitoring are substantial and the reliability of the results is often limited and questionable. Commonly, soil spatial monitoring is conducted via a network of sampling points, such as grid or transect sampling (Ishizuka *et al.*, 2005 and Allaire *et al.*, 2012). Often this method does not enable reliable estimation at the field scale. Thus, alternatively, proximal soil sensing technology (PSS) was used as a quantitative method to infer spatial patterns. Such PSS measurements were apparent soil electrical conductivity and gamma ray spectroscopy. The efficacy of using PSS in relation to GHG emissions lies in an understanding of the spatial and temporal soil property variations. Because there is a limitation in sensors related to spatial soil biological activities, the measurement or estimation of soil physical properties can be done via PSS technologies. Other than biological activities, the variation in soil physical properties changed the formation of soil aggregates, pore spaces, and water content, consequently, altering the rate of the soil gas diffusion. Alternatively, understanding soil mineralogy using the gamma ray method may help in predicting GHG rates.

The use of PSS technology as a method of GHG mitigation for agriculture is a relatively new approach. Soil EC_a measurements at different times may be used to predict different levels of GHG fluxes; however, local and detailed interpretations are imperative. For instance, Allaire *et al.* (2012) used multi depths of the soil EC_a profile to investigate its co-relationship to CO₂, and found a negative correlation between CO₂ and soil EC_a. To date, there has not been a comprehensive study on the application of γ-ray spectra to actual GHG production. The closest study measured available soil carbon through a predictive approach. An early study by Macias and Barker (1978) attempted to predict bulk available oxygen and nitrogen gas in a coal sample using a gamma ray spectrometer. Along with other properties of interest, they found an indication of good correlation with more than 95 %. In contrast, recent findings on nitrogen gas by Chapyzhnikov *et al.* (2005) found no significant correlation with nitrogen gas. However, both studies achieved good correlation of gamma ray spectra of the carbon content. This may lead to better predictions of CH₄ or CO₂ emissions. Spatial and temporal interaction of the GHG and the soil physical properties also were subjects of interest. The spatial variability of soil carbon across the field can be predicted using Cesium (¹³⁷Cs) in the soil (Johnston *et al.*, 2004; Dierke and Werban, 2013). The data suggest that measurements of ¹³⁷Cs in soils can be useful for understanding carbon distribution patterns in surface soil. A few studies reported good correlation between γ-ray with texture clay content. Rodrigues *et al.* (2015) performed a combination of soil EC_a and gamma ray measurements in CEC and clay content. In addition, soil chemical properties also resulted in a very significant relationship, for instance, a strong correlation with potassium (K) (Piikki *et al.*,

2013). Bulk density and soil water content also were predicted using γ -ray measurements (Gurr, 1964). Good prediction with potassium (K) content and soil texture in the soil was found (Wong and Harper, 1999, Wong et al, 2010); however, this may not hold in all areas due to landscape heterogeneity and other soil forming factors.

The objective of this study was to identify representative locations in monitoring GHG fluxes based on field heterogeneity information using proximal soil sensing (PSS) technologies. Spatial variation of soil EC_a and γ -ray were used in delineating the field for the gas chambers at prescribed locations. Spatial soil variability within a field can be quite extensive, which means that defining representative locations for the agricultural GHG and environmental management decisions is challenging.

6.2 Materials and Methods

6.2.1 Site Characteristics

The study location, Field 26 (F26) with an area of approximately 11 ha, was located at one of the farm production areas of Macdonald Campus of McGill University, Quebec, Canada. The field was under no till practice, cultivated with soybean (*Glycine max L.*) for 2014 season, and previously grown with alfalfa (*Medicago sativa L.*) and mixed pasture for forage. During this study, the field did not receive fertilizer applications during the growing season; however, liquid manure was applied during the previous fall season. In addition to the crop and soil management, roundup herbicide was applied on two different dates: 19 Jun and 18 July 2014, after the soybeans emerged.

It was found that the variations in soil properties are mainly governed by the landscape position across the field especially related to changes in elevation. The soil at F26 was composed of a wide range of soil series and types, varying from pure muck (organic) to mineral soil, and the soil drainage ranged from excellent to very poor (Table 12). The leading soil type in this field is classified as muck soil (organic) containing a minimum of 30 % organic matter, or 17 % of organic carbon, which covers about 7.3 ha area (Canadian Soil Classification, 1998). Of the total field area, shallow and deep layers of muck soil were developed over the mineral soil layer at the north (about 29 %) and south (about 34 %) parts of the field, respectively. Muck soil regions were located at lower elevations (between 6.9 – 7.2 m above sea level) developed from plant residue (fibre) and mosses, hence, resulting in a water depression area and causing very poor drainage. The organic soil layer was about 1-1.5 m depth across field.

The remaining 37 % coverage was mineral soil, which covered from the centre and extended to the west and north-west of the field and included several mineral soil types: St. Zotique (18 % of total area), Soulanges (2.4 % of total area), Chicot (1 % of total area) and Upland (0.4 % of total area). St. Zotique soils occupied from the centre to north-west part of the field, and it provided the second largest soil type coverage after muck soil. This soil type was mainly developed from historical alluvial soil with fine silt loam with very poor drainage, located at 7.6 to 7.9 m above sea level. Due to poor drainage, these soils are commonly associated with muck and Soulanges soil types. For the latter soil type, drainage was considered to be at the moderate level. The Soulanges soils were silt loam gently undulating over the landscape (about 8.1 – 8.2 m to the west of the field). At higher elevations (8.5 – 9.0 m), there were two soil types, Chicot and Upland soils. On one hand, these soils were built up from the same basis: sand. On the other, the Chicot soils mainly build up from sandy loam soil resulting in very poor drainage. Upland soils appeared as deep deposits at the center of the field and they are well-drained soil, hence, low in soil nutrients. In between, St. Damase (about 5.5 % of the total area) located at the same elevation as Chicot and Upland soils, contains mainly light sandy loam with a similar drainage level as Soulanges soils. The Farmington soil type (about 7.5 % of total area) is a relatively dry shallow clay loam overlay over the bedrock, lightly stony soil. Further, Farmington soils area well drained soils located at the south-east of the field (high elevation 8.2 – 9.3 m). A couple of small patches of Chateauguay soils (about 1.7 % of total area) were found at the south-east and south-west sections of the field containing mainly loam soil, with a similar level of drainage as the Farmington soil type.

Despite a variation in soil types, soil texture, and drainage capability heavy and stony soil are not fully subjected to a serious handicap for cultivation since there is a conventional tile drainage system installed and stretched from the top to the bottom of the field to facilitate drainage and improve crop production. The tile drainage was installed mainly at the lower elevation, where very poor soil drainage occurred (Figure 8d).

The humid continental climate of this area is characterized by a variation in both temperature and precipitation typical of the eastern Canada region. For 2012 to 2014, recorded total daily precipitation (mm) along with other weather parameters were retrieved from Sainte-Anne-De-Bellevue, QC, Canada, weather station, located about 0.6 km from the F26 field, as shown in Figure 23. Average ambient temperature in 2014 was about 18 °C in the gas sampling period. Recorded precipitation events from the nearby weather station measured a total of 825 mm of

rain in 2014 (Figure 24), higher than the average 171 mm in the two previous years. The range of precipitation varied in intensity from 0.2 to 49.4 mm, with an average of about 8 mm. About 252 mm of rain occurred within the gas sampling events, with heavy rains occurring prior to the sampling dates on 3 June and 24 June 2014 with about 46 and 49 mm of water, respectively.

Soil samples at the same location were collected and geo-referenced with RTK GPS on 12 May 2014, before planting using the standard soil probe at 0–20 cm depth, using a stratified random sampling scheme based on soil EC_a distribution maps. The five sub samples per location were homogenized to become one sample. Each sample was placed in the soil bag and marked with the sampling location ID for the lab soil physical and chemical analysis. The particle size distribution was analyzed by gravitational sedimentation using a hydrometer, after organic matter oxidized by hydrogen peroxide, air dried at 105°C and passed the fine components through a 2 mm sieve. Soil pH was determined using a 1:5 soil/water ratio with a compound glass electrode (Si *et al.*, 2007). The 2014 yield of soybeans at F26 was harvested using a combine harvester (TR87, New Holland Agriculture, Turin, Italy) in late November 2014. Average yield recorded via the combine yield monitoring system resulted in an average of 2.4 t/ha at 13 % moisture content.

Table 12. Wide range of soil series and its characteristic at F26

Legend	Soil series	Soil texture	Water holding capability	Drainage
A	Muck (organic)	Fibres, mosses,	High	Poor
B	St. Zotique	Fine silt loam	Very high	Very poor
C	Soulanges	Silt loam	Moderate	Moderate
D	Chicot	Sandy loam	High	Very poor
E	Upland	Sand	Poor	Very good
F	St. Damase	Light sandy loam	Moderate	Moderate
G	Farmington	Clay loam	Poor	Very good
H	Chateauguay	Loam	Poor	Very good

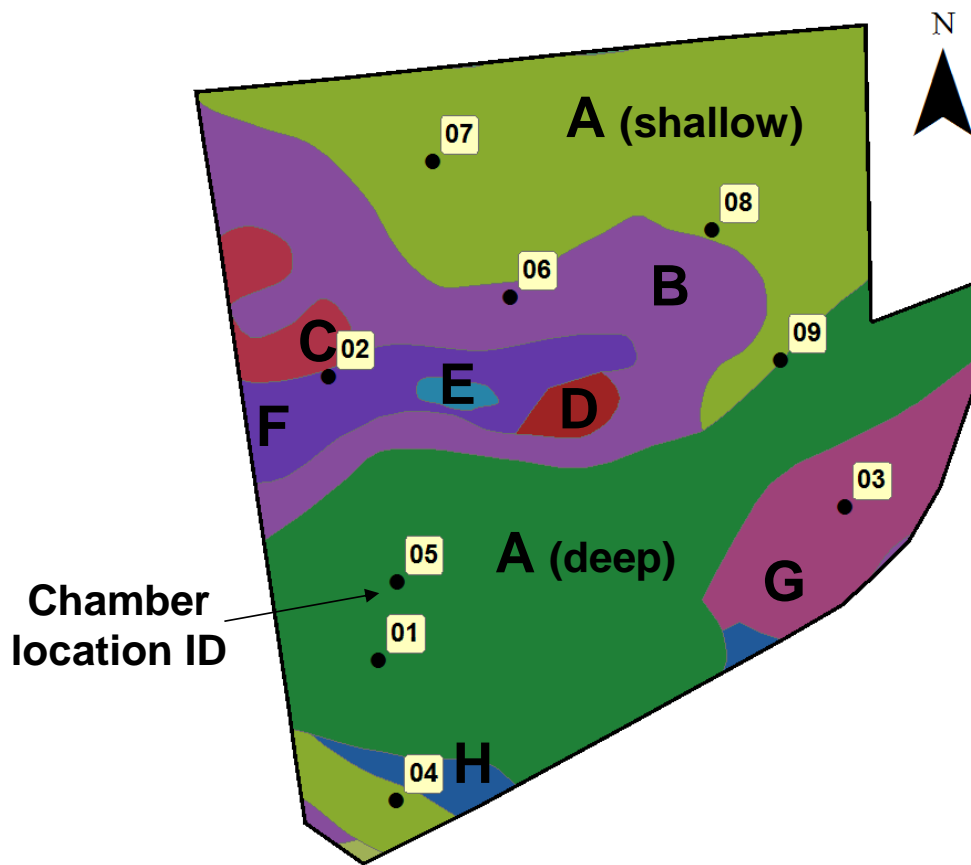


Figure 23: Soil series map ranged from organic to mineral soil located at F26 (Soil Canada Survey Map, 1971). The letters is the legend as explained in Table 12

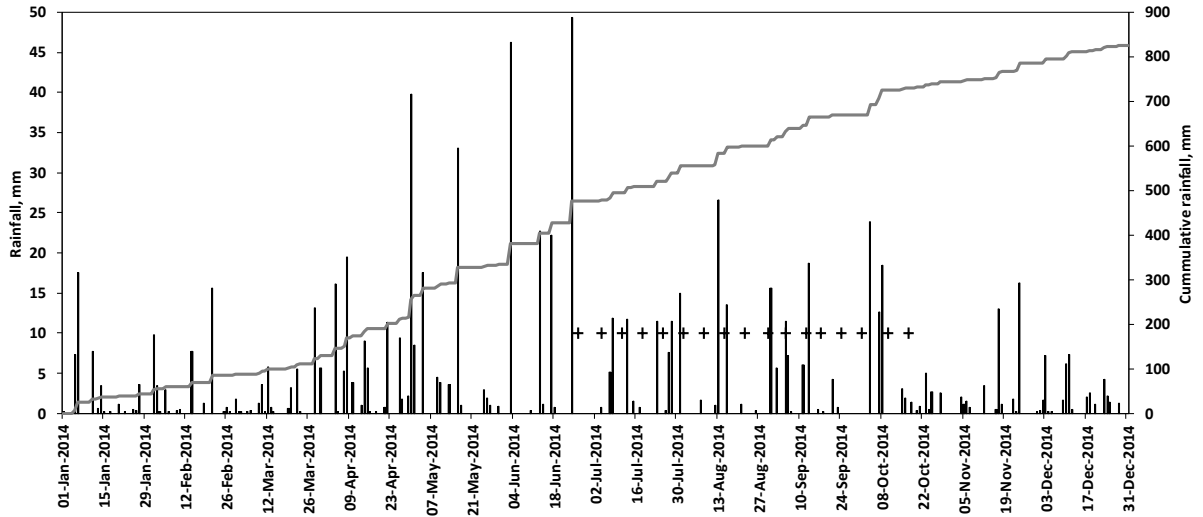


Figure 24: Precipitation data of 2014 at F26. The respective sampling date was marked as "+"

6.2.2 Field Survey

To acquire high resolution soil EC_a , the DUALEM-21S (Dualem, Inc., Milton, ON, Canada) instrument was used to characterize the spatial heterogeneity of soil EC_a data, surveyed on 13 October 2013 as shown in Figure 25. On this date, the soil at F26 was at field capacity with an average daily ambient temperature about 14°C. The on-the-go surveys were conducted at travel speeds of approximately 5 km/h at an average 12 m swath width, which resulted in about 5023 measurements. Elevation was obtained using the RTK GNSS receiver (Trimble RTK/PP-4700 GPS, Trimble Navigation Limited, Sunnyvale, CA, USA) and the data was recorded at 1 Hz using the preprogrammed LabVIEW software (National Instrument, Inc., TX, USA). Although the soil EC_a included two sets of measurements: 1 and 2 m of horizontal co-planar (HCP) and perpendicular co-planar (PRP), only the latter mode of measurements was used and focused in relation to the GHG analysis since the gas productions were related to the top soil layer (0.54 and 1.03 m, respectively) as was discussed in Chapter 3.

In addition to the soil EC_a survey, a formation and distribution of soil mineralogy of F26 was also derived by a passive sensor, the SoilOptix™ sensor (Practical Precision, Inc., Ravistock, ON, Canada) deployed in F26 on 18 November 2013, at a daily average ambient temperature of 7.6°C (Figure 25). A total of 6245 high resolution γ -ray spectra data paired with the RTK GNSS were measured during the on-the-go survey. The data were acquisitioned using proprietary software supplied with the sensor at 1 Hz (Table 13).

Table 13. Gamma ray specifications

Parameters	Value
Radiation sensor	40 cm x 15 cm dim. CsI crystal detector
Weight	~5 kg (approximate)
Channel	512 MCA
Power	12V DC
Measurements, (Bq/kg)	Total Count, ⁴⁰ K, ²³⁸ U, ²³² Th, Cs
Communication	Ethernet / serial connectivity
Data rate	1 Hz

A γ -ray emission detector made from Caesium Iodine (CsI) crystal attached to a photomultiplier at 512 channel multi-channel analyzer (MCA) was utilized to predict the concentration of γ -ray emission (Loonstra and van Egmond, 2009). The sensing unit was mounted in front of the ATV, 0.5 m off the ground. The average travel speed was about 6.2 km/h at about 11 m swath width (Figure 25). This sensor measured the natural radioelement concentrations decay from the γ -ray energy emitted by the soil and rocks at the top soil profile (0-30 cm). The decay energy was captured by the photomultiplier measured in the unit of Becquerel per kilogram (Bq/kg) to predict the concentration of γ -ray emission radioactivity, mainly the total radiometric count or total count (TC), potassium (⁴⁰K), Uranium (²³⁸U), Thorium (²³²Th), and Caesium (¹³⁷Cs). The response of the γ -ray was measured using the full-spectrum analysis method (Van Egmond *et al.*, 2010).

6.2.3 Gas Sampling and Flux Analysis

Spatial and temporal variations of GHG fluxes were characterized at F26 from nine locations with a total of 18 chambers (two duplicated chambers per location) using a square, non-steady state (NSS) chamber design, deployed during the growing season (June to December 2014). The nine locations were selected to maximize D-optimality criterion for both EC_a and TC as well as field elevation (similarly to Adamchuk *et al.*, 2011b). This way gas chambers represent the most unique PSS measurement combinations that exist in this field. Gas chambers were positioned between soybean rows with base (bottom square collar) dimensions of 0.556 x 0.556 x 0.140 m, and the top cover (0.564 x 0.564 x 0.130 m) was vented with a small air channel of 0.05 m clear polyvinyl tube to avoid pressure perturbations (Figure 26). The chamber was a customized design built from sturdy PVC materials, and protected with an aluminum sheet to minimize the temperature effect from sunlight to the gas inside chamber (Rochette and Eriksen-Hamel, 2008).

A simple white soft cushion tape was taped along the cover and base contact surface acted as a seal for the chamber system from air leaks.

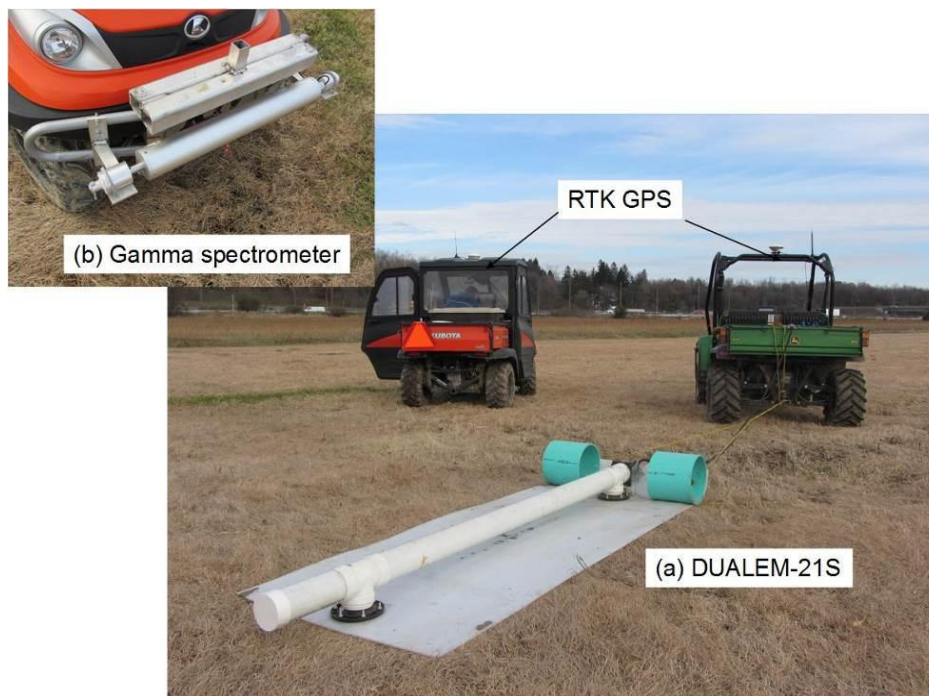


Figure 25: Proximal soil sensing survey (a) DUALEM-21S and (b) Gamma ray spectrometer.



Figure 26: Non-steady state chamber design deployed between soybean crop, covered with aluminum sheet to minimized the effect direct thermal from the sun.

The chamber base was preinstalled at the beginning of the season, and gently pushed down with approximately 10 cm remaining above the soil surface. This provided an average of effective

total height of 0.23 m. The effective height is the most crucial parameter in linear flux and emission estimation using the NSS method. Other than being used as a marking location, the installation of the base at the beginning of the season is important to avoid direct disturbance of the soil, crop and the root system from interfering with repeated gas sampling measurements. The location of the chambers is also considered for in-farm traffic activities. Over the season, the weeds were minimal and left in their natural state, if present on the inside of the chamber.

The gas samples were taken at 15 min intervals for an hour total duration. The gas samples were extracted from the chamber headspace using a 20 ml gas exetainer, transferred using tight syringes. All samples were then injected into pre-evacuated or vacuum exetainers of 12 ml (Labco, Wycombe, UK) fitted with an extra 60 mil (60 mil equal to 1/16 in or 0.0625 in) Teflon-silicon septa (National Scientific, Rockwood, TN, USA), and then stored in cool conditions. Samples were brought immediately to the Soil Ecology Research Laboratory of Macdonald campus, McGill University, and analyzed for the three main trace GHG gases: N₂O, CH₄ and CO₂ concentrations using customized Bruker-Varian 450 gas chromatograph (GC) (Bruker, Bremen, Germany). As a result, a total of 1531 gas samples were collected from 17 sampling dates using NSS chambers, when bi-weekly measurements were performed between 12 noon to 7 p.m. The first gas sampling followed three weeks after seeding and roundup herbicide application. All sampling locations were geo-referred with RTK GPS with a precision of about 1 mm accuracy.

Fluxes were determined from the median slope of the linear regression model of the mixing ratio change with five sequential samples measured at 0, 15, 30, 45, and 60 min after chamber closure. 1-D array interpolation was imposed to estimate the in-season emission as explained in Chapter 4. The median slope method is superior to the typical average method as it allows for disregarding the outliers dataset, if the dataset contains erroneous measurements. Full automatic fluxes and emissions estimations were made via the MATLAB scripts. This approach allows for large batch data processing and took, on average, about 60 seconds (64-bit, Window 7 operating system) to produce the summary results. The reported flux and emission of the GHG were made in base gas species such as N₂O-N, CH₄-C and CO₂-C. The minimum detection limit of the GC for the measured gas was measured by using the standard 0.15, 0.17 and 300 ppm for N₂O, CH₄ and CO₂, respectively. These minimum values were set as the minimum threshold values during data processing, and any value below would be disregarded.

Simultaneous soil temperature and moisture measurements at 0 – 30 cm from the soil surface were made at the time of gas sampling at all individual gas chambers. Time domain reflectometry

(TDR) moisture sensor (Model: HH2, Delta-T Devices Ltd., Cambridge, United Kingdom) was used to record the moisture variations in terms of volumetric water content (%), and a single thermocouple probe sensor (Model: HI98509, Hanna Instrument, Rhode Island, USA) measured the soil temperature levels in degree Celsius (°C). An average value of a minimum of three measurements at each chamber location was used, and manually recorded in the log book. The measurements were calibrated for the specific mode, soil mineral and organic soil type, prior to the field work.

6.2.4 Data Analysis

Spatial and temporal variation of soil properties and GHG fluxes were analyzed in two stages. In the first stage, to allow for a comparison of the measured sensors' survey, the data obtained were synchronized using the same geographic coordinates of the nine sampling locations using an average value within a 5x5 m grid. The estimation procedure was achieved after each of the survey sensors data were interpolated using ordinary kriging conducted using ArcGIS software. Then, the predicted value of the soil properties was matched with the sampling IDs. As a result of the 5x5 m grid, about 4468 of the same geo-coordinates were created. A spatial analysis clustering method was used principally by finding the distance where spatial correlation was strongest.

The second stage involved the statistical analysis conducted to evaluate the findings. The estimated soil EC_a, gamma ray, and elevation were used as a single value and repeated over the temporal data (GHG, and soil temperature and moisture). All data in the nine locations, including temporal GHG fluxes from two replicated chambers at each location, were subjected to linear correlation analysis, carried out using 17.0 SPSS Statistic (SPSS Inc., Chicago, IL, USA) to obtain the basic descriptive statistics and Pearson correlation coefficient (r) using the method of minimum squares ($p < 0.05$). Due to the fact that the data distribution was not normal for the GHG fluxes, the non-parametric pair-wise comparison was used to compare the effect of fluxes on two different soils (i.e. organic versus mineral soil base on average value). Stepwise multi-linear analysis was performed for the GHG emissions prediction for each chamber using measured soil physical properties.

6.2.5 Representative monitoring locations (RML) for the GHG fluxes

The only limitation of the chamber numbers to be installed across the soil for spatial variation depends upon the (i) total sampling locations, (ii) duration of the sampling, and (iii) availability of

the chambers. The nine locations were chosen based on the optimality of the sampling locations, where the PSS technologies helped in delineating the field into the corresponding soil heterogeneity. Finding the representative locations would not be feasible without the knowledge of on-the-go mapping of high resolution soil spatial variations. Secondly, logistically, the total number of chambers to be installed reflected the total duration of the sampling procedure, where the gas sampling activities were conducted during diurnal time. Therefore, for all of the gas chambers to be within appropriate walking and sampling times during the growing season, this limits the optimal number of chambers.

In reporting the GHG fluxes or the overall field emission, the RML must be selected among the located chamber to represent a single value of field GHG emissions. Representative locations are defined as the locations of the chamber where measure GHG fluxes either are close to the average fluxes or a combination of chambers transformed to obtain such averages (Vanderlinden *et al.*, 2012). Several methods were proposed to define the representative location. The simplest method is to use the location with the means relative different (MRD) closest to zero (Vachaud *et al.*, 1985). The used of MRD was first was introduced to monitor seasonal and annual variation of the soil water content, which is the same behavior with the GHG fluxes.

There are two steps to characterize the temporal stability (TS) as described in Vanderlinden *et al.* (2012). The first step, the MRD was calculated of all observations made during the sampling periods. The second step used a multiple pair of observation times and calculates the similarity in the spatial patterns between those times. Non-parametric Spearman rank correlation is one of the most commonly chooses (Vachaud *et al.*, 1985) to compare fluxes at two different observations times. Spearman rank correlation was established to rank of the temporal observation. The second method uses the combination of times and calculates the similarity in the spatial patterns between those times. More details of some other methods in identifying MRD are given by Vanderlinden *et al.* (2012) and Biswas (2014).

Briefly, if the GHG fluxes at i^{th} location and t^{th} date is $f_{i,t}$ and the spatial mean GHG fluxes is \bar{f}_t from the same chamber ID, the different (Δ) between individual determinations is

$$\Delta_{i,t} = f_{i,t} - \bar{f}_t \quad (12)$$

The spatial mean GHG fluxes was calculated from

$$\bar{f}_t = \left(\frac{1}{n} \right) \sum_{i=1}^n f_{i,t} \quad (13)$$

Where n is the number of measurement from the total chamber ($n=18$). Then the relative difference, $\delta_{i,t}$ was calculated as

$$\delta_{i,t} = \frac{\Delta_{i,t}}{f_t} \quad (14)$$

The relative difference provides an estimation of difference that is unbiased to the magnitude of the mean value. The temporal MRD was calculated as

$$\delta_i = \left(\frac{1}{m} \right) \sum_{t=1}^m \delta_{i,t} \quad (15)$$

where m is the number of sampling days (in this case $m = 17$). The standard deviation of mean relative different (SDMRD) as

$$\sigma(\delta_i) = \sqrt{\frac{\sum (\delta_{i,t} - \bar{\delta}_i)^2}{m-1}} \quad (16)$$

Thus, each location will have one MRD value and its associated SDMRD. The MRD values are then sorted from the smallest to the largest to identify the RML, which has the MRD closest to zero and smaller SDMRD. The MRD value can be positive or negative, which corresponds to the underestimated or overestimation, respectively. As RMLs identification approach, Jacob *et al.*, (2004) proposed to select the lowest of the root mean square error (RMSE) which can be calculated from combination of MRD and SDRD as;

$$RMSE_i = \sqrt{MRD_i^2 + SDMRD_i^2} \quad (17)$$

Finding the only one site to be representative with small MRD and SDMRD can be quite challenging, and the results may not end up at the same chamber ID number for separate GHG fluxes. This is similarly being reported by Tallon and Si (2003) for soil water content study. The SDMRD indicates the

$$MRD_{Abs} = |\delta|_i \quad (18)$$

6.3 Results and Discussions

6.3.1 Descriptive Statistics

Data distribution of the on-the-go soil physical properties mapping activities and geostatistical study was described using classical descriptive statistics (Table 14). Elevation variation measured using RTK GPS resulted in 7.64 ± 0.57 m (mean \pm STD) at about 7 % of the coefficient of variation (CV). An increase in soil EC_a was observed with depth, where HCP measurements were higher than PRP. The PRP measurements were the most stable with low SD of the soil EC_a survey (SD is 6.97 mS/m for PRP 1.1 m, and 11.56 mS/m for PRP 2.1 m). Thus, the overall range HCP 2 m measured in 2013 averaged 14.99 mS/m and had the highest CV (61 %). CVs from the on-the-go soil physical mapping indicated a potentially significant spatial variability and suggested defining different field soil zone heterogeneity.

Table 14. Descriptive statistics of the 5x5 m data on-the-go measurement; SD, standard deviation; CV, coefficient of variation; N = 4467.

Variable	Mean	Median	SD	Min	Max	CV (%)	Kurtosis	Skewness
Elevation, m	7.64	7.41	0.57	6.72	9.27	7.42	0.12	1.12
2013 HCP 1 m	25.27	25.74	11.68	3.67	50.98	46.23	-1.28	0.02
2013 HCP 2 m	25.42	25.43	14.16	2.64	52.04	55.69	-1.40	0.03
2013 PRP 1 m	16.61	16.83	6.97	1.51	35.24	41.94	-0.86	0.13
2013 PRP 2 m	23.09	23.65	11.56	1.36	49.24	50.08	-1.25	0.00
TC	308.32	315.70	53.83	152.96	434.76	17.46	-0.02	-0.52
⁴⁰ K	260.64	252.46	106.47	26.77	509.45	40.85	-0.88	-0.02
²³² Th	16.40	16.65	4.99	1.53	28.70	30.46	-0.34	-0.23
²³⁸ U	13.16	12.94	3.40	0.71	27.42	25.84	0.26	0.28
Yield	2.44	2.49	0.85	0.44	3.79	34.79	-1.08	-0.24

With respect to the soil mineralogy, ⁴⁰K was the predominant property resulting in an average of 261 Bq/kg, and with the highest SD (106 Bq/kg); ²³²Th, ²³⁸U and TC constituted an average of 16, 13 and 308 Bq/kg, respectively. The later measurements resulted in the lowest CV (17 %) among the γ -ray sensing measurements. The field average yield of soybeans was at 2.4 t/ha, ranging from 0.44 to 3.79 t/ha. For mineral soils, a low count number was observed on a high percentage of sand content since the soil characteristic tended to have a leached profile, as similarly reported by Mahmood *et al.*, 2011. Good correlations between radionuclide data and

different soil properties suggest a potential role of gamma-ray spectroscopy in soil property mapping.

For all proximally sensed soil physical properties, including responses such as yield, mean and median values, they were very similar, which indicated that the data were derived from a normal distribution. This was supported by the fact that low skewness values were obtained; in addition, coefficients of kurtosis were under 3 (standard data normal distribution). This information is important in geostatistical and clustering analyses using the procedure as discussed in the methodology method.

Table 15 shows the actual variation at different locations of sampling IDs. High variation of OM (overall average = 308 g/kg and SD = 256 g/kg) in the soil indicated the field varied in landscape positions. Different average OM between organic and mineral soils was close to 80 %. Average soil EC_a in organic soil was about 61 – 66 % higher than in mineral soil for both years. The TC of the γ -ray emissions also varied between sampling location with an average TC about 303 Bq/kg at SD = 85 Bq/kg. Average ⁴⁰K was about 265 Bq/kg with the highest variance (SD = 160 Bq/kg), and with a similar average between ²³⁸U and ²³²Th. However, there was slightly higher SD in the later measurements. Average TC in organic soil was 53 % lower than mineral soil. More than double average ²³⁸U emissions were found in mineral soil as compared to organic soil. However, there was no difference in average ²³²Th emissions from both soil types. Top soil clay content varied from 52 - 350 g/kg, and sandy soil ranged from 272-624 g/kg. Respective overall average clay and sandy soil content was 184 and 448 g/kg, with similar variations. Clay content in organic soil was higher by about 32 % than mineral soil. In contrast, the sand content in organic soil was less by 19 % than mineral soil. The elevation difference was about 0.8 m from the lowest to the highest location with average and SD elevation of 7.69 ± 0.75 m. The lowest part of the sampling location in the field was at 6.92 m. only 13 % difference in average elevation between organic versus mineral soil locations. This variation varied the soybean yield by an average of 2.32 ± 1.02 t/ha, with only 6 % difference between yield under organic vs. mineral soil. The soil pH was slightly acidic and alkaline, drifting from the neutral line and ranging from 5.85 to 7.51 ± 0.61. As expected, the soil pH in organic soil was lower than in mineral soil; however, the average soil pH indicated only 6 % difference. Other macronutrients also show great variations. Average P, K and Al were higher in mineral soil as compared to organic soil, 163, 134, 637 mg/kg, and 85, 128, and 334 mg/kg, respectively. However, average Ca and Mg is about 58 % higher in organic than in mineral soil.

Table 15. Descriptive statistic of soil EC_a, gamma ray measurement, and other soil properties measured at all 9 locations.

Parameter	HCP 1 m	HCP 2 m	PRP 1 m	PRP 2 m	Total Count	40K	238U	232Th
	2013, mS/m				Bq/kg			
Minimum	8.14	4.70	5.14	6.03	166.87	28.10	4.79	3.85
Median	27.71	29.59	16.44	26.88	309.31	319.12	13.63	17.98
Maximum	42.74	49.14	31.13	41.19	425.52	459.93	23.07	22.41
Average	25.00	24.43	17.02	23.18	303.80	264.57	14.12	15.03
SD	14.37	16.46	9.22	14.31	84.74	160.30	4.91	6.98
Parameter	Clay	Sand	Silt	OM	K	Ca	Mg	Al
	g/kg				mg/kg			
Minimum	52.40	271.71	214.86	54.71	56.00	1460.00	190.00	186.00
Median	223.52	455.86	387.48	183.50	114.00	5930.00	779.00	511.00
Maximum	350.26	623.75	647.18	728.25	266.00	10700.00	1700.00	1082.00
Average	184.08	448.29	367.64	308.19	131.44	5647.78	876.11	502.67
SD	100.12	105.90	134.46	256.31	58.26	3085.61	483.54	262.33
Parameter	Elevation, m	pH	Yield, t/ha	P mg/kg				
Minimum	6.92	5.85	1.00	51.23				
Median	7.44	6.51	2.27	115.66				
Maximum	9.12	7.51	3.60	249.68				
Average	7.69	6.69	2.32	128.35				
SD	0.75	0.61	1.02	63.99				

SD = Standard deviation, N = 9 sampling points

6.3.2 Locating the Gas Chambers

The accuracy of the chamber placement over the selected locations as a representative area for the GHG monitoring sites were evaluated based on the coefficient of determination (R^2) between measured soil spatial properties (Figure 27). Spatial heterogeneity of the soil EC_a along with gamma ray and elevation were used to define the targeted locations for the GHG chambers. Soil EC_a variations were mainly governed by the landscape position. Soil EC_a at PRP 1 m and 2 m modes measured in 2012 and 2013 were used since the presented soil EC_a were measured at top soil profiles, 0.54 and 1.03 m from the soil surface, respectively. These profiles were considered since GHG fluxes were mostly produced within the sub meter soil depth. Respective R^2 between elevation versus total count of gamma ray and 2013 soil EC_a at PRP 1 m mode was 0.32 and 0.64 for gas chamber location, and 0.34 and 0.50 for all locations (Figure 27a and 27b) respectively. In addition, the R^2 between 2013 soil EC_a at PRP 1 m mode vs. total count of γ -ray was $R^2=0.69$ for gas chamber locations and $R^2=0.37$ for all locations (Figure 27c).

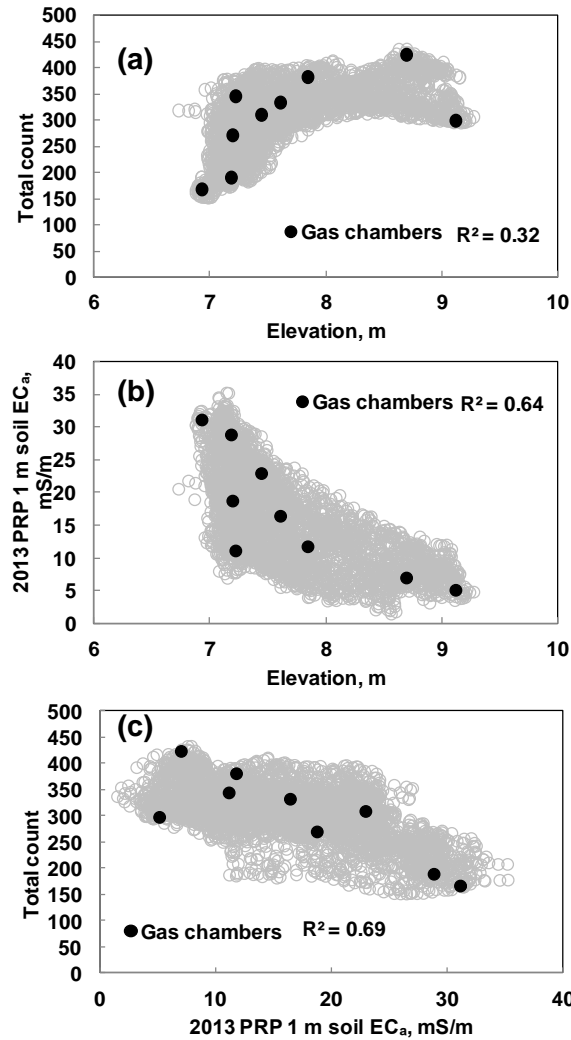


Figure 27: Comparison of the R^2 between various field measured on-the-go soil physical properties; Elevations vs. (a) total count of the gamma ray and (b) 2013 soil EC_a at PRP 1 m mode; and (c) 2013 soil EC_a at PRP 1 m vs. total count of gamma ray.

The field measurements were interpolated using ordinary kriging method in ArcGIS to share the same coordinate locations based on 5x5 meter grids as shown in Figures 28 and 29. These maps indicated the spatial heterogeneity of the measured properties was strongly correlated with the field elevation. The actual values of the PSS measurements and other soil properties are presented in the summary table (Table 16) and according to different soil textures (Table 17).

Table 16. Actual data set at 9 sampling locations

Sampling ID	HCP 1 m	HCP 2 m	PRP 1 m	PRP 2 m
	<i>2013, mS/m</i>			

01*	38.71	31.05	31.13	38.23				
02	9.96	9.19	5.14	7.18				
03	8.14	4.70	7.02	6.03				
04	14.17	9.55	11.78	12.57				
05*	42.74	41.52	28.85	41.19				
06	31.11	35.71	16.44	27.62				
07*	27.71	29.59	18.76	26.88				
08*	41.62	49.14	22.95	38.38				
09	10.82	9.44	11.15	10.58				
Sampling ID	Total Count	⁴⁰ K	²³⁸ U	²³² Th	Clay	Sand	Silt	OM
	<i>Bq/kg</i>				<i>g/kg</i>			
01*	166.87	28.10	11.71	4.81	233.42	365.00	401.58	632.70
02	299.25	374.21	4.79	17.98	130.29	623.75	245.96	77.65
03	425.52	459.93	23.07	21.77	256.00	464.51	279.49	74.92
04	385.27	438.35	12.47	22.41	241.77	488.93	269.30	54.71
05*	190.16	55.02	13.04	3.85	87.93	455.86	456.20	728.25
06	333.73	319.12	13.63	18.78	52.40	560.13	387.48	178.83
07*	271.78	152.94	16.95	10.30	223.52	369.81	406.67	505.15
08*	309.31	207.38	14.65	18.65	350.26	434.88	214.86	337.97
09	352.30	346.08	16.79	16.72	81.11	271.71	647.18	183.50
Sampling ID	Elevation, m	pH	Yield, t/ha	P	K	Ca	Mg	Al
				<i>mg/kg</i>				
01*	6.92	6.90	1.23	78.32	108.00	10700.00	1700.00	206.00
02	9.12	5.85	2.24	140.05	56.00	1460.00	190.00	1082.00
03	8.69	7.35	1.00	99.71	124.00	3600.00	622.00	461.00
04	7.84	7.37	2.27	115.66	112.00	2860.00	598.00	511.00
05*	7.18	6.11	1.15	51.23	112.00	9400.00	1530.00	186.00
06	7.60	6.30	2.64	210.63	114.00	3600.00	575.00	517.00
07*	7.19	6.31	3.51	87.67	171.00	7280.00	1090.00	402.00
08*	7.44	6.51	3.60	122.19	120.00	6000.00	801.00	543.00
09	7.22	7.51	3.28	249.68	266.00	5930.00	779.00	616.00

* = organic soil

Table 17. Average of measured properties under organic and mineral soil.

Soil type	HCP 1 m	HCP 2 m	PRP 1 m	PRP 2 m	Clay	Sand	Silt	OM
	<i>2013, mS/m</i>				<i>g/kg</i>			
Organic	37.69	37.82	25.42	36.17	223.78	406.39	369.83	551.02
Mineral	14.84	13.72	10.31	12.79	152.31	481.80	365.88	113.92
Soil type	Total Count	⁴⁰ K	²³⁸ U	²³² Th				
	<i>Bq/kg</i>							
Organic	234.53	110.86	14.09	9.40				
Mineral	359.21	387.54	14.15	19.53				
Soil type	Elevation, m	pH	Yield, t/ha	P	K	Ca	Mg	Al
				<i>mg/kg</i>				
Organic	7.18	6.46	2.37	84.85	127.75	8345.00	1280.25	334.25
Mineral	8.09	6.88	2.29	163.15	134.40	3490.00	552.80	637.40

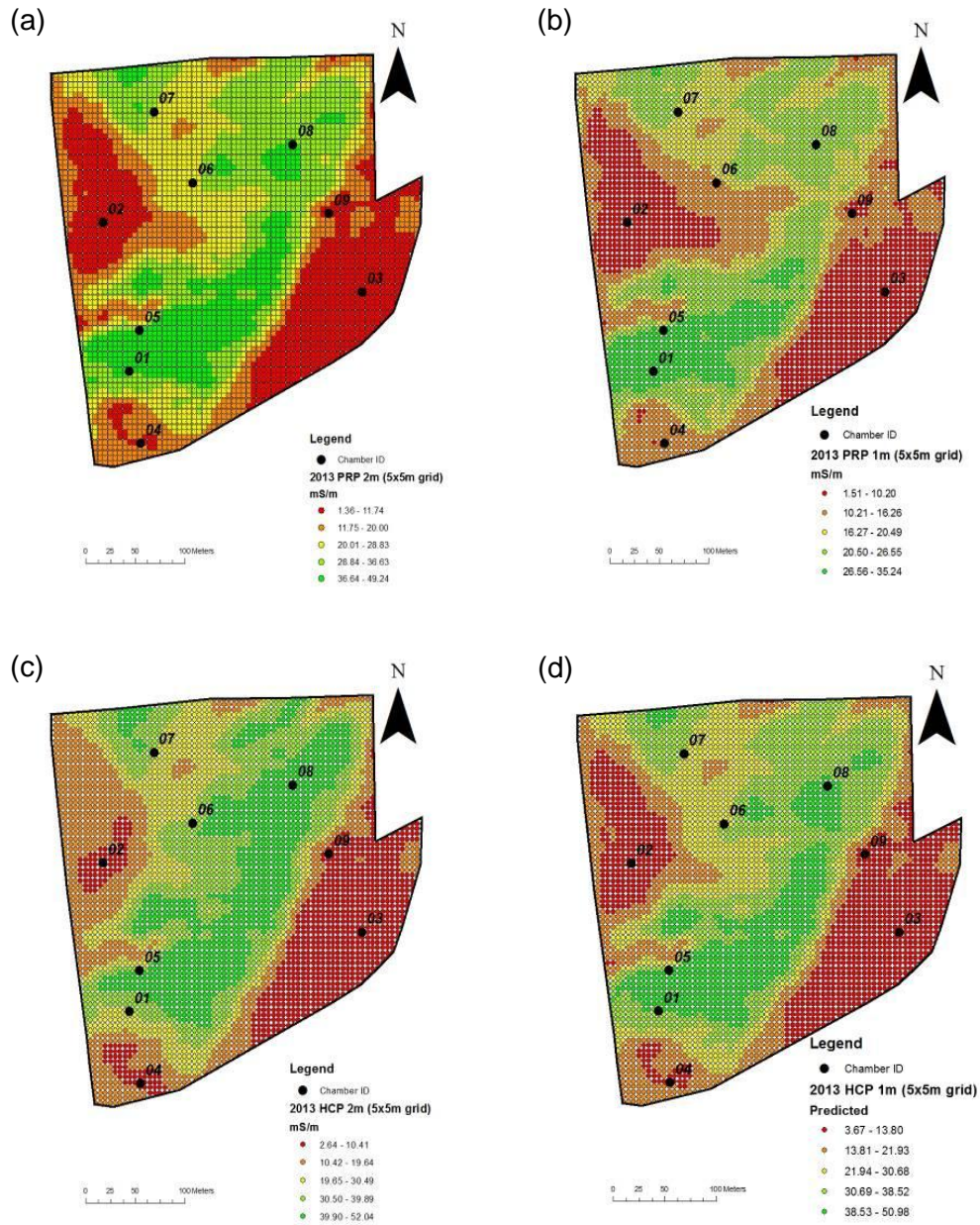


Figure 28: The 5x 5 m grid of soil physical properties measured using on-the-go system; 2013 soil EC_a measured on different configuration of (a) perpendicular 2 m, (b) perpendicular 1 m, (c) horizontal 2 m, and (d) horizontal 1 m

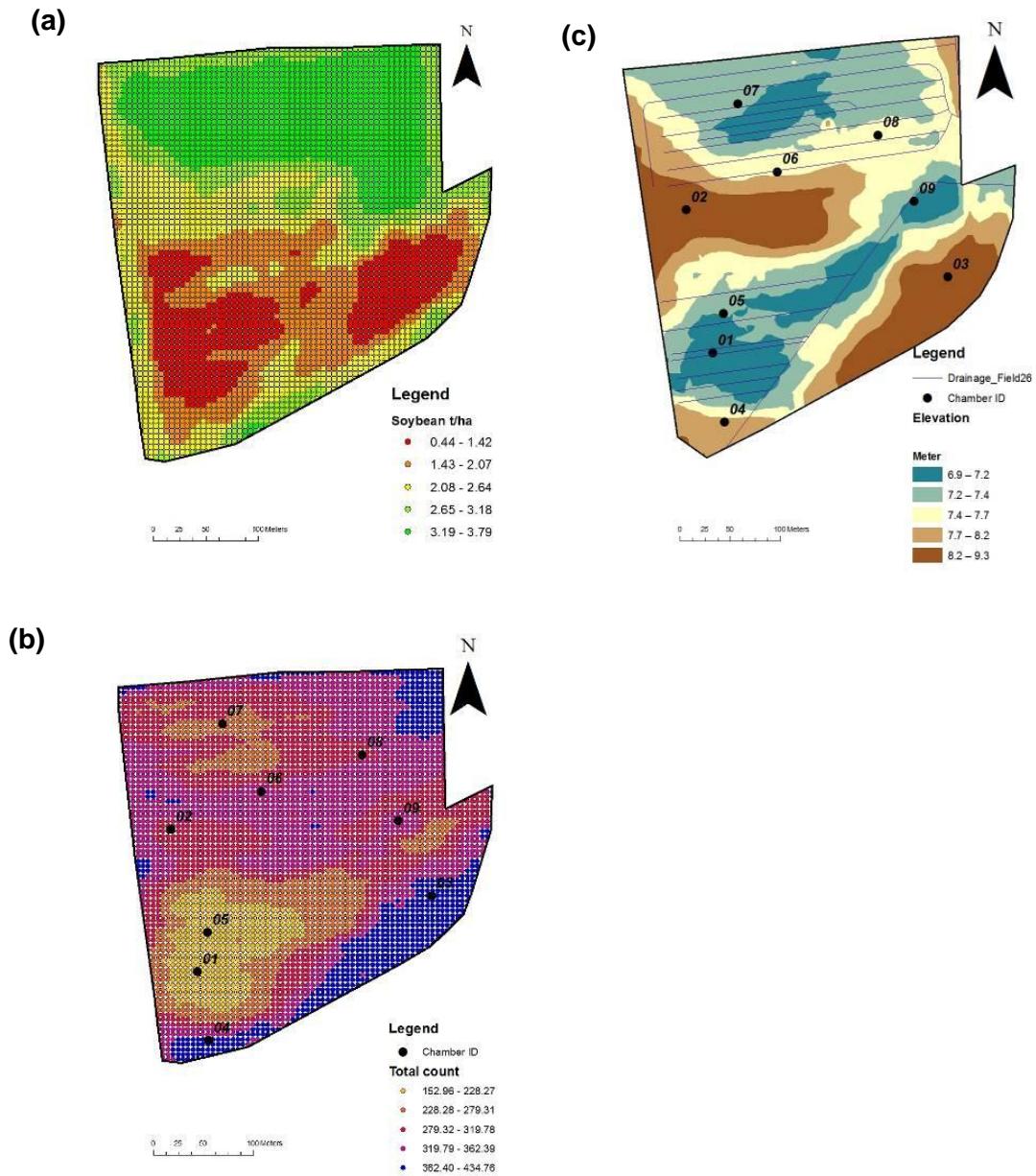


Figure 29: The 5x5 m grid of (a) the soybean yield (t/ha) measured using yield monitor on the combine harvester, (b) Total count of gamma ray signal, and (c) Elevation and irrigation line map of F26. The conventional sub-irrigation stretched from east to west of the field mainly at the depression area at sub meter depth, spacing approximately from 6-30 m apart.

6.3.3 GHG flux and emission

In general, soil moisture and temperature measured at all gas chambers were mostly stable and cooler towards the end of the growing season (Figure 30-31). There was a clear break at 40 % moisture level between organic soil and mineral soil. The soil moisture was higher in organic soil (46.46 ± 17.20 %) than mineral soil (33.00 ± 9.00 %); however, the temporal pattern of soil moisture maintained a stable level throughout the growing season. Meanwhile, the soil temperature (Figure 32) under mineral soil was slightly warmer than in organic soil with respective variation of 23.00 ± 6.00 °C and 21.72 ± 4.96 °C. The soil temperature was relatively stable over the season until it reached the lowest point between 8–10°C towards the end of the growing season for both soil types. Soil moisture and temperature data were missing for the 4th of July 2014 (for chamber IDs 5, 11, 12, and 14), on 15th August 2014 (all chambers) and on 12th September 2014 (all chambers).

All GHG exhibited a large variation both temporally and spatially. Figures 32, 33 and 34 show the different GHG variations under different soil conditions for each gas chamber. In addition, Figure 35 summarizes the estimated total in-season GHG emissions. The GHG uptake mostly occurred at the beginning of the growing season. Over, the growing season, high spatial variation in soil temperature, with a seasonal variation between 9–36°C may affect the soil respiration both from the microbial and plant root respiration. The prescribed locations for the GHG monitoring sites were able to monitor the gas responses from a wide range of soil textures, especially when dealing with variations in soil types (i.e. organic and mineral soil). Each GHG gas showed great variations both temporally and spatially, similar to other auxiliary measurements. This is due to soil moisture, temperature variations, farm management and soil texture.

Table 18 shows the linear Pearson correlation between estimated fluxes and the other field measured soil properties. The average estimated diurnal N₂O-N emission production was about 49 % higher in organic soil than in mineral soil with about 0.068 ± 0.31 mg·m⁻²·h⁻¹ and 0.026 ± 0.067 mg·m⁻²·h⁻¹, respectively. Linear analysis of Pearson correlation indicated no significant relationship between N₂O-N fluxes and all measured soil properties. Low N₂O-N fluxes response are mostly affected by the total available organic N in the soil. Since F26 was cultivated with soybeans, the crop itself fixing N from the air, and the field was not fertilized except with liquid manure during the fall of the previous year. In addition, the decreased response towards the end of the season may be due to the crop starting to dry out and ready to be harvested. From the

correlation analysis, there were no measured soil physical properties correlated with the N₂O-N fluxes. However, the average of the total N₂O-N emissions from the chambers located on organic soil was considerably higher than on mineral soil, 0.841 g/m² and 0.174 g/m², respectively.

The key factors that derive the spatial variations of the GHG emissions were due to different level topography and soil pH. Soil pH is the master soil chemical property governing N₂O-N fluxes, however the lab data indicates the field was relatively at neutral level between pH6-7. This is particularly true when the lab measured soil pH indicated that higher N₂O-N fluxes were found in organic soil than in mineral soil. The organic carbon content of the ploughed layer is an important soil feature, which regulates many soil functions. For instance, the N₂O-N fluxes (Figure 33) show great variation with respect to different soil water content, soil texture (organic vs. mineral) and timing. The field received no additional irrigation, and the main source was from natural rainfall. Thus, regular rainfall naturally stored water and increased the soil water content. Heavy rain and more frequent raining events significantly increased the soil water content in the soil at the beginning of the season. Therefore, some of the GHG locations emitted higher GHG levels at the beginning of the season than later in the season. In addition, due to the fact that organic soil texture holds more pores than mineral soil, its ability to hold more water is superior to mineral soil. In addition, the organic soil also is susceptible for compaction due to machinery application.

6.3.4 N₂O–N fluxes and emissions

In this study, increased soil moisture (> 41 % VWC) and relatively stable and warm soil temperatures produced relatively high N₂O–N and CH₄–C fluxes in organic soil than in mineral soil. In result of poor drainage in organic soil, prolonged moisture reduced the soil pH i.e. locations ID under muck soil. Overall, N₂O-N fluxes were relatively high at the beginning of the season, especially during the soybean flowering and seed formation stage around July and August, 2014. At this stage, it has been suggested that the biological fixation of N (active bacteria nodules) contributed to the N₂O-N emission and potential nitrate leach. The active symbiosis activity between bacteria and the crop improved the N uptake from the air for crop growth, hence, enhancing N₂O-N emissions. Towards the end of the season, the uptake of N may be depleted (Torstensson *et al*, 2006) as indicated by the reduction of N₂O-N fluxes. In September and October 2014, the soybeans were fully ready to be harvested, and photosynthesis dramatically decreased due to the cold weather and occasional freezing; as a result, this degraded the nodules' activities.

Sub-classification according to soil type indicated muck soils with higher soil organic content emitted higher N₂O–N fluxes than mineral soils. This can be seen particularly at gas chamber IDs of 01, 05, 07, and 08. These responses might be due to higher soil water content (> 40%) with relatively stable soil temperatures. This is due to the fact that these locations were mostly located at lower elevations and this means greater water accumulation. Thus, there was a significant increase in soil moisture levels over time. It also suggested that the combined effect of high soil moisture and soil OM leads to N production. However, neither soil moisture nor soil temperature provided a statistical significant correlation to N₂O–N fluxes.

Secondly, it also suggested that high GHG fluxes occurred due to crop responses to the organic matter decomposition process and management practices i.e. herbicide applications (19 June and 18 July 2014). The fluxes located under muck soils were relatively high in N₂O–N fluxes at the beginning of the season, and this might be due to the active bacterial (soybean was at V1 stage, with nodules visible) accumulated energy from available N in the atmosphere being converted to organic N. With the symbiosis of bacteria and legume crop i.e. soybean, N can be susceptible to leaching or transform into N₂O gas in two ways: during the biological fixation in full cycle, and left over crop residues (Torstensson *et al*, 2006). Considering the latter effect, as the herbicide was applied between the 1st and 2nd gas sampling, the plant residues may have decomposed. If they were rich in N (low C:N ratio), then they become susceptible to leaching or N₂O production. This situation was seen not only in muck soil, but also in mineral soil, but higher emissions in the latter soil type. High water content in muck soils govern anaerobic activity, thus, this may increase the denitrification process. The reduction process reduces the soil pH level which mostly occurs under saturated muck soil. Table 18 shows the Pearson correlation results analyzed in SPSS indicated that no other soil properties correlated to the N₂O–N fluxes.

6.3.5 CH₄–C fluxes and emissions

CH₄–C fluxes had the most dramatic gas variation throughout the season. Differences in field elevation play a key role in flux emissions. Most of the CH₄ fluxes were an indication of the uptake of gas from the soil. Depression areas, due to high soil water content, and with the relatively warm temperatures (above 20 °C) emitted more CH₄–C fluxes on organic soil than in mineral soil. In addition, the fluxes resulted in sinks (negative flux) at most of the chamber locations. The average and standard deviation of the fluxes in organic versus mineral soil were $-0.008 \pm 0.019 \text{ mg}\cdot\text{m}^{-2}\cdot\text{h}^{-1}$ and $-0.007 \pm 0.007 \text{ mg}\cdot\text{m}^{-2}\cdot\text{h}^{-1}$, respectively. Estimated net emissions showed a similar pattern

with chamber ID of 3 showing methane production estimated to be about 0.025 g/m² of CH₄-C. The depression area of location ID of 01 located at the lowest spot of the field (6.92 m above mean sea level) was the main source of the CH₄-C fluxes. Overall, the linear Pearson correlation indicated poor correlations between methane fluxes and measured parameters. Only methane had a significant correlation with other field and lab measured soil properties. Soil moisture content had a positive correlation with methane production ($r = 0.372$, significant at 99 %), but no correlation found for soil and ambient temperature. Soil EC_a measured using DUALEM-21S in 2012 from PRP 1.1 m and 2.1 m mode measurements indicated positive correlations (with $r = 0.269$ and $r = 0.127$ significant at 99 %) respectively. However, for 2013 measurements, only PRP 1 m indicated a positive correlation ($r = 0.131$ significant at 99 %), and not significant for PRP 2 m. This clearly indicated that surface conductivity (PRP 1 m mode) is more predominant for the GHG responses.

In contrast, gamma ray measurements such as total count, ²³²Th, and ²³⁸U were the only parameters with negative correlations ($r = -0.194$, -0.161 , and -0.204 at 99 % significant level), similarly yield, clay and K also had negative correlations ($r = -0.276$, -0.131 , and -0.185 at 99 % significant level), and Mg ($r = 0.161$ at 99 % significant level). Methane was considered to have a negligible effect on the environment. Considering most of the CH₄ net emissions were consumed in agricultural soil, this may support the view that the agricultural field is potentially a source of methane uptake and could become a substantial input for a mitigation policy. Higher methane fluxes were due to an increase in soil moisture content (>40 %) after the precipitation event, and during relatively warm soil conditions. The methane productions were mainly due to high decomposition occurring during the wet and warm climate. Further stepwise linear regression shows relatively low $R^2=0.115$, and has very weak practical value for the GHG prediction. Yet, CH₄ a strong correlation with carbon dioxide, and total count of the gamma ray (Equation 12). The methane flux can be predicted using multi regression analysis as in equation below.

Prediction model for methane:

$$CH_4 - C Flux (mg/m^2 h) = 0.008 - 4.641 \times 10^{-5} \cdot CO_2 - C - 3.355 \times 10^{-5} \cdot Total Count \quad (19)$$

$$F(2,95) = 19.552, p < 0.005, R^2 = 0.115$$

6.3.6 CO₂-C fluxes and emissions

Most of the representative locations showed positive CO₂-C fluxes which mostly increased during warm climate conditions (Figure 34). The highest fluxes were at the beginning of the season with the average ambient temperature of about 26 °C. The majority of the chosen locations were above 100 mg·m⁻²·h⁻¹ except for location ID of 01 (chamber 3 and 4) which was slightly lower than the rest. The mean and STD from organic and mineral soils were 108.40 ± 84.57 mg·m⁻²·h⁻¹ and 106.65 ± 80.49 mg·m⁻²·h⁻¹. The CO₂-C flux production was significantly affected at higher ambient and soil temperatures (positive Pearson correlation of $r = 0.336$ and 0.412 at significant level of 99 %, respectively). Furthermore, CO₂-C fluxes had a negative correlation with methane fluxes and soil pH ($r = -0.278$ and $r = -0.140$ significant at 99 % and 95 % respectively). Further, stepwise linear regression shows $R^2=0.261$ and strong correlation with methane gas, soil temperature, and soil pH (Equation 13).

High emissions of CO₂-C during warm climate and CH₄ during wet soil occurred at the lowest elevation. As the observed soil temperature measurements decreased towards the end of the growing season, a similar pattern was observed with the CO₂-C fluxes production. This suggests that the soil microbial uptake of the CH₄-C from the surface soil (negative value of fluxes). CO₂-C fluxes tended to decrease towards the end of the season, suggesting that as the weather gets cooler, there is a reduction in soil and crop respiration. High CO₂-C emission fluxes were expected at all locations. However, this value did not take into consideration the respiration source from the plants or weeds from inside the chamber during gas sampling. This is negligible since the chamber was located between the crop rows, and with minimum weeds growing inside the chamber.

Prediction model for carbon dioxide:

$$CO_2 - C Flux (mg / m^2 h) = 60.18 - 1645.264 \cdot CH_4 - C + 6.582 \cdot Soil\ temperature - 16.278 \cdot Soil\ pH$$

$F(3,95) = 30.895, p < 0.005, R^2 = 0.261$

6.3.7 Correlation between on-the-go measurements and soil properties

Good correlation with soil EC_a on PRP 1 m mode is the most representative measurement since it is related to the sub meter top soil layer. This shortcoming inhibits accurate mapping of large agricultural areas without compromising the major spatial and temporal soil heterogeneity.

Over time, the stability of the organic carbon and soil organic matter under muck soil suggest that the decomposition of these components is less tolerant to soil temperature due landscape variations (Cambardella, 1992). Thus, the organic matter is maintained at the same level (>30 %).

Table 19, 20 and 21 summarize the cross correlations between soil EC_a, and gamma ray spectroscopy with other measured soil parameters. On-the-go measurements (i.e. soil EC_a and gamma ray) were mostly controlled by the landscape position with both having strong correlations with elevation despite going in different directions (negative correlation with soil EC_a and positive with gamma ray). Variations in field elevations controlled the temporal and spatial soil moisture content and soil properties. Correlation analysis indicated that several soil attributes appeared strongly correlated to the soil EC_a measured in 2012 and 2013. Soil EC_a measured in both years shows a relatively strong negative correlation with elevation ($r = -0.607$ to -0.282 significant at 99 %), and soil pH ($r = -0.564$ to -0.266 significant at 99 %) but not significant with the soil texture and yield. To reiterate, the soil EC_a was measured using the DUALEM-21S sensor, measured at two different pseudo depths of 1 and 2 m, at HCP and PRP modes. Because the top soil profiles exhibited distinct textural differences across the landscape, there was no significant correlation between the main soil texture (clay, sand and silt) for both years, 2012 and 2013. However, there was a strong positive correlation between organic matter content and soil EC_a (range of $r = 0.40$ to 0.72 significant at 99 %). These observations indicate that there may be a correlation between soil EC_a readings and soil water content at this site, assuming that soil water content would closely follow the precipitation patterns.

On-the-go gamma ray spectroscopy measurements were similar to soil EC_a as the strongest correlation between ⁴⁰K, total count, ²³²Th with organic matter content, however, a negative relationship ($r = -0.934$, to -0.777 significant at 0.01). All lab measured soil chemical properties (K, Ca, and Mg) show a moderate strength relationship of the gamma ray measurement (range from $r = -0.677$ to -0.849 significant at 0.01). However, other soil properties such as yield, Al, soil textures and soil pH were poorly correlated (positive correlation under $r < 0.612$).

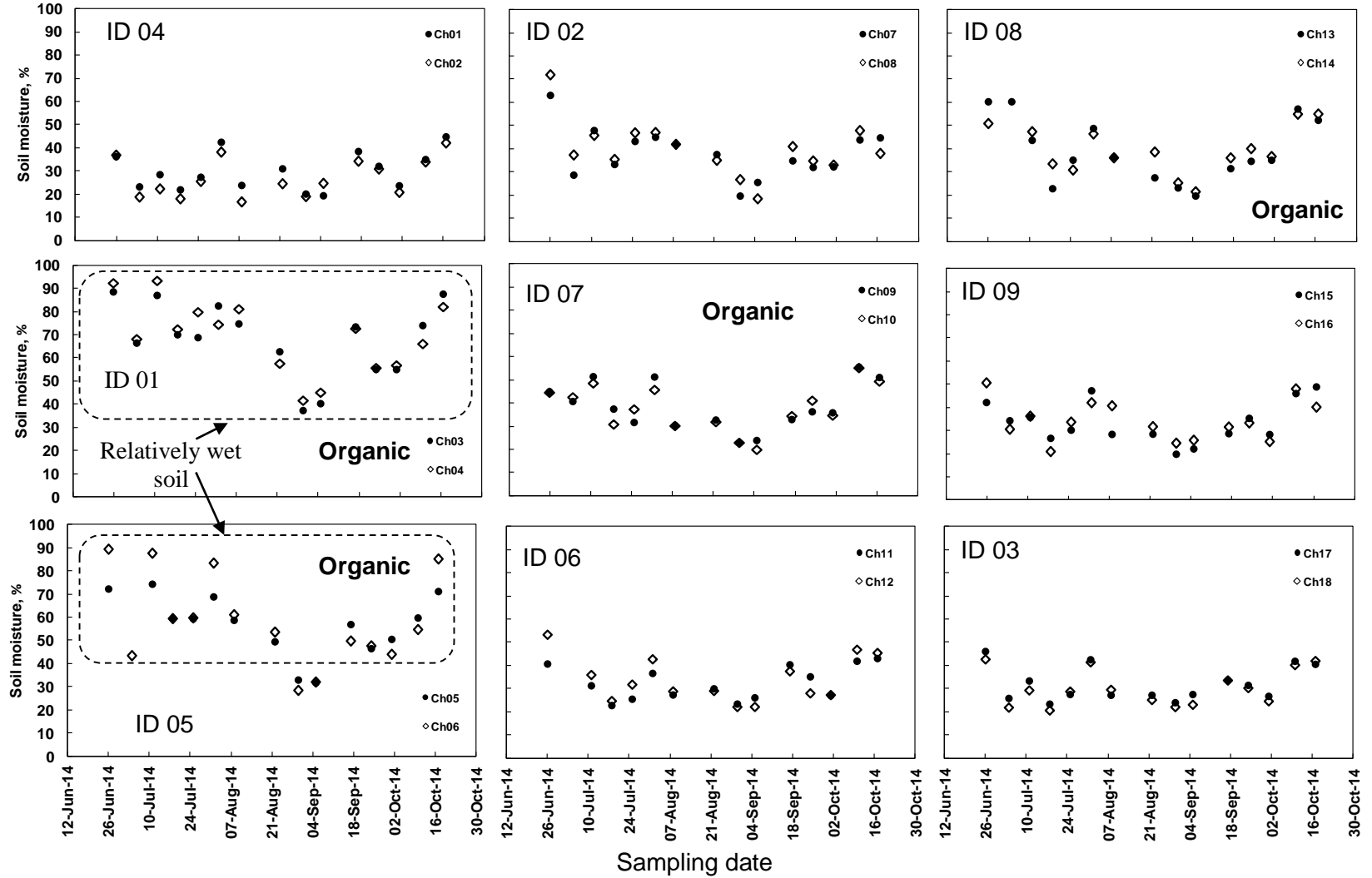


Figure 30: Soil moisture variability.

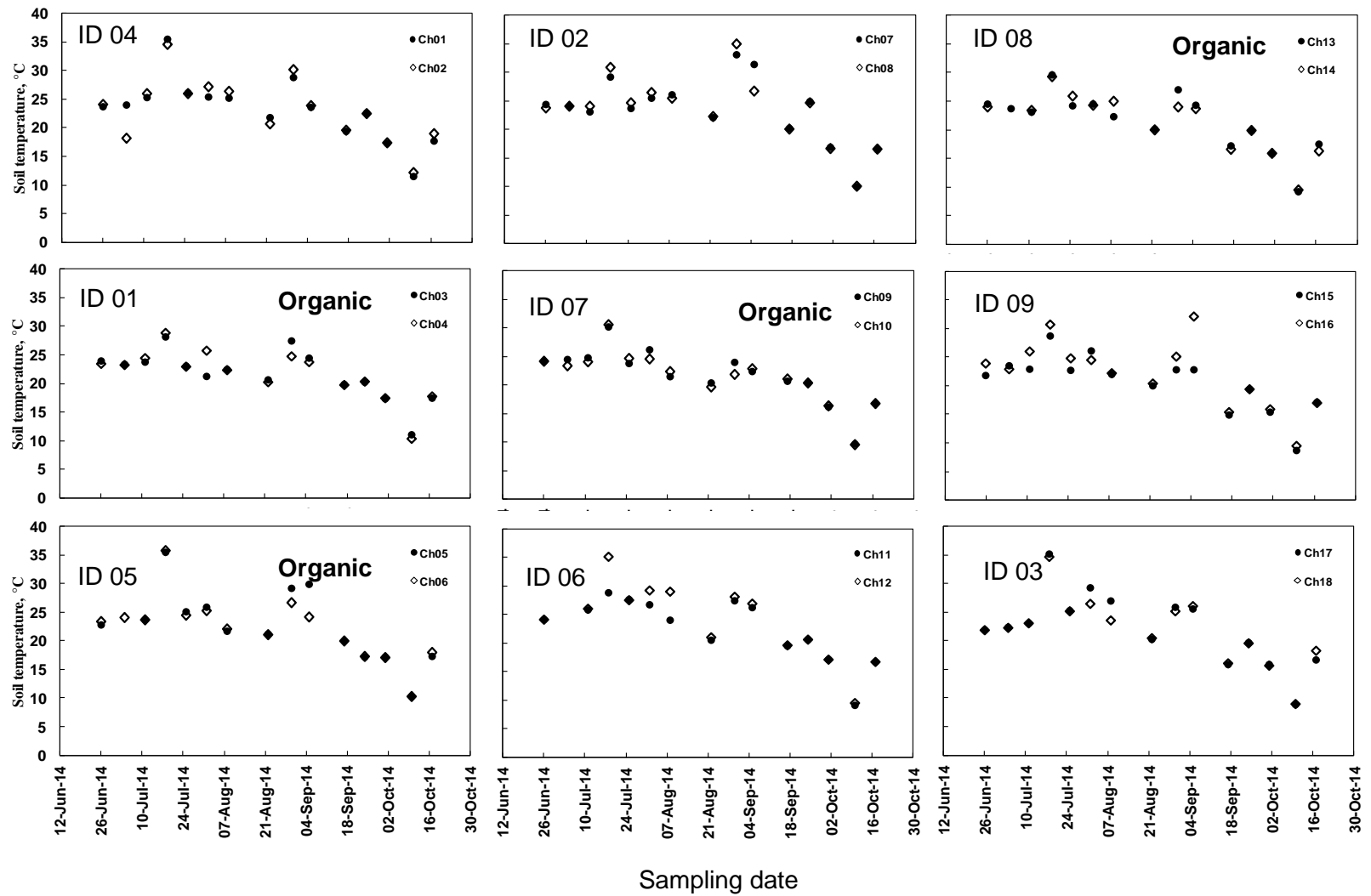


Figure 31: Soil temperature variability.

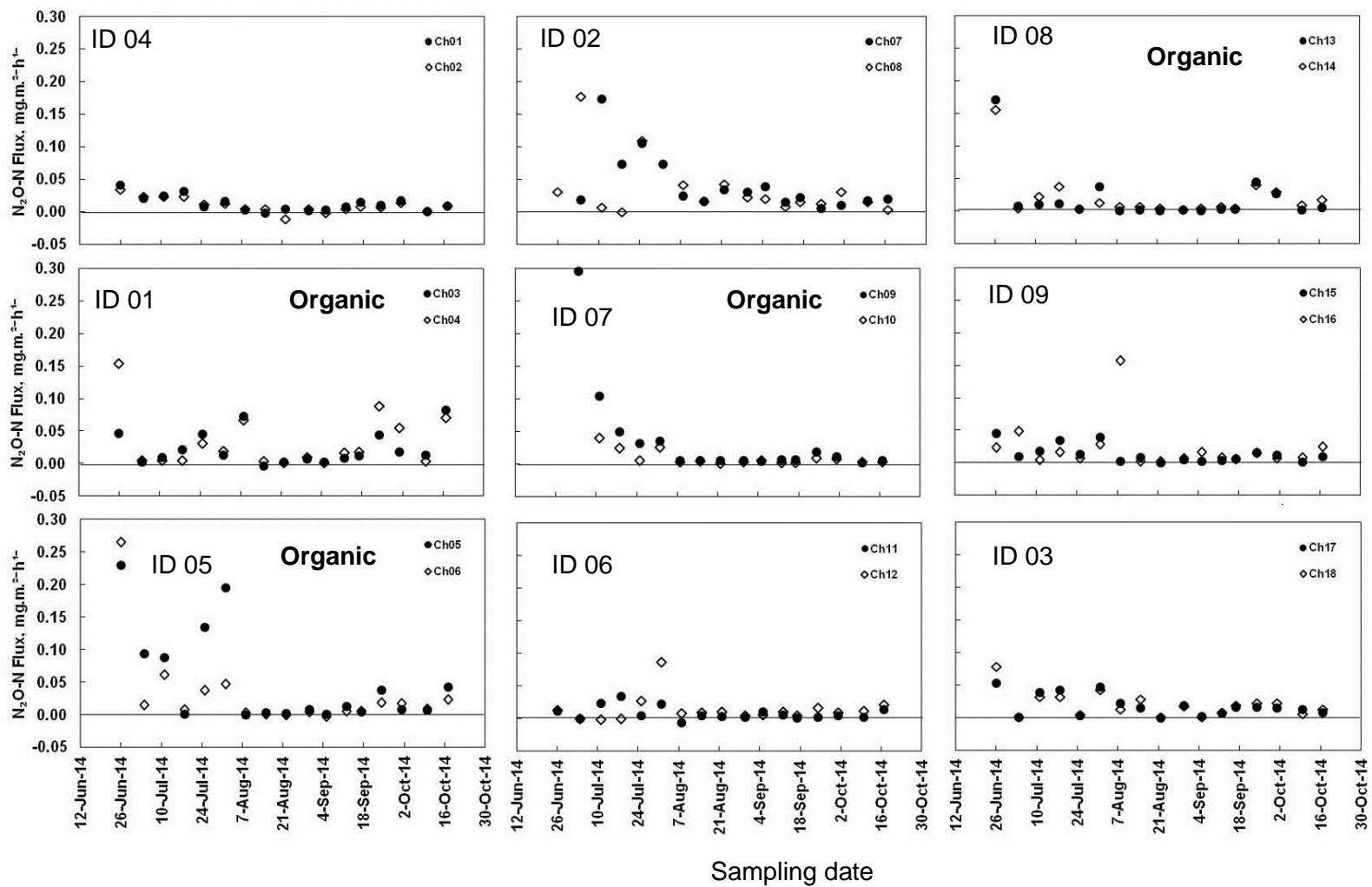


Figure 32: N_2O-N fluxes variation

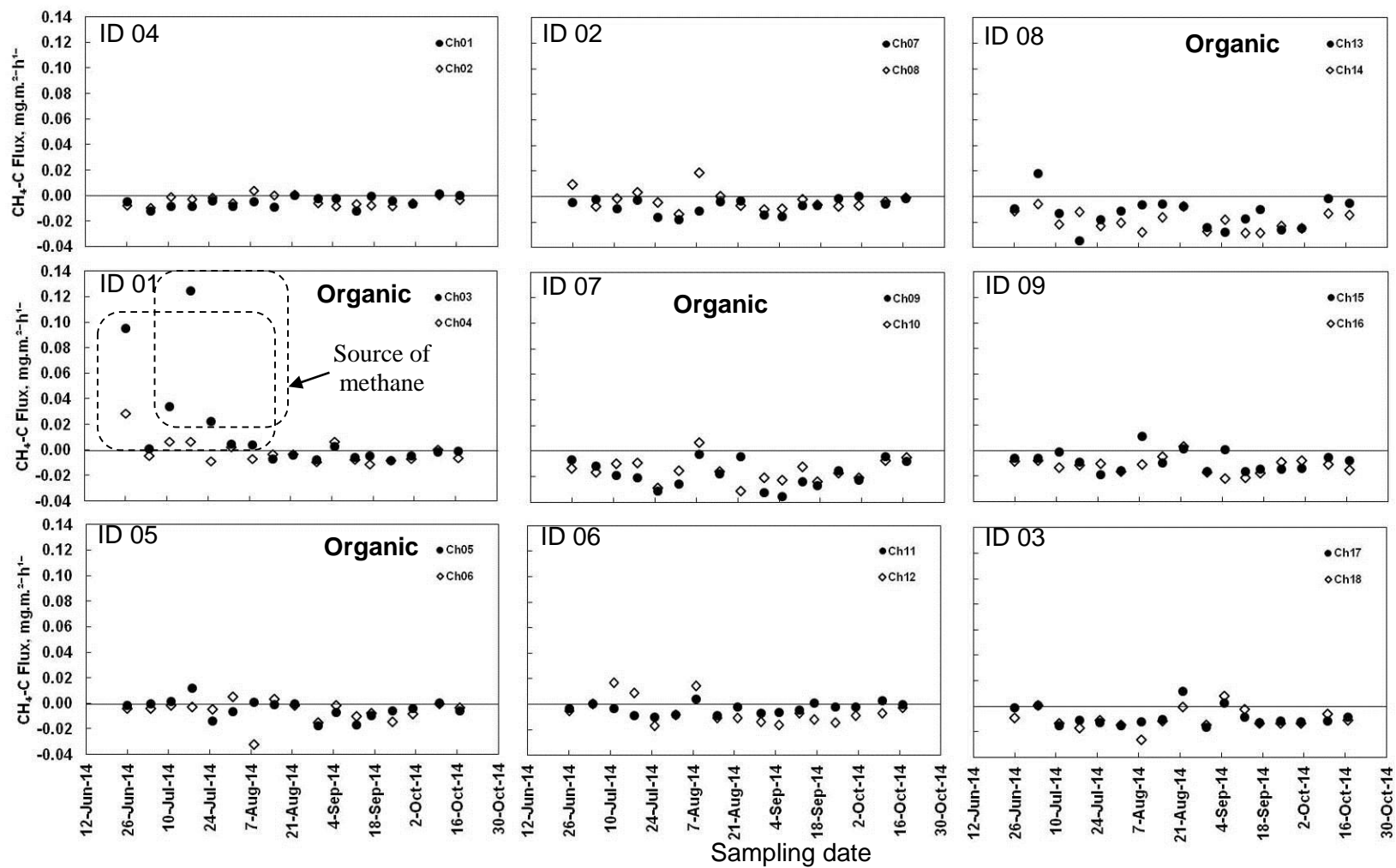


Figure 33: CH₄-C fluxes variation

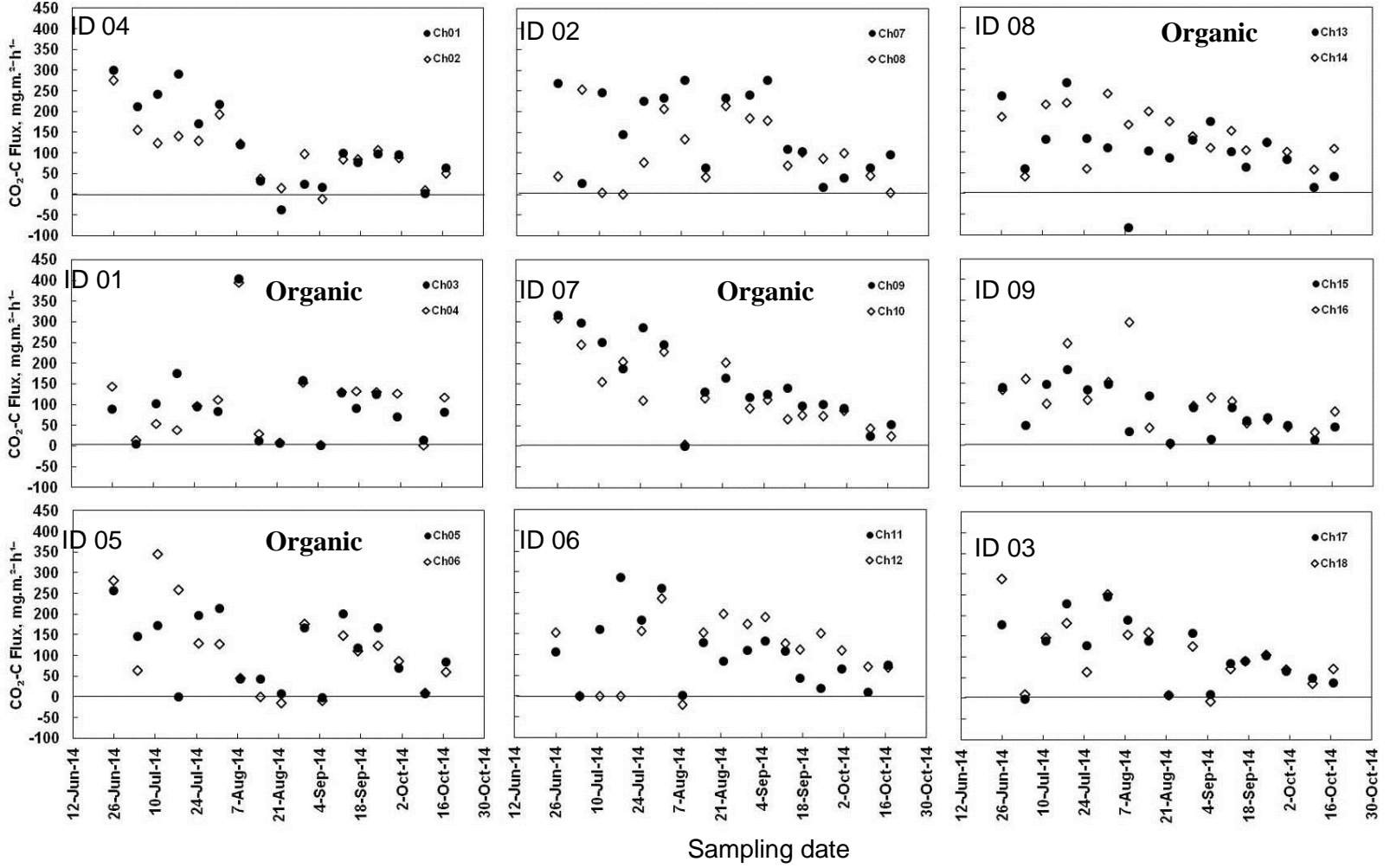


Figure 34: CO₂-C fluxes variation

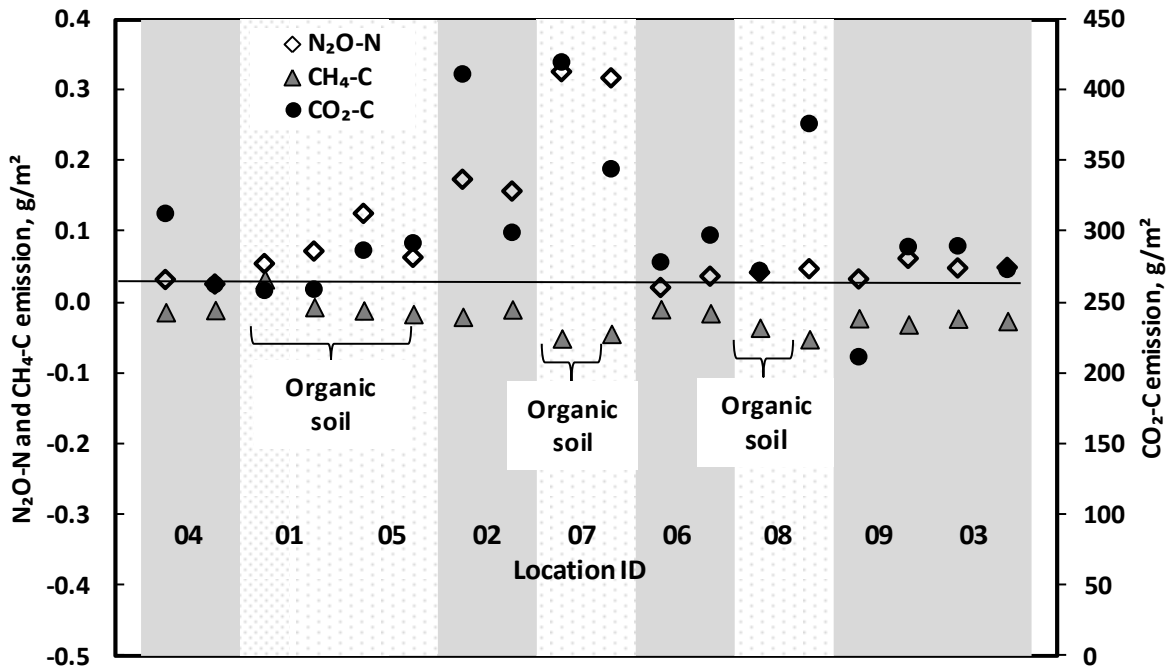


Figure 35: Estimated in-season net GHG emissions under organic and mineral soil

Table 18: Pearson correlation of GHG and soil properties (N = 306).

Parameters	N ₂ O–N flux, mg/m ² .h	CH ₄ –C flux, mg/m ² .h	CO ₂ –C flux, mg/m ² .h
N ₂ O–N flux, mg/m ² .h	1		
CH ₄ –C flux, mg/m ² .h	ns	1	
CO ₂ –C flux, mg/m ² .h	ns	–0.278**	1
Ambient temperature, °C	ns	ns	0.336**
Soil temperature, °C	ns	ns	0.412**
Soil moisture, %	ns	0.372**	ns
Elevation, m	ns	ns	ns
2013 HCP 1 m	ns	ns	ns
2013 HCP 2 m	ns	ns	ns
2013 PRP 1 m	ns	0.131*	ns
2013 PRP 2 m	ns	ns	ns
Count	ns	–0.194**	ns
⁴⁰ K	ns	ns	ns
²³² Th	ns	–0.161**	ns
²³⁸ U	ns	–0.204**	ns
Caesium	ns	ns	ns
Yield, kg/ha	ns	–0.276**	ns
Sand, %	ns	ns	ns
Silt, %	ns	ns	ns
Clay,%	ns	–0.131*	ns
pH	ns	ns	–0.140*
OM, %	ns	ns	ns
K	ns	–0.185**	ns
P_ppm	ns	ns	ns
Ca	ns	ns	ns
Mg	ns	0.161**	ns
Al	ns	ns	ns

* = Correlation is significant at the 0.05 level; **= Correlation is significant at the 0.01 level; ns = not significant

Table 19: Correlation coefficient (r) between the soil EC_a and other soil parameters.

Attributes	2013			
	HCP 1 m	HCP 2 m	PRP 1 m	PRP 2 m
<i>Site</i>				
Yield, kg/ha	ns	ns	ns	ns
Elevation, m	-0.535**	-0.444**	-0.710**	-0.607**
<i>Soil</i>				
Clay, g/kg	ns	ns	ns	ns
Sand, g/kg	ns	ns	ns	ns
Silt, g/kg	ns	ns	ns	ns
OM, g/kg	0.558**	0.442**	0.717**	0.613**
pH	-0.508**	-0.564**	-0.266*	-0.436**
K, mg/kg	ns	ns	ns	ns
Ca, mg/kg	0.411**	0.287*	0.655**	0.502**
Mg, mg/kg	0.325*	ns	0.541**	0.383**
Al, mg/kg	ns	ns	-0.373**	ns

* = Correlation is significant at the 0.05 level; ** = Correlation is significant at the 0.01 level; ns = not significant

Table 20: Correlation coefficient between the Gamma ray and site and soil parameters (N= 56).

Attributes	Total count	⁴⁰ K	²³⁸ U	²³² Th
Yield, kg/ha	Ns	-0.281*	ns	ns
Elevation, m	0.517**	0.750**	ns	0.418**
Clay, %	ns	ns	0.327*	ns
Sand, %	ns	0.450**	ns	0.266*
Silt, %	-0.300*	-0.334*	ns	ns
OM, %	-0.864**	-0.934**	ns	-0.777**
pH	0.292*	ns	0.292*	ns
K, mg/kg	ns	ns	0.329*	ns
Ca, mg/kg	-0.772**	-0.849**	ns	-0.748**
Mg, mg/kg	-0.710**	-0.835**	ns	-0.677**
Al, mg/kg	0.546**	0.549**	ns	0.612**

* = Correlation is significant at the 0.05 level; ** = Correlation is significant at the 0.01 level; ns = not significant;

Table 21: Correlation coefficient between the soil EC_a and Gamma ray.

Attributes	2013			
	HCP1m	HCP2m	PRP1m	PRP2m
Count	- 0.508**	- 0.398**	- 0.650**	- 0.558**
⁴⁰ K	- 0.584**	- 0.471**	- 0.734**	- 0.638**
²³⁸ U	ns	ns	ns	ns
²³² Th	- 0.325*	ns	- 0.503**	- 0.390**
Cae	ns	ns	ns	ns
Count rate	- 0.548**	- 0.437**	- 0.691**	- 0.598**

*Correlation is significant at the 0.05 level; ** Correlation is significant at the 0.01 level; ns - not significant;

6.3.8 Identification of the representative chamber location

Figure 36 shows the MRD values for each of individual gas. It was found for the N₂O-N, the most temporally stable is from chamber ID 18, 3, 16, 10 and 17 (the mean of the relative different was close to 0), for the CH₄-C is from chamber ID 8, 7, 6 and 2, for the CO₂-C is from chamber ID 8 and 16. For the N₂O-N emission, chamber ID 15 resulted the minimum variances (variance = 0.373), however, cannot be presented as the representative chamber and considered as underestimated. Chamber ID 9, 8 and 7 shows the values of the MRD is overestimated and cannot be used as a representative location since the variances were relatively high. Similar rules apply to the other two cases. Wet location (see Figure 9) is prone to be the source of the CH₄-C emission as show on of chamber ID 3. Thus suppressed the graph and produced very significant fluxes as compared to others. The CO₂-C fluxes were quite stable over time, and Chamber ID 15 more stable, but consistence during the gas sampling.

When the average GHG fluxes were mapped spatially on the field map, it's clearly indicate there is a spatial differences of the GHG flux productions as shown in Figures 37 a-c. Figures 38-40 represents the average of the GHG fluxes versus other measured field parameters. For an example, based on the average N₂O-N fluxes (Figure 38), it's clearly indicated that different soil type have an impact on the scale of the fluxes (organic vs mineral, > 30 % of OM considered as organic soil layer). High N₂O-N fluxes had a clear break on different range of soil EC_a (above 10 mS/m) which produce the most of the emission. Chamber located at the lowest spot of the field produced the highest average N₂O-N fluxes. Total count had no direct relationship with the average N₂O-N fluxes.

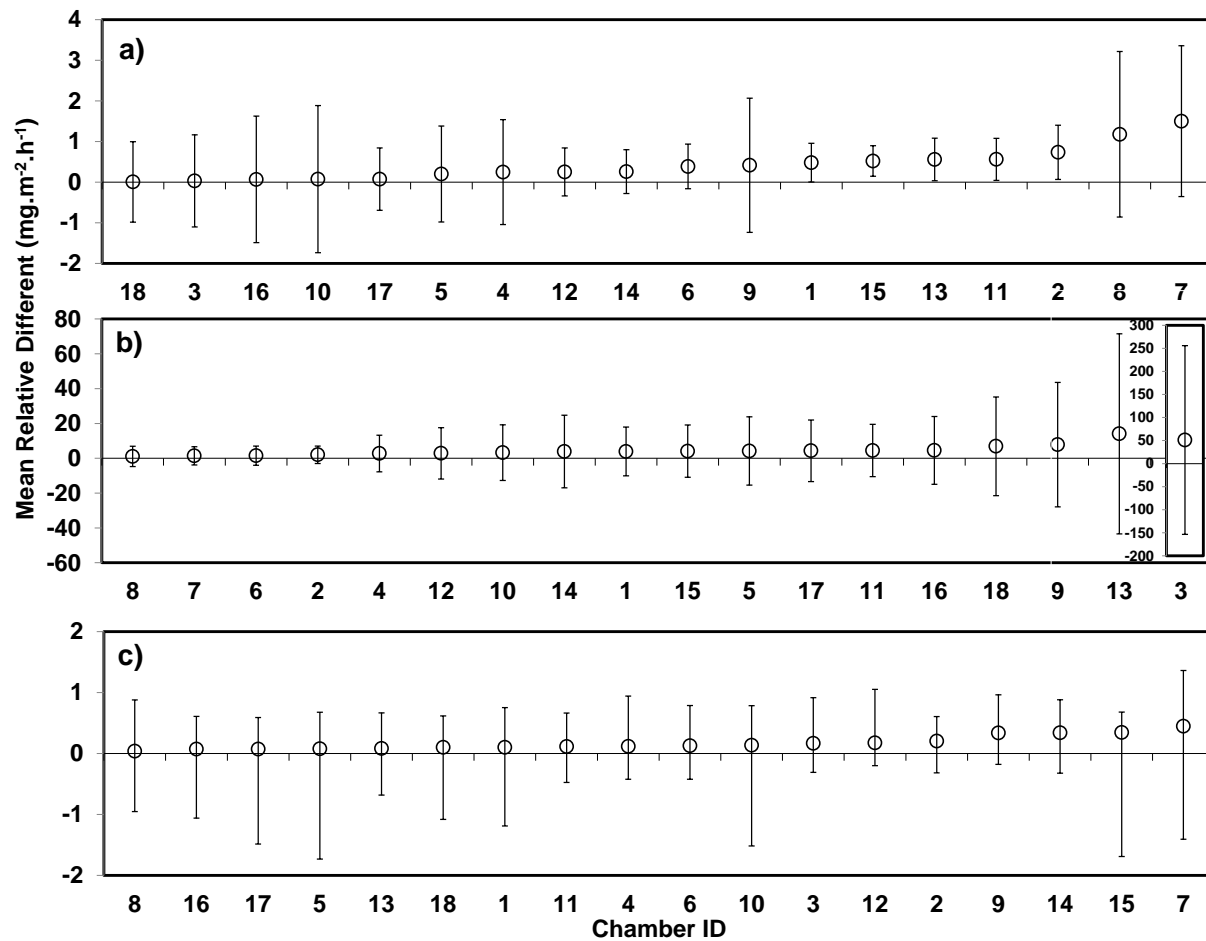


Figure 36: Ranked mean relative different of the fluxes for (a) N₂O-N, (b) CH₄-C, and (c) CO₂-C. The error bars indicate the standard deviation of the MRD of the fluxes.

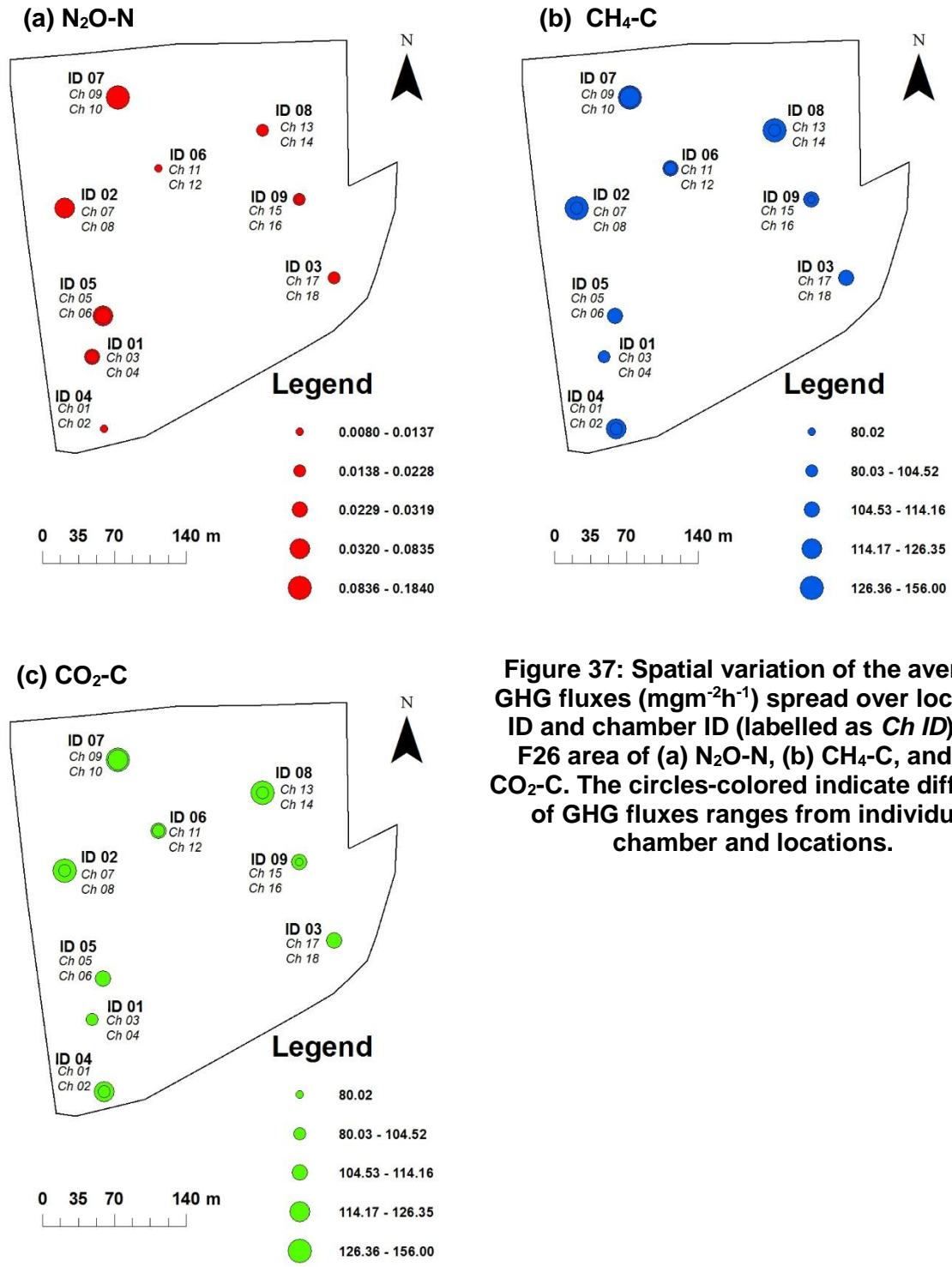


Figure 37: Spatial variation of the average GHG fluxes ($\text{mgm}^{-2}\text{h}^{-1}$) spread over location ID and chamber ID (labelled as *Ch ID*) the F26 area of (a) N₂O-N, (b) CH₄-C, and (c) CO₂-C. The circles-colored indicate different of GHG fluxes ranges from individual chamber and locations.

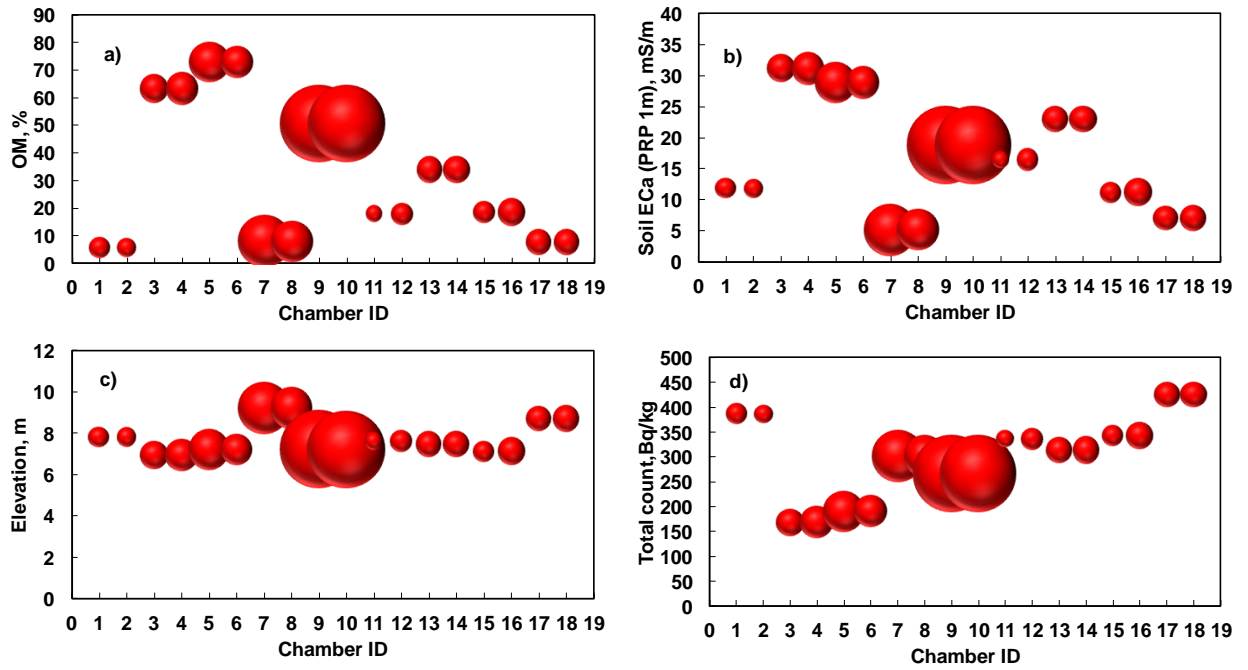


Figure 38: Spatial relationship between the average of the N_2O-N fluxes versus (a) OM (b) soil EC_a , (c) field elevation and (d) total count. CH_4-C , and (c) CO_2-C . The circles-colored indicate different of GHG fluxes ranges from individual chamber and locations.

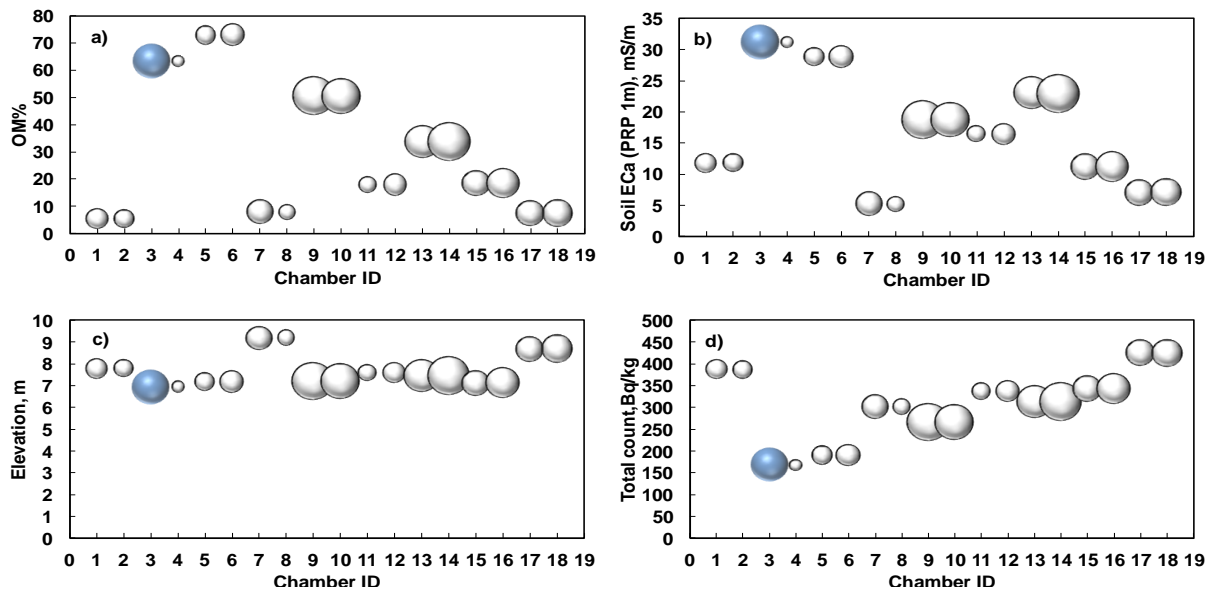


Figure 39: Spatial relationship between the average of the CH_4-C fluxes versus (a) OM (b) soil EC_a , (c) field elevation and (d) total count.

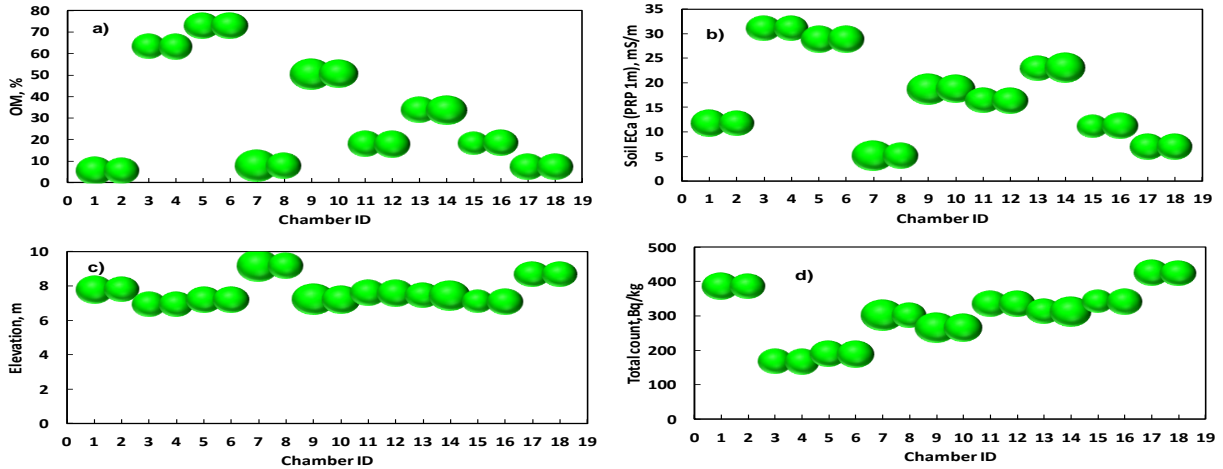


Figure 40: Spatial relationship between the average of the CO₂-C fluxes versus (a) OM (b) soil EC_a, (c) field elevation and (d) total count.

6.4 Conclusions

Overall, PSS was able to detect the field heterogeneity based on soil EC_a maps. The emissions of GHG were mainly derived from spatial and temporal field variations. They also varied from one location to another although side by side chambers were relatively close to each other. Over time, stability of soil organic carbon and soil organic matter under muck soils suggest that the decomposition of these components is less tolerant to soil temperature due to landscape variations (e.g. depressions). Thus, the organic matter was maintained at the same level (>30 %) and varied the GHG, i.e. the CO₂-C emission production. Increased soil salinity detected by soil EC_a measurements (indicated by variations in soil moisture) resulted in an increase in N₂O-N flux emissions. Mapping field heterogeneity might be useful for farm GHG CO₂ mapping in large-scale agriculture production areas in order to improve the efficiency of seasonal GHG emissions auditing. The identification of the most representative chamber locations is essential for producing high quality estimates of overall field GHG flux and emission values.

CHAPTER 7

SUMMARY AND GENERAL CONCLUSIONS

7.1 Summary

Field heterogeneity assessment to characterize the spatial and temporal GHG emissions from agricultural land was achieved by using soil EC_a data collected via PSS technology to provide insight for annual environmental assessments. Total emission distribution of the GHG monitoring locations throughout the field proved more reliable in terms of spatial variability in considering flux and emission estimations rather than a single, or a few locations. In addition, the optimal number of samples can be planned at a relatively low cost with more representative results.

In the first study, information on the quality of soil EC_a data is essential prior to using soil EC_a data for any agriculture application. The stability of soil EC_a readings was assessed based on temporal and operational tests. The temporal test involved 4.5 h to collect static soil EC_a measurements over a long period of time for both GCR and EMI sensors. Similarly, the operational test involved a test for height above ground (0 and 10 cm), while $\pm 10^\circ$ roll and pitch was tested only for EMI sensors. GCR was followed by DUALEM-21S measurements (1.1 and 2.1 m) where the PRP results were superior to the HCP measurement modes. Changes in the internal temperature due to prolonged exposure to sunlight or during typical mapping exercises were the main issues that contributed to differences in stability of the soil EC_a readings from EMI sensors.

During the second study, processing and management of the database for the GHG flux and emissions from large datasets imposed a challenge for manual calculations. Thus, a streamlined approach using MATLAB scripts was developed to avoid calculation errors. The flux was estimated using the median slopes approach with the purpose of disregarding outliers in the dataset, i.e. eliminating erroneous measurements. The emissions were estimated using the PCHIP with the 1-D array interpolation method. MATLAB was capable of analyzing all datasets from the six sites at once with maximum operating time, on average, of 3 min per 10,000 datasets per year.

In the third study, a WSN was implemented to monitor the relationship between physical soil properties and GHG fluxes overtime in large-scale vegetable production. Three stations were

set up based on different levels of organic soil decomposition, namely, mineralized, moderate, and pure organic soil. The results were evaluated for modeling of the GHG temporal variations.

Lastly, in the fourth study, PSS technology based upon the soil EC_a measurements was used to evaluate field heterogeneity for the purpose of environmental assessment. The purpose was to optimize the number and location GHG monitoring sites at optimal cost.

7.2 General Conclusions

All four studies were related to the optimization of GHG assessment of an agricultural field from a set of representative locations with consideration of field heterogeneity. The main challenge in the implementation of GHG assessments is poor estimation accuracy when extrapolating across large agriculture fields with relatively low-cost and widely distributed chambers. By using PSS technology to reveal field heterogeneity, researchers will be able to better predict the annual GHG emissions when developing climate change mitigation strategies.

CHAPTER 8

CONTRIBUTIONS TO KNOWLEDGE AND SUGGESTIONS FOR FUTURE RESEARCH

8.1 Contributions to Knowledge

The following are the contributions to knowledge derived from this research:

1. The thesis presents an evaluation of soil EC_a stability over a long period of time as well as determining typical conditions of the operational test. The tests conducted using a side-by-side test of all soil EC_a instruments has not been reported in depth, especially when comparing the latest models for three of the most popular instruments. This test provided an overview of the overall performance of sensors which are widely available.
2. The GHG fluxes and emission estimations based upon the NSS measurements were used to build a large centralized dataset covering multiple research studies. The streamlined approach required a standard protocol from a standardized input sheet for fast and accurate flux and emission estimation. Approximately 30,000 data records over the three year study were used and a automated system developed in MATLAB helps other researchers to perform fast flux and emission calculations. In addition, another group of researchers utilized the results from this study for the producing an cost-benefit analysis for agricultural GHG mitigation strategies.
3. Understanding the GHG variations over the temporal changes in the physical soil properties measured using WSN on muck soil will help the grower to reduce water usage and minimize GHG emissions during the growing season. The ability to understand the co-factors that contribute to high GHG, i.e. irrigation schedules and amounts of fertilizer, helps reduce the environment impact from large scale agriculture production.
4. The information on the factors affecting GHG emission under different cropping systems and water management strategies will contribute to the IPCC soil factors as listed under the IPCC (2006). For instance, the emission factor for agricultural crop production under peat soil will be the main contribution for the national inventory as this information is relatively new for an agricultural area cultivated under organic soil. This information could provide a benchmark value for the emission factors for the Tier II IPCC database program.
5. This thesis presents a unique approach in placement optimization for the GHG monitoring sites using soil EC_a measurements to reveal field heterogeneity. Yet, to date, the approach has not been fully implemented for the application of PSS for environmental purposes.

6. The MATLAB code developed provides a basis for other researchers. Although, this code is specially developed for the purposes of this study, the author intends for this software to be freely available for further improvement by future researchers.

8.2 Suggestions for Further Research

1. In the first study, the replicated dataset on DUALEM–21S should be tested in more detail at the multi-scale of roll and pitch. The test on soil EC_a should be extended to more complex combinations such as roll and pitch tests up to 30° with 5° increments. This would allow the study to determine changes of the signal on the horizontal coplanar mode (HCP) of the DUALEM–21S instrument at different angles, both for roll and pitch. The challenge lies in the consistency of the test since the heating of the instrument might reduce soil EC_a if the test was conducted in direct sunlight. Ultimately, this will help in generalizing the soil EC_a effects or changes caused by the sensors relative orientation and position during mapping.
2. Over the long run, the temporal effect seems to be the major factor controlling soil EC_a variations. Thus, the author suggests performing additional tests on EMI sensors with and without the cover during the test. This will justify the effect of the soil EC_a quantification, especially for the newly developed sensor.
3. In the second study, relying on a linear model did not always produce the best results, but provided the simplest method for flux estimation. The minimum threshold value based on the ambient temperature should be used for data quality assessment.
4. The MATLAB scripts can be improved by integrating them with more complex calculation methods, such as the non-linear method for flux and emission estimation
5. In the third study, the use of a better sensor specifically designed for muck soil is necessary because muck soil tends to dry faster during the summer, thus, increasing the pore space within the sensor area and limiting the contact between the muck soil and the sensor. This results in poor sensor response. In this case, the capacitance sensor based may provide better measurement.
6. Lastly, the method of the GHG monitoring in Chapter 6 should be improved with continuous measurement rather than static measurement. This will give better result of the GHG estimation with more presentable dataset for diurnal estimation. The design of the portable GHG monitoring chamber would provide cost effective of the overall spatial and temporal variation of the field area.

REFERENCES

- Abdu, H., D. Robinson, and S. B. Jones. 2007. Comparing bulk soil electrical conductivity determination using the DUALEM-1S and EM38-DD electromagnetic induction instruments. *Soil Science Society of America Journal* 71(1):189-196.
- Adamchuk, V., A. Mat Su, R. Eigenberg, and R. Ferguson. 2011a. Development of an angular scanning system for sensing vertical profiles of soil electrical conductivity. *Transactions of the ASABE* 54(3):757-767.
- Adamchuk, V.I., Viscarra Rossel, R.A., Marx, D.B., Samal, A.K., 2011b. Using targeted sampling to process multivariate soil sensing data. *Geoderma* 163, 63-73.
- Allaire, S.E., Lange, S.F., Lafond, J.A., Pelletier, B., Cambouris, A.N., Dutilleul, P., 2012. Multiscale spatial variability of CO₂ emissions and correlations with physico-chemical soil properties. *Geoderma* 170, 251-260.
- Allred, B., J. J. Daniels, and M. R. Ehsani. 2008. *Handbook of agricultural geophysics*. CRC Press.
- Allred, B., M. Ehsani, and D. Saraswat. 2005. The impact of temperature and shallow hydrologic conditions on the magnitude and spatial pattern consistency of electromagnetic induction measured soil electrical conductivity. *Transactions of the ASAE* 48(6):2123-2135.
- Allred, B., M. R. Ehsani, and D. Saraswat. 2006. Comparison of electromagnetic induction, capacitively-coupled resistivity, and galvanic contact resistivity methods for soil electrical conductivity measurement. *Applied engineering in agriculture* 22(2):215-230.
- Amidu, S. A., and J. A. Dunbar. 2008. An evaluation of the electrical-resistivity method for water-reservoir salinity studies. *Geophysics* 73(4):G39-G49.
- Berglund, Ö., Berglund, K., 2011. Influence of water table level and soil properties on emissions of greenhouse gases from cultivated peat soil. *Soil Biology and Biochemistry* 43, 923-931.
- Biswas, A., 2014. Season-and depth-dependent time stability for characterising representative monitoring locations of soil water storage in a hummocky landscape. *Catena* 116, 38-50.
- Brevik, E. C., T. E. Fenton, and A. Lazari. 2006. Soil electrical conductivity as a function of soil water content and implications for soil mapping. *Precision Agriculture* 7(6):393-404.

- Brevik, E., T. Fenton, and A. Lazari. 2003. Differences in EM-38 Readings Taken Above Crop Residues Versus Readings Taken with Instrument-Ground Contact. *Precision Agriculture* 4(4):351-358.
- Brevik, E., T. Fenton, and R. Horton. 2004. Effect of Daily Soil Temperature Fluctuations on Soil Electrical Conductivity as Measured with the Geonics® EM-38. *Precision Agriculture* 5(2):145-152.
- Brillante, L., B. Bois, O. Mathieu, V. Bichet, D. Michot, and J. Lévêque. 2014. Monitoring soil volume wetness in heterogeneous soils by electrical resistivity. A field-based pedotransfer function. *Journal of Hydrology* 516:56-66.
- Buchanan, S., Triantafyllis, J., 2009. Mapping Water Table Depth Using Geophysical and Environmental Variables. *Ground Water* 47, 80-96.
- Cambardella, C.A., Elliott, E.T., 1992. Particulate Soil Organic-Matter Changes across a Grassland Cultivation Sequence. *Soil Sci. Soc. Am. J.* 56, 777-783.
- Canada Soil Survey Committee, Subcommittee on Soil Classification. 1978. The Canadian system of soil classification. Can. Dep. Agric. Publ. 1646. Supply and Services Canada (Pb), Ottawa, Ontario. 83pp
- Chapyzhnikov, B.A., Badyukov, D.D., Tsipenyuk, Y.M., 2005. Determination of carbon and nitrogen in meteorites using gamma-ray activation analysis. *J Anal Chem* 60, 45-48.
- Corwin, D. L., and S. M. Lesch. 2005. Apparent soil electrical conductivity measurements in agriculture. *Computers and Electronics in Agriculture* 46(1–3):11-43.
- Corwin, D., and S. Lesch. 2003. Application of soil electrical conductivity to precision agriculture. *Agronomy Journal* 95(3):455-471.
- De Jong, E., A. Ballantyne, D. Cameron, and D. Read. 1979. Measurement of apparent electrical conductivity of soils by an electromagnetic induction probe to aid salinity surveys. *Soil Science Society of America Journal* 43(4):810-812.
- Dierke, C., Werban, U., 2013. Relationships between gamma-ray data and soil properties at an agricultural test site. *Geoderma* 199, 90-98.
- Doolittle, J., K. Sudduth, N. Kitchen, and S. Indorante. 1994. Estimating depths to claypans using electromagnetic induction methods. *Journal of Soil and Water Conservation* 49(6):572-575.
- Eichner, M.J., 1990. Nitrous oxide emissions from fertilized soils: summary of available data. Environment and Climate Change Canada. A Report, 2013. Available online at <http://ec.gc.ca/ges-ghg/default.asp?lang=En&n=E0533893-1>. Access on 15 Jan 2015.

- Eswaran, H., Van Den Berg, E., Reich, P., 1993. Organic carbon in soils of the world. *Soil science society of America journal* 57, 192-194.
- Farahani, H., and G. Buchleiter. 2004. Temporal stability of soil electrical conductivity in irrigated sandy fields in Colorado. *Transactions of the ASAE* 47(1):79-90.
- Fowler, D. 1999. Experimental designs appropriate for flux determination in terrestrial and aquatic systems. In: A.F. Bouwman (Ed.). *Approaches to scaling of trace gas fluxes in ecosystems. Developments in Atmospheric Science* 24. Elsevier Science, Amsterdam, pp. 101-121.
- Fritsch, F. N., and R. E. Carlson. 1980. Monotone piecewise cubic interpolation. *SIAM Journal on Numerical Analysis* 17(2):238-246.
- Gurr, C., 1964. Calculation of soil water contents from gamma ray readings. *Soil Research* 2, 29-32.
- Halvorson, A.D., Del Grosso, S.J., Reule, C.A., 2008. Nitrogen, tillage, and crop rotation effects on nitrous oxide emissions from irrigated cropping systems. *Journal of environmental quality* 37, 1337-1344.
- Hénault, C., Devis, X., Lucas, J.L., Germon, J.C., 1998. Influence of different agricultural practices (type of crop, form of N-fertilizer) on soil nitrous oxide emissions. *Biol Fertil Soils* 27, 299-306
- Holland, E.A., Robertson, G.P., Greenberg, J., Groffman, P.M., Boone, R.D. and Gosz, J.R. 1999. Soil CO₂, N₂O, and CH₄ exchange. In: Robertson G.P., Coleman D.C., Bledsoe C.S., Sollins P. (Eds.), *Standard Soil Methods for Long term Ecological Research*. Oxford University Press, New York, pp. 185–201.
- Howard, D. M., and P. J. A. Howard. 1993. Relationships between CO₂ evolution, moisture-content and temperature for a soil types. *Soil Biology & Biochemistry*. 25 (11): 1537-1546.
- Hutchinson, G.L. and Livingston, G.P. 1993. Use of chamber systems to measure trace gas fluxes. In: Harper L.A., Mosier A.R., Duxbury J.M. and Rolston D.E. (Eds.) *Agricultural Ecosystem Effects on Trace Gases and Global Climate Change*. ASA Publ. 55, ASA-CSSA-SSSA, Madison, WI, pp.63-78.
- Hutchinson, G.L. and Mosier, A.R. 1981. Improved soil cover method for field measurement of nitrous oxide fluxes. *SSSA*. 45: 311-316.
- IPCC (2006). 2006 IPCC Guidelines for National Greenhouse Gas Inventories, prepared by the National Greenhouse Gas Inventories Programme (eds. Eggleston HS, Buendia L, Miwa K, Ngara T, Tanabe K). IGES, Japan. Access on 7 February 2015. Available at: <http://www.ipcc-nggip.iges.or.jp/public/2006gl/>

- IPCC (2007). IPCC Fourth Assessment Report: Climate Change 2007. Intergovernmental Panel on Climate Change. Cambridge University Press, Cambridge.
- Ishizuka, S., Iswandi, A., Nakajima, Y., Yonemura, S., Sudo, S., Tsuruta, H., Muriyarso, D., 2005. Spatial patterns of greenhouse gas emission in a tropical rainforest in Indonesia. *Nutrient Cycling in Agroecosystems* 71, 55-62.
- Johnston, C.A., Groffman, P., Breshears, D.D., Cardon, Z.G., Currie, W., Emanuel, W., Gaudinski, J., Jackson, R.B., Lajtha, K., Nadelhoffer, K., 2004. Carbon cycling in soil. *Frontiers in Ecology and the Environment* 2, 522-528.
- Kachanoski, R., I. V. Wesenbeeck, and E. Gregorich. 1988. Estimating spatial variations of soil water content using noncontacting electromagnetic inductive methods. *Canadian Journal of Soil Science* 68(4):715-722.
- Kasimir - Klemedtsson Å., Klemedtsson L., Berglund K., Martikainen P., Silvola J., and Oenema O. Greenhouse gas emissions from farmed organic soils: a review. *Soil use and management*. 1997 Dec 1;13(s4):245-50.
- Kern, J., Johnson, M., 1993. Conservation tillage impacts on national soil and atmospheric carbon levels. *Soil Science Society of America Journal* 57, 200-210.
- Kroon, P. S., A. Hensen, W. C. M. Van Den Bulk, P. A. C. Jongejan, and A. T. Vermeulen. 2008. The importance of reducing the systematic error due to non-linearity in N₂O flux measurements by static chambers. *Nutrient Cycling in Agroecosystems* 82(2):175-186.
- Lal, R., 2004. Carbon emission from farm operations. *Environment international*, 30(7), pp.981-990.
- Leirós, M. C., C. Trasar-Cepeda, S. Seoane, and F. Gil-Sotres. 1999. Dependence of mineralization of soil organic matter on temperature and moisture. *Soil Biology and Biochemistry* 31(3):327-335.
- Lesch, S. M., D. J. Strauss, and J. D. Rhoades. 1995. Spatial prediction of soil salinity using electromagnetic induction techniques: 1. Statistical prediction models: A comparison of multiple linear regression and cokriging. *Water Resources Research* 31(2):373-386.
- Li, H., Qiu, J., Wang, L., Tang, H., Li, C., Van Ranst, E., 2010. Modelling impacts of alternative farming management practices on greenhouse gas emissions from a winter wheat–maize rotation system in China. *Agriculture, Ecosystems & Environment* 135, 24-33.
- Linn, D., and J. Doran. 1984. Effect of water-filled pore space on carbon dioxide and nitrous oxide production in tilled and nontilled soils. *Soil Science Society of America Journal* 48(6):1267-1272.

- Livingston, G.P., Hutchinson, G.L., Spartalian, K., 2005. Diffusion theory improves chamber-based measurements of trace gas emissions. *Geophysical Research Letters* 32, 1-3.
- Loonstra, E., van Egmond, F., 2009. On-the-go measurement of soil gamma radiation. *Precision Agriculture* 9, 415-422.
- Macias, E., Barker, J., 1978. Simultaneous oxygen, carbon, nitrogen, sulfur and silicon determination in coal by proton induced gamma-ray analysis. *J. Radioanal. Chem.* 45, 387-394.
- Mahmood, H., Hoogmoed, W., Van Henten, E., 2011. Estimating soil properties with a proximal gamma ray spectrometer using windows and full-spectrum analysis methods. *Proceedings of the Second Global Workshop on Proximal Soil Sensing, Montreal, Canada*, pp. 15-18.
- MATLAB and Statistics Toolbox Release 2012b, The MathWorks, Inc., Natick, MA, United States.
- McGinn, S., Beauchemin, K., Coates, T., McGeough, E., 2014. Cattle Methane Emission and Pasture Carbon Dioxide Balance of a Grazed Grassland. *Journal of Environmental Quality* 43, 820-828.
- Michot, D., Y. Benderitter, A. Dorigny, B. Nicoullaud, D. King, and A. Tabbagh. 2003. Spatial and temporal monitoring of soil water content with an irrigated corn crop cover using surface electrical resistivity tomography. *Water Resources Research* 39(5):1138.
- Mikkelsen, R. L. 2011. The “4R” nutrient stewardship framework for horticulture. *HortTechnology* 21(6):658-662.
- Mukherjee, A., Lal, R., Zimmerman, A., 2014. Effects of biochar and other amendments on the physical properties and greenhouse gas emissions of an artificially degraded soil. *Science of The Total Environment* 487, 26-36.
- Nikièma, P., Rothstein, D.E., Miller, R.O., 2012. Initial greenhouse gas emissions and nitrogen leaching losses associated with converting pastureland to short-rotation woody bioenergy crops in northern Michigan, USA. *Biomass and Bioenergy* 39, 413-426.
- Paillet, Y., N. Cassagne, and J.-J. Brun. 2010. Monitoring forest soil properties with electrical resistivity. *Biology and Fertility of Soils* 46(5):451-460.
- Pan, L., V. Adamchuk, S. Prasher, R. Gebbers, R. Taylor, and M. Dabas. 2014. Vertical Soil Profiling Using a Galvanic Contact Resistivity Scanning Approach. *Sensors* 14(7):13243-13255.

- Pan, L., V. I. Adamchuk, D. L. Martin, M. A. Schroeder, and R. B. Ferguson. 2013. Analysis of soil water availability by integrating spatial and temporal sensor-based data. *Precision Agriculture* 14(4):414-433.
- Parasnis, D.S. *Principles of Applied Geophysics*, 5th ed.; Chapman & Hall: London, UK, 1997; pp. 456.
- Parkin, T. B., R. T. Venterea, and S. K. Hargreaves. 2012. Calculating the detection limits of chamber-based soil greenhouse gas flux measurements. *J Environ Qual* 41(3):705-715.
- Paul G. Lajoie. Soil survey of Argenteuil, two mountains and Terrebonne counties, Quebec. Research Blanch, Canada Department of Agriculture in co-operation with Quebec Department of Agriculture and Macdonald College, McGill University 1960. Available online: <http://sis.agr.gc.ca/cansis/publications/surveys/pq/pq2/index.html> (accessed on 8 November 2014). Canadian soil Classification
- Pedersen, A. R., S. O. Petersen, and F. P. Vinther. 2001. Stochastic diffusion model for estimating trace gas emissions with static chambers. *Soil Science Society of America Journal* 65(1):49-58.
- Pedersen, A. R., S. O. Petersen, and K. Schelde. 2010. A comprehensive approach to soil-atmosphere trace-gas flux estimation with static chambers. *European Journal of Soil Science* 61(6):888-902.
- Peterjohn, W.T., Melillo, J.M., Steudler, P.A., Newkirk, K.M., Bowles, F.P., Aber, J.D., 1994. Responses of trace gas fluxes and N availability to experimentally elevated soil temperatures. *Ecological Applications*, 617-625.
- Piikki, K., Söderström, M., Stenberg, B., 2013. Sensor data fusion for topsoil clay mapping. *Geoderma* 199, 106-116.
- Rehman, S.A.U., 2014. Agricultural Impact on Climate Change: A comparison of GHGs emissions from Organic and Conventional Agricultural practices. *Emirates Journal of Food and Agriculture* 27.
- Reijnders, L., Huijbregts, M., 2008. Palm oil and the emission of carbon-based greenhouse gases. *Journal of cleaner production* 16, 477-482.
- Robinson, D. A., I. Lebron, S. M. Lesch, and P. Shouse. 2004. Minimizing Drift in Electrical Conductivity Measurements in High Temperature Environments using the EM-38. *Soil Sci. Soc. Am. J.* 68(2):339-345.
- Rochette, P., 2011. Towards a standard non-steady-state chamber methodology for measuring soil N₂O emissions. *Animal Feed Science and Technology* 166–167, 141-146.

- Rochette, P., and N. S. Eriksen-Hamel. 2008. Chamber Measurements of Soil Nitrous Oxide Flux: Are Absolute Values Reliable? *Soil Sci. Soc. Am. J.* 72(2):331-342.
- Rochette, P., Chantigny, M.H., Ziadi, N., Angers, D.A., Bélanger, G., Charbonneau, É., Pellerin, D., Liang, C., Bertrand, N., 2014. Soil Nitrous Oxide Emissions after Deposition of Dairy Cow Excreta in Eastern Canada. *Journal of Environmental Quality* 43, 829-841.
- Rochette, P., N. Tremblay, E. Fallon, D. Angers, M. Chantigny, J. MacDonald, N. Bertrand, and L. É. Parent. 2010. N₂O emissions from an irrigated and non - irrigated organic soil in eastern Canada as influenced by N fertilizer addition. *European Journal of Soil Science* 61(2):186-196.
- Rodrigues Jr, F.A., Bramley, R.G.V., Gobbett, D.L., 2015. Proximal soil sensing for Precision Agriculture: Simultaneous use of electromagnetic induction and gamma radiometrics in contrasting soils. *Geoderma* 243–244, 183-195.
- Roy, A. 1972. Depth of investigation in Wenner, three-electrode and dipole-dipole DC resistivity methods. *Geophysical Prospecting* 20(2):329-340.
- Saey, T., D. Simpson, H. Vermeersch, L. Cockx, and M. Van Meirvenne. 2009. Comparing the EM38DD and DUALEM-21S sensors for depth-to-clay mapping. *Soil Science Society of America Journal* 73(1):7-12.
- Sathaye, J., Cannell, M., Kauppi, P., 1995. Management of forests for mitigation of greenhouse gas emissions.
- Serrano, J., S. Shahidian, and J. M. d. Silva. 2014. Spatial and Temporal Patterns of Apparent Electrical Conductivity: DUALEM vs. Veris Sensors for Monitoring Soil Properties. *Sensors* 14(6):10024-10041.
- Shcherbak, I., Millar, N., Robertson, G.P., 2014. Global metaanalysis of the nonlinear response of soil nitrous oxide (N₂O) emissions to fertilizer nitrogen. *Proceedings of the National Academy of Sciences* 111, 9199-9204.
- Sheets, K. R., and J. M. H. Hendrickx. 1995. Noninvasive Soil Water Content Measurement Using Electromagnetic Induction. 1944-7973.
- Si, B., Kachanoski, R., Reynolds, W., Carter, M., Gregorich, E., 2007. Analysis of soil variability. *Soil sampling and methods of analysis* 2nd ed CRC Press Boca Raton, FL 1163, 1191.
- Simpson, D., M. Van Meirvenne, T. Saey, H. Vermeersch, J. Bourgeois, A. Lehouck, L. Cockx, and U. W. A. Vitharana. 2009. Evaluating the multiple coil configurations of the EM38DD and DUALEM-21S sensors to detect archaeological anomalies. *Archaeological Prospection* 16(2):91-102.

- Skinner, C., Gattinger, A., Muller, A., Mäder, P., Fließbach, A., Stolze, M., Ruser, R., Niggli, U., 2014. Greenhouse gas fluxes from agricultural soils under organic and non-organic management—A global meta-analysis. *Science of the Total Environment* 468, 553-563.
- Slavich, P., and G. Petterson. 1993. Estimating the electrical conductivity of saturated paste extracts from 1: 5 soil, water suspensions and texture. *Soil Research* 31(1):73-81.
- Smyth, C., Stinson, G., Neilson, E., Lemprière, T., Hafer, M., Rampley, G., Kurz, W., 2014. Quantifying the biophysical climate change mitigation potential of Canada's forest sector. *Biogeosciences Discussions* 11, 441-480.
- Snyder, C., Bruulsema, T., Jensen, T., Fixen, P., 2009. Review of greenhouse gas emissions from crop production systems and fertilizer management effects. *Agriculture, Ecosystems & Environment* 133, 247-266.
- Sommer, R., Bossio, D., 2014. Dynamics and climate change mitigation potential of soil organic carbon sequestration. *Journal of environmental management* 144, 83-87.
- Statistics Canada. 2012. Fruit and Vegetable Production. Catalogue no. 22-003-X. Available at: <http://www.agr.gc.ca/eng/industry-markets-and-trade/statistics-and-market-information/by-product-sector/horticulture/horticulture-canadian-industry/sector-reports/a-snapshot-of-the-canadian-vegetable-industry-2010/?id=1330373416993>
- Sudduth, K. A., N. R. Kitchen, D. B. Myers, and S. T. Drummond. 2010. Mapping depth to argillic soil horizons using apparent electrical conductivity. *Journal of Environmental & Engineering Geophysics* 15(3):135-146.
- Sudduth, K. A., S. T. Drummond, and N. R. Kitchen. 2001. Accuracy issues in electromagnetic induction sensing of soil electrical conductivity for precision agriculture. *Computers and Electronics in Agriculture* 31(3):239-264.
- Taylor, R.; and Holladay, J. Accurate electromagnetic measurement of apparent conductivity: Issues and applications. In 3rd Global Workshop on Proximal Soil Sensing 2013; International Union of Soil Sciences Working Group on Proximal Soil Sensing: Potsdam, Germany, 2013; pp. 62-69.
- Tetegan, M., C. Pasquier, A. Besson, B. Nicoulaud, A. Bouthier, H. Bourenane, C. Desbourdes, D. King, and I. Cousin. 2012. Field-scale estimation of the volume percentage of rock fragments in stony soils by electrical resistivity. *Catena* 92:67-74.
- Torstensson, G., Aronsson, H., Bergström, L., 2006. Nutrient use efficiencies and leaching of organic and conventional cropping systems in Sweden. *Agronomy Journal* 98, 603-615.

- United Nations Framework Convention on Climate Change. Access on: 9 June 2015. Available at http://unfccc.int/national_reports/annex_i_ghg_inventories/national_inventories_submissions/items/8812.php
- Urdanoz, V., and R. Aragüés. 2012. Comparison of Geonics EM38 and Dualem 1S electromagnetic induction sensors for the measurement of salinity and other soil properties. *Soil Use and Management* 28(1):108-112.
- Vachaud, G., Passerat de Silans, A., Balabanis, P., Vauclin, M., 1985. Temporal stability of spatially measured soil water probability density function. *Soil Science Society of America Journal* 49, 822-828.
- Van Egmond, F., Loonstra, E., Limburg, J., 2010. Gamma ray sensor for topsoil mapping: The Mole. *Proximal Soil Sensing*. Springer, pp. 323-332.
- Vanderlinden, K., H. Vereecken, H. Hardelauf, M. Herbst, G. Martínez, M. H. Cosh, and Y. A. Pachepsky. 2012. Temporal stability of soil water contents: a review of data and analyses. *Vadose Zone Journal* 11(4).
- Venterea, R. T. 2010. Simplified method for quantifying theoretical underestimation of chamber-based trace gas fluxes. *Journal of Environmental Quality* 39(1):126-135.
- Venterea, R. T., K. A. Spokas, and J. M. Baker. 2009. Accuracy and precision analysis of chamber-based nitrous oxide gas flux estimates. *Soil Science Society of America Journal* 73(4):1087-1093.
- Veris Technologies, Inc. Available online: <http://www.veristech.com/the-soil/soil-ec> (accessed on 17 November 2014).
- Villarino, S.H., Studdert, G.A., Lateral, P., Cendoya, M.G., 2014. Agricultural impact on soil organic carbon content: Testing the IPCC carbon accounting method for evaluations at county scale. *Agriculture, Ecosystems & Environment* 185, 118-132.
- Wagner - Riddler, C., Furon, A., Mclaughlin, N.L., Lee, I., Barbeau, J., Jayasundara, S., Parkin, G., Von Bertoldi, P., Warland, J., 2007. Intensive measurement of nitrous oxide emissions from a corn–soybean–wheat rotation under two contrasting management systems over 5 years. *Global Change Biology* 13, 1722-1736.
- Weiske, A., Vabitsch, A., Olesen, J.E., Schelde, K., Michel, J., Friedrich, R., Kaltschmitt, M., 2006. Mitigation of greenhouse gas emissions in European conventional and organic dairy farming. *Agriculture, ecosystems & environment* 112, 221-232.
- West, T.O., Marland, G., 2002. A synthesis of carbon sequestration, carbon emissions, and net carbon flux in agriculture: comparing tillage practices in the United States. *Agriculture, Ecosystems & Environment* 91, 217-232.

- Wiant, H. V. 1967. Influence of temperature on the rate of soil respiration. *Journal of Forestry* 65(7):489-490.
- Williams, B. G., and D. Hoey. 1987. The use of electromagnetic induction to detect the spatial variability of the salt and clay contents of soils. *Soil Research* 25(1):21-27.
- Wong, M., Wittwer, K., Oliver, Y., Robertson, M., 2010. Use of EM38 and gamma ray spectrometry as complementary sensors for high-resolution soil property mapping, Proximal soil sensing. Springer, pp. 343-349.
- Wong, M.T.F., Harper, R.J., 1999. Use of on-ground gamma-ray spectrometry to measure plant-available potassium and other topsoil attributes. *Soil Research* 37, 267-278.
- Wood, R., Lenzen, M., Dey, C., Lundie, S., 2006. A comparative study of some environmental impacts of conventional and organic farming in Australia. *Agricultural Systems* 89, 324-348.

APPENDICES

A. MATLAB programs for data analysis, flux and emission estimation (Chapter 4)

```
close all; clear all; clc; rehash;
tic
disp('GHG Analysis: Fluxes & Emission Estimation Calculation, Version:
ASMS2013-06');
disp('Author: Ahmad S. Mat Su, Bioresource Eng. Department, McGill
University');
disp('Email: ahmad.matsu@mail.mcgill.ca | asuhaizil@gmail.com');
disp(' ');
%% Last updated: March 20, 2014          Version: V-AGGP-ASMS201403
%% GLOBAL INPUT VARIABLES
% INPUT FILES
inName = '140731_AGG2012_Gas_Clean.xls'; % Input filename
%% ## For multiple sheet entry
%inSheets =
[cellstr('Leamington'),cellstr('Harrow'),cellstr('Sherrington'),cellstr('St-
Emmanuel'), cellstr('Saint-Louis-de-Blandford'),cellstr('Truro')];
%% ## For single sheet entry
%site = input('Which study site (Answer:1=HR, 2=LE, 3=SE, 4=SH, 5=SL or 6=TR)
: ', 's');
% USER INPUT PROMPT
site = input('Which study site? (Ans:1=HR/2=LE/3=SE/4=SH/5=SL/6=TR) : ');
disp ' '
year = input ('What year of the data (Ans: 2012/2013/2014):');
% Site, planting and harvest date setting
if site == 1 % HR: Harrow
    inSheets = [cellstr('Harrow') ];
    Chambers = 24;
    if year == 2012
        planting = 41054; % Date in time format
        harvest = 41218;
    elseif year == 2013
        planting = 41432;
        harvest = 41555;
    elseif year == 2014
        planting = 0;
        harvest = 0;
    else
        disp 'Input in incorrect!'
    end
elseif site == 2 % LE: Leamington
    inSheets = [cellstr('Leamington') ];
    Chambers = 10;
    if year == 2012
        planting = 41049; harvest = 41166;
    elseif year == 2013
        planting = 41417; harvest = 41534;
    elseif year == 2014
        planting = 0; harvest = 0;
    else
        disp 'Input in incorrect!'
    end
end
```

```

end
elseif site == 3    % SE: St Emmanuel
inSheets = [cellstr('St-Emmanuel') ];
Chambers = 12;
if year == 2012
    planting = 41047;    harvest = 41159;
elseif year == 2013
    planting = 41393;    harvest = 41567;
elseif year == 2014
    planting = 41393;    harvest = 41567;
else
    disp 'Input in incorrect!'
end
elseif site == 4    % SH: Sherrington
inSheets = [cellstr('Sherrington') ];
Chambers = 24;
if year == 2012
    planting = 41053;    harvest = 41150;
elseif year == 2013
    planting = 41397;    harvest = 41550;
elseif year == 2014
    planting = 0;    harvest = 0;
else
    disp 'Input in incorrect!'
end
elseif site == 5    % SL: St Louis De Blandford
inSheets = [cellstr('Saint-Louis-De-Blandford') ];
Chambers = 15;
if year == 2012
    planting = 41059;    harvest = 41217;
elseif year == 2013
    planting = 41386;    harvest = 41571;
elseif year == 2014
    planting = 0;    harvest = 0;
else
    disp 'Input in incorrect!'
end
elseif site == 6    % TR: Truro
inSheets = [cellstr('Truro') ];
Chambers = 18;
if year == 2012
    planting = 41032;    harvest = 41220;
elseif year == 2013
    planting = 41402;    harvest = 41529;
elseif year == 2014
    planting = 41402;    harvest = 41529;
else
    Chambers = 00;
    disp 'Input in incorrect!'
end
else    % Unknown
inSheets = [cellstr('Unknown') ];
Chambers = 0;
if year == 2012
    planting = 0;

```

```

        harvest = 0;
    elseif year == 2013
        planting = 0;
        harvest = 0;
    elseif year == 2014
        planting = 0;
        harvest = 0;
    else
        disp('Input in incorrect!')
    end
    disp('Please input correct site name!')
end

disp('Your site is:'); disp(site);
disp('Chambers is:'); disp(Chambers);
disp(planting); disp(harvest);

%% OUTPUT FILES
[~, locations] = size(inSheets); % "~" means ignore/ thrown away the scalar
[data, text, raw] = xlsread(inName, char(inSheets)); % import data
outname = 'Flux Summary';

%% LOCAL VARIABLES
% Converstion factors of lppmv unit to mg/m^3
f_N2O = 1.16596; %mg/m^3.ppm
f_CH4 = 0.4999; %mg/m^3.ppm
f_CO2 = 0.4999; %mg/m^3.ppm
factor = [f_N2O, f_CH4, f_CO2];
% Chamber's Spec
H = 0.179; % Total height, m (Base + chamber cover)
%H = 0.139; % If installed only with cover, m
%H = 0.25; % H (meter) at Truro using cylinder base for 2012 season
A = 0.30914; % Area,m^2
V = H*A; % Volume inside the chamber,m^3
% Filter parameters | treshold, min value to be considered
N2O_filter = 0.15*f_N2O; % unit ppm * = mg/m^3
CH4_filter = 1.7*f_CH4; % unit ppm new filter 1.7 ppm! = mg/m^3
CO2_filter = 300*f_CO2; % unit ppm = mg/m^3
% Time for flux calculation
T = 0:0.25:1;
Cid = 1:1:Chambers;

%% MAIN-DO FOR ALL LOCATIONS
for i = 1:locations
    [data, text, raw] = xlsread(inName, char(inSheets(i))); % import data
    formatIn = 'dd/mm/yyyy';
    datesAll = datenum(raw(2:end,1),formatIn);
    datesUnique = unique(datesAll); % all sampling dates-individual date
    % datetime = raw(2:end,1)
    % For all Unique Dates
    for j = 1:length(datesUnique) % for all unique dates
        % Find all matching dates
        matches = find(datesAll == datesUnique(j));
    end
end

```

```

% slope = diff(y)./diff(x)

% For all matches date
results = cell(length(matches),11); %11 column to create empty matrix
for k = 1:length(matches)
    results(k,:) = raw(matches(k)+1,:);
end

%% FORMATING
semiformatted = results(:,3:end);
resultsFormatted = sortrows(semiformatted,1); % sort by chamber_ID
%resultsFormatted = sortrows (raw,{'Chamber_ID','Sequence'});

%% SLOPE CALCULATIONS ON ALL CHAMBERS
slope = @(data, int) cell2mat(data)/int;
chamberNames = unique(resultsFormatted(:,1));
for chamberID = 1:length(chamberNames)

    % FOR EACH CHAMBER FIRST REMOVE AMBIENT VALUES
    all = resultsFormatted(:,1);
    tmp = strfind(all, chamberNames{chamberID}); % unformatted, has
empties
    rowsTotal = find(not(cellfun('isempty', tmp))); % returns
indicies for rows of i-th chamber names
    z=1;
    for row = 1:length(rowsTotal)
        if strcmp('Ambient',resultsFormatted(row, 2))
            % do nothing, lose 'Ambient'
        %
        % elseif strcmp('Ambient',resultsFormatted(row, 2))
        %
        % % do nothing, lose 'Ambient'
        %
        % elseif strcmp('Ambient',resultsFormatted(row, 2))
        %
        % % do nothing, lose 'Ambient'
        else
            rowsData(z) = rowsTotal(row); % YAYA
            z = z + 1; % stepper
        end
    end
end

    data = cell2mat(resultsFormatted(rowsData, 4:6)) % Raw data of
Col14: N2O, Col15: CH4,Col16: CO2

%% UNIT CONVERSTION AND FILTER [ppmv to mg/m^3]
    N2O_mgm3 = data(:,1)*f_N2O; % Converted ppmv to mg/mg3
    N2O_mgm3(N2O_mgm3<=N2O_filter) = NaN % replace values
in filfer with NAN % The filter val is in mg/m3

    CH4_mgm3 = data(:,2)*f_CH4;
    CH4_mgm3(CH4_mgm3<=CH4_filter) = NaN % replace values
in filfer with NAN % The filter val is in mg/m3

    CO2_mgm3 = data(:,3)*f_CO2;
    CO2_mgm3(CO2_mgm3<=CO2_filter) = NaN % replace values
in filfer with NAN % The filter val is in mg/m3

```

```

data_mgm3 = [N2O_mgm3, CH4_mgm3, CO2_mgm3]

%% FLUX CALCULATION
% convert call to numbers
for k = 1:1:3; %Number of column-position of the gas
dataset in excel
gasdata = data_mgm3 ; % gas data is in mg/m^3 unit

% For three gas-2012 Truro, use below command!
%[Allslopes,MedSlope] = CAL_SLOPE_TR2012(gasdata(:,k)) ;

[Allslopes,MedSlope] = CAL_SLOPE(gasdata(:,k));
if k == 1 % Col 1 in excel
N2O_slope = horzcat(Allslopes,MedSlope)*H %
Concatenate all fluxes + medflux
N2O_slope1(chamberID,:)=N2O_slope;
elseif k == 2 % Col 2 in excel
CH4_slope = horzcat(Allslopes,MedSlope)*H
CH4_slope1(chamberID, :)= CH4_slope;
else k == 3
CO2_slope = horzcat(Allslopes,MedSlope)*H
CO2_slope1(chamberID, :)= CO2_slope;
end
end

end

%% OUTPUT- Export flux data into Excel files

% Export raw value of gas in Excel format
xlswrite(char(inSheets(i)), resultsFormatted,
datestr(datesUnique(j)), 'A2');%

% Export slopes value of gas in Excel format
slopedata = [N2O_slope1 ; CH4_slope1; CO2_slope1];
xlswrite(char(inSheets(i)), slopedata,
datestr(datesUnique(j)), 'M3');%

% Header of the exported excel files
header1 = {'Chamber_ID', 'Sequence', 'Sample_ID',
'N2O_ppm', 'CH4_ppm', 'CO2_ppm', 'Air_temp_C', 'Soil_temp_C', 'Soil_mois_%' };
xlswrite(char(inSheets(i)), header1,
datestr(datesUnique(j)), 'A1');
row_header2 = {'Chamber_ID', 'slope1', 'slope2', 'slope3',
'slope4', 'slope5', 'slope6', 'slope7', 'slope8', 'slope9', 'slope10', 'medslope_mg/
m2.hr' };
xlswrite(char(inSheets(i)), row_header2,
datestr(datesUnique(j)), 'L2');
A = 1:1:chamberID;

```

```

        %header3 = {'A', 'A', 'A' };
        xlswrite(char(inSheets(i)), A', datestr(datesUnique(j)), 'L3');
        %xlswrite(char(inSheets(i)), A', datestr(datesUnique(j)), 'L3
+length(A) ');

        matches = []; %To clear everytime loops for a new date to be
saved
        results = [];
        slopedata= [];

    end
end

%% EXPORT TO SUMMARY FLUX TABLE
disp ' Exporting summary flux on different dates....'
disp ' '
dates = datestr(datesUnique);
TotalDate = j;
TotChambers = 1:1:length(chamberNames);
% j is the total sampling days
for d = 1:1:j
    medslope(:,d) = xlsread (char(inSheets), dates(d,:), 'W:W');

    % for Truro 2012
    %medslope(:,d) = xlsread (char(inSheets), dates(d,:), 'P:P');
end
medslope(isnan(medslope)) = 0;
medslope;
days = 1:1:j;
%% OUTPUT -
%Flux Summary sheet

xlswrite (char(inSheets),TotChambers, outname, 'C3');
xlswrite (char(inSheets),days', outname, 'B4');
xlswrite (char(inSheets),medslope', outname, 'C4');

% Export date in number format MATLAB to EXCEL
    sampdates = datesUnique - datenum('30-Dec-1899');
    xlswrite(char(inSheets),sampdates, outname, 'A4');
disp 'FINISH calculating & exporting flux summary'
disp ' '
disp ' Now..calculating the EMISSION values...'

%% 1-D INTERPOLATION
% Importing fluxes data
    ifname = char(inSheets); % read input file name
    ishname = outname; % read input sheet name
    flux = xlsread(ifname, ishname);
    [row, col] = size(flux);
    id = 3; %First column data is on 3rd column
    last = col; %Last column data on data(end).

```

```

Date = flux(2:end,1);           % Date of sampling-in numerical format
x1 = Date;                     % Data in number format, Growing days
x2 = Date(1,1):1:Date(end);
fil = planting:1:harvest;      % Choose the site planting and harvesting dates
    % Interpolation of emission over sampling date
Flux_sampling = interp1(x1,flux(2:end,3:end),x2,'pchip');
    % Interpolation of emission In-Season date
Flux_InSeason = interp1(x1,flux(2:end,3:end),fil,'pchip');

%% EMISSION (mg/day or g/day)
% Sampling
Emission_Sampling = Flux_sampling*24;
Total_Emis_sampling = sum(Emission_Sampling);
N20Emiss_sampling = (Total_Emis_sampling(1,1:Chambers))*0.001; % In unit of
g/m^2
CH4Emiss_sampling = (Total_Emis_sampling(1,Chambers+1:Chambers*2))*0.001; %
In unit of g/m^2
CO2Emiss_sampling = (Total_Emis_sampling(1,(Chambers*2)+1:Chambers*3))*0.001;
% In unit of g/m^2

GasSummary_sampling = [N20Emiss_sampling  CH4Emiss_sampling
CO2Emiss_sampling];
Summary_Sampling = [Emission_Sampling; Total_Emis_sampling;
GasSummary_sampling];

% InSeason
Emission_InSeason = Flux_InSeason*24;
Total_Emis_InSeason = sum(Emission_InSeason);
N20Emiss_InSeason = (Total_Emis_InSeason(1,1:Chambers))*0.001; % In unit of
g/m^2
CH4Emiss_InSeason = (Total_Emis_InSeason(1,Chambers+1:Chambers*2))*0.001; %
In unit of g/m^2
CO2Emiss_InSeason = (Total_Emis_InSeason(1,(Chambers*2)+1:Chambers*3))*0.001;
% In unit of g/m^2

GasSummary_InSeason = [N20Emiss_InSeason  CH4Emiss_InSeason
CO2Emiss_InSeason];
Summary_InSeason = [Emission_InSeason; Total_Emis_InSeason;
GasSummary_InSeason];

%% OUTPUT DATA

sampdates = datestr(datenum(dates),'dd-mmm-yyyy');
xlswrite(char(inSheets),cellstr(sampdates), outname,'A4');

% EMIS_Summary sheet
xlswrite(char(inSheets),TotChambers,'EMIS_Summary','B4');
xlswrite(char(inSheets),TotChambers,'EMIS_Summary','G4');
xlswrite(char(inSheets),N20Emiss_sampling,'EMIS_Summary','C4');
xlswrite(char(inSheets),N20Emiss_sampling,'EMIS_Summary','C4');
xlswrite(char(inSheets),CH4Emiss_sampling,'EMIS_Summary','D4');
xlswrite(char(inSheets),CO2Emiss_sampling,'EMIS_Summary','E4');
xlswrite(char(inSheets),N20Emiss_InSeason,'EMIS_Summary','H4');
xlswrite(char(inSheets),CH4Emiss_InSeason,'EMIS_Summary','I4');

```

```

xlswrite (char(inSheets),CO2Emiss_InSeason', 'EMIS_Summary', 'J4');

% InterpoFlux-Sampling sheet
xlswrite (char(inSheets),TotChambers, 'InterpoFlux-Sampling', 'B3');
xlswrite (char(inSheets),x2', 'InterpoFlux-Sampling', 'A4');
xlswrite (char(inSheets),Flux_sampling, 'InterpoFlux-Sampling','B4');
% InterpoFlux-InSeason sheet
xlswrite (char(inSheets),TotChambers, 'InterpoFlux-InSeason', 'B3');
xlswrite (char(inSheets),fil', 'InterpoFlux-InSeason', 'A4');
xlswrite (char(inSheets),Flux_InSeason, 'InterpoFlux-InSeason','B4');

% Emis_Sampling sheet
xlswrite (char(inSheets),TotChambers, 'Emis_Sampling', 'B3');
xlswrite (char(inSheets),x2', 'Emis_Sampling', 'A4');
xlswrite (char(inSheets),Summary_Sampling, 'Emis_Sampling', 'B4');
% Emis_InSeason sheet
xlswrite (char(inSheets),TotChambers, 'Emis_InSeason', 'B3');
xlswrite (char(inSheets),fil', 'Emis_InSeason', 'A4');
xlswrite (char(inSheets),Summary_InSeason, 'Emis_InSeason', 'B4');

%% DISPLAY SIMPLE SUMMARY [DATES AND TOTAL SAMPLING]
disp(cellstr(inSheets))
disp ' Sampling Dates'
disp (datestr(datesUnique)) , disp 'Total sampling date:', disp (j)

disp 'End'
rehash
toc

```